Pattern formation in Hamiltonian systems with continuous spectra; a normal-form single-wave model

N. J. Balmforth[*]

Department of Mathematics,
University of British Columbia, Vancouver,
Canada

P. J. Morrison[†]

Department of Physics and Institute for Fusion Studies,
University of Texas at Austin,
Austin, TX 78712,
USA

J.-L. Thiffeault[‡]

Department of Mathematics,
University of Wisconsin,
Madison, WI 53706,
USA

Pattern formation in biological, chemical and physical problems has received considerable attention, with much attention paid to dissipative systems. For example, the Ginzburg–Landau equation is a normal form that describes pattern formation due to the appearance of a single mode of instability in a wide variety of dissipative problems. In a similar vein, a certain "single-wave model" arises in many physical contexts that share common pattern forming behavior. These systems have Hamiltonian structure, and the single-wave model is a kind of Hamiltonian mean-field theory describing the patterns that form in phase space. The single-wave model was originally derived in the context of nonlinear plasma theory, where it describes the behavior near threshold and subsequent nonlinear evolution of unstable plasma waves. However, the single-wave model also arises in fluid mechanics, specifically shear-flow and vortex dynamics, galactic dynamics, the XY and Potts models of condensed matter physics, and other Hamiltonian theories characterized by mean field interaction. We demonstrate, by a suitable asymptotic analysis, how the single-wave model emerges from a large class of nonlinear advection-transport theories. An essential ingredient for the reduction is that the Hamiltonian system has a continuous spectrum in the linear stability problem, arising not from an infinite spatial domain but from singular resonances along curves in phase space whereat wavespeeds match material speeds (wave-particle resonances in the plasma problem, or critical levels in fluid problems). The dynamics of the continuous spectrum is manifest as the phenomenon of Landau damping when the system is stable, and when the system becomes unstable, an embedded neutral mode appears within the continuum. The single-wave model captures the dynamics of the embedded mode if the system is perturbed so as to make the mode unstable, or if perturbations destroy that mode and the system remains stable. As a consequence, the model describes a range of universal phenomena: for a bifurcation to instability, the model fea-

tures the so-called "trapping scaling" dictating the saturation amplitude, and the "cats-eye" structures that characterize the resulting phase-space patterns. In the stable situation, the model offers one of the simplest descriptions of Landau damping, and illustrates how this can be arrested by nonlinearity. Such dynamical phenomena have been rediscovered in different contexts, which is unsurprising in view of the normal-form character of the single-wave model.

* njb@math.ubc.ca

† morrison@physics.utexas.edu

‡ jeanluc@math.wisc.edu

CONTENTS

I. INTRODUCTION

A. Perspective

The dynamics of forming patterns in biological, chemical, and physical systems has received considerable attention over recent years (see e.g. Cross and Hohenberg, 1993). In the simplest settings, one deals with spatial patterns that form as a result of the appearance of a small number of "modes" of instability, such as a convection cell in a fluid contained between differentially heated plates. These are the eigenmodes of the linear stability problem and provide a natural set of tools to describe the forming spatial patterns. In particular, by decomposing perturbations about the unpatterned equilibrium into the eigenmodes and exploiting the center-manifold reduction, the full system of governing equations can be approximated by a low-order set of amplitude equations near the onset of linear instability (e.g. Crawford, 1991; Manneville, 1995).

The center-manifold reduction works because, in spatially bounded, dissipative systems, the eigenvalues of the normal modes compose a set of distinct points on the spectral plane, and instability arises when one of these modes becomes unstable. The purpose of the present article is to summarize extensions of some of these ideas to non-dissipative systems that suffer instabilities that cannot be described in low-dimensional terms, and for which the patterns that form occur naturally in the associated phase space. These systems are Hamiltonian systems that have a neutrally stable continuous spectrum of eigenvalues in the linear stability problem. Moreover, this spectrum is not the result of the problem being couched in an infinite spatial domain, but due to singularities in the linear eigenvalue problem that arise due to a resonant interaction between wave-like perturbations and the background equilibrium state; the singular resonances occur along curves in phase space whereat wavespeeds match material speeds. Such systems are also commonplace, and include ideal plasmas, inviscid fluids, self-gravitating stellar systems, and various other Hamiltonian models characterized by mean-field interactions. The plasma problem is that of electrostatic instability in an ideal, single-species plasma (van Kampen, 1955), which was the original building block in understanding a multitude of more complicated instabilities in plasma theory and fusion science. The fluid problem is the instability of inviscid shear flow or vortices (Case, 1960), which are also key problems in fluid mechanics. Another mean-field Hamiltonian model of interest is that with the XY interaction (see Chaikin and Lubensky,

1995), which models spin-spin interaction and has been used to describe e.g. superfluid helium and hexatic liquid crystals (see the 'Hamiltonian Mean Field' model of Campa *et al.*, 2009 for an extensive treatment).

The mathematical issue which underlies our discussion is that, although instability is described by an exponentially growing discrete eigenmode, the mode detaches from the continuous spectrum when it becomes unstable. Consequently, at onset, the distinguished mode cannot be isolated from an infinite number of other, singular eigensolutions representing the continuum (the center-manifold reduction relies on such a spectral gap). This aspect of the problem fundamentally affects the weakly nonlinear description, which, as a consequence, has to proceed down a relatively novel and much more tortuous pathway.

As we outline in this review, the outcome of following this pathway is a reduced description of the dynamics that is closely related to the single-wave model of O'Neil *et al.* (1971) and Onishchenko *et al.* (1971). Following the plasma physics terminology, we refer to the reduced description as simply the "single-wave model". However, one could take this as an abuse of terminology as there are some key differences between our weakly nonlinear theory and the classical single-wave model of plasma physics. More specifically, the classical model is often written down largely as a minimal description of the interaction of between wave with a beam of particles, not after a reduction from some governing set of equations. By taking this more qualitative approach, one simply poses the single-wave model and is allowed complete freedom in fixing the initial conditions describing the starting arrangement of the wave and particles. By contrast, although the reduced description of the weakly nonlinear theory furnishes evolution equations that are formally identical to those of the classical single-wave model, special initial conditions are also selected that rule out many of the solutions studied by O'Neil *et al.* and others since. The special initial and boundary data are the descendants of certain conditions placed on the original governing system at the outset of the calculations, and reflect how that system is positioned in the sense of linear stability theory. Of course, one could view such restrictions negatively, given the convenience and simplicity afforded by those solutions. However, as a weakly nonlinear description, the restrictions are essential to constraint properly the bifurcation to instability.

Indeed, our single-wave model is a Hamiltonian normal form that describes the transition to instability described above in a wide variety of physical systems of fluid, plasma, and other disciplines. The model captures the dynamics of the patterns that form in the phase space of the system due to the growth and nonlinear saturation of the unstable mode detaching from the continuous spectrum. All of the physical models for which the single-wave model is appropriate are hyperbolic Hamiltonian systems with Hamiltonian characteristic equations. Thus the patterns occur in a conventional phase space with canonically conjugate coordinates, and consequently have a Liouville theorem and other Hamiltonian properties, all of which help to recognize the circumstances that lead to the single-wave model.

For the physical systems we treat as examples, the patterns have two characteristic features: there is a relatively smooth, wave-like pattern ocupying most of the domain, coupled to a more complicated, finely scaled structure appearing over a localized region surrounding the resonance of linear theory. The larger-scale wave pattern reflects the shape of the embedded neutral mode. The finely scaled structure is generated by the interaction of that mode with a locally resonant packet of the continuous spectrum, and takes the form of either localized "holes" in the plasma distribution function (see, e.g., Eliasson and Shukla, 2007), "cat's-eye" vortices in the fluid shear flow, and 'magnetization' zones in the XY model. Explicating the universal nature of these patterns as described by the single-wave model is the main goal of this article.

B. Single-wave model preview

The single-wave model is a Hamiltonian normal form that captures the dynamics of Landau damping in stable situations, and the nonlinear saturation of unstable modes (see §VI). In light of its origin, the model must be of Hamiltonian and transport form (see §II.A), and be defined in a phase space that we take, for simplicity, to be two-dimensional. The basic dynamical variables are a density-like variable $Q(x, y, t)$, and an amplitude variable $A(t)$. The density Q depends on the coordinates (x, y), describing the phase space over the resonant, finely scaled region. The amplitude $A(t)$ depends purely on time, and represents the amplitude of the embedded neutral mode; given that mode's eigenfunction, one can reconstruct the large-scale wave pattern outside the resonant region. In its normal form (described in §V.B), the single-wave model is

compactly given by following:

$$Q_t + [Q, \mathcal{E}] = 0 \,, \tag{1}$$

$$\varphi = A\mathrm{e}^{\mathrm{i}x} + A^*\mathrm{e}^{-\mathrm{i}x} \,, \tag{2}$$

$$\mathrm{i}A_t = \left\langle Q\,\mathrm{e}^{-\mathrm{i}x} \right\rangle \,, \tag{3}$$

where $\mathcal{E} = y^2/2 - \varphi$,

$$[f, g] = f_x g_y - f_y g_x \,, \quad \text{and} \quad \langle \,\cdot\, \rangle = \frac{1}{2\pi} \int_{-\infty}^{\infty} dy \int_{0}^{2\pi} dx \ \cdot \tag{4}$$

and $f_x := \partial f/\partial x$, etc. Equation (1) is the transport equation for Q that resembles the Vlasov or Euler equation, with dependence on the variable φ through $\mathcal{E}$, an energy for the characteristic 'particle orbit' equations. From Eqs. (2) it is clear that φ represents a wave of amplitude A, with its single-wave spatial dependence upon the variable x being obvious, while equation (3) gives the temporal evolution of A, which is driven in an integral manner by the rearrangements of Q throughout the entire resonant region.

In addition, the model contains parameters that must be adjusted to characterize the physical system of interest. There are two, γ and κ, which are contained in the definition of the equilibrium, $\overline{Q}(y) = \gamma y - \frac{1}{2}\kappa y^2$, about which the system develops. Section Y outlines in detail how these parameters are determined, as well as deriving in a fairly general setting the single-wave model. We also need initial conditions, which are guided by the need to perturb the system off this equilibrium by nudging the unstable mode; formally, this corresponds to taking $Q(x, y, t = 0) = \overline{Q}(y) + \kappa\varphi(x, t = 0)$ and $A(t = 0) = A_0$, with $|A_0| \ll 1$. An alternative, which amounts to a very similar initialization but can be more convenient as a numerical strategy, is to take $Q(x, y, t = 0) = \overline{Q}(y)$ and $A(t = 0) = 0$, and then kick the system into action by adding a small, transient forcing to (3), such as $0.1t \exp(-200t^2)$. This type of forcing corresponds to engineering a "dynamically accessible" initial condition in view of the underlying Hamiltonian structure of the problem (Morrison and Pfirsch, 1992), and mimics certain experimental protocols (Balmforth et $al.$, 2001a). A solution of (1)–(3) with $\kappa- = 0$ and $\gamma = -1$, exploiting this initial forcing, is presented in Fig. 1.

The figure shows five snapshots of the density $Q(x, y, t)$ on the (x, y)-phase plane (panel a), together with a time series of the mode amplitude $A(t)$ (panel b). For the earliest snapshot, $Q(x, y, t)$ has undergone only minor rearrangements which the deformation of the initial state (with $\kappa = 0$, the equilibrium is simply a linear gradient in y), determined by the shape of the unstable mode (see §VI). For the later times, the Q distribution becomes increasingly twisted up into a cats-eye pattern; simultaneously, the mean ($x-$averaged) profile of the distribution becomes flattened over the region occupied by the cat's eye. This dynamics is described more thoroughly in §VII. The solution illustrates the universal pattern seen in many physical systems described by the single-wave model, and is typical of vortex formation in fluid mechanics (§II.C.1), the development of particle holes in plasma physics (§II.C.2), and analogous structure formation in systems like the XY model (§II.C.3).

The system of Eq. (2)-(3) is a Hamiltonian field theory and the equations are equivalent to the alternative, Poisson bracket form,

$$Q_t = \{Q, H\} \qquad \text{and} \qquad A_t = \{A, H\} \tag{5}$$

where the Hamiltonian is given by

$$H = \int_{-\infty}^{\infty} dy \int_{0}^{2\pi} dx \left(\mathcal{E}Q + \kappa|A|^2 \right) \tag{6}$$

and the Poisson bracket $\{\, , \,\}$ is

$$\{F, G\} = \frac{i}{2\pi} \left(\frac{\partial F}{\partial A} \frac{\partial G}{\partial A^*} - \frac{\partial F}{\partial A^*} \frac{\partial G}{\partial A} \right)$$
$$+ \int_{-\infty}^{\infty} dy \int_{0}^{2\pi} dx\, Q \left[\frac{\delta F}{\delta Q}, \frac{\delta G}{\delta Q} \right] \,; \tag{7}$$

functional derivatives such as $\delta F/\delta Q$ are defined in Sec. II. This Hamiltonian structure (derived and discussed in more detail in §V.C) is inherited from that of the various 'parent' models for which the single-wave model is an encompassing normal form.
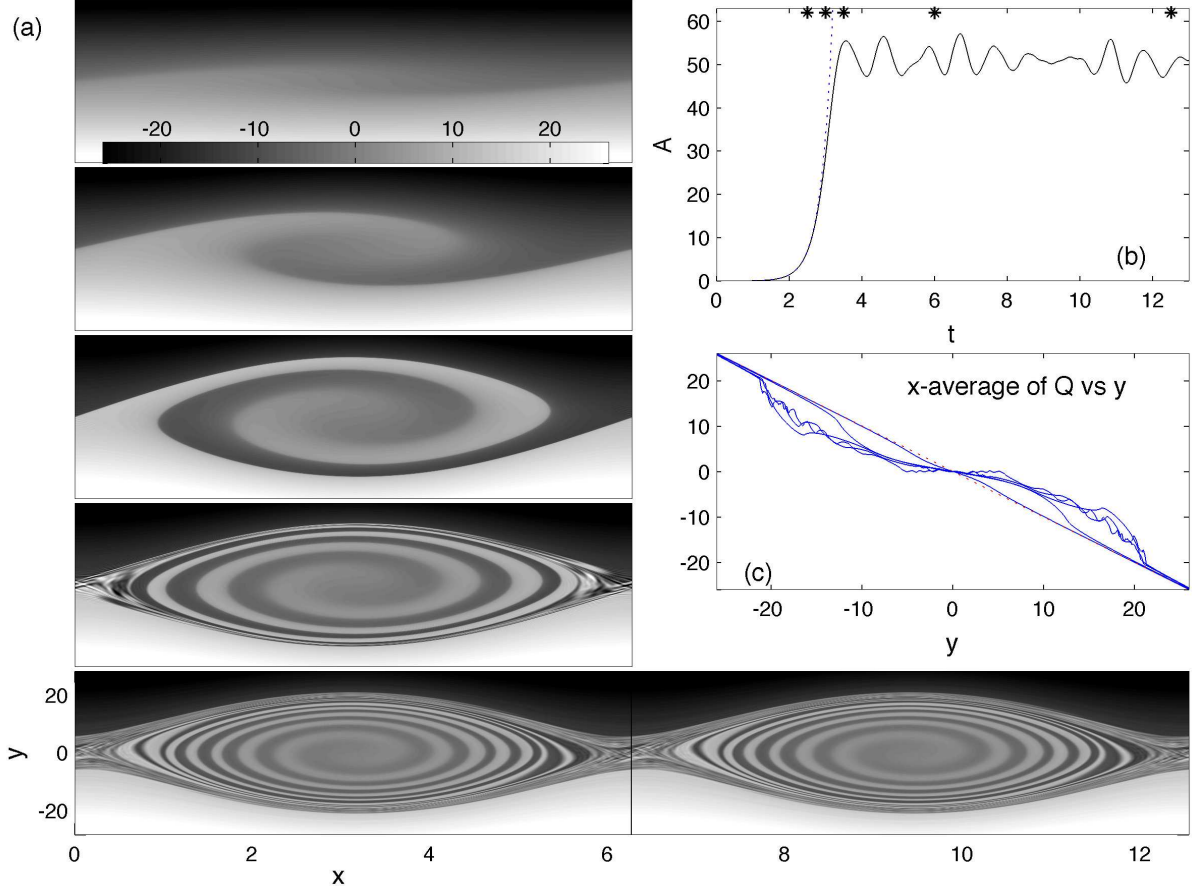
FIG. 1 A solution of the single-wave model in its normal form. Parameter values are $\kappa = 0$ and $\gamma = -1$ (cf. Sec. V). The system is initialized with $A(0) = 0$ and $Q(x, y, 0) = -y$ and then kicked into action by adding a forcing term $0.1t \exp(-200t^2)$ to the mode amplitude equation (see Balmforth and Piccolo, 2001 for further details of the computational scheme). Panel (a) shows five snapshots of $Q(, x, y, t)$ as densities on the (x, y)-plane. Two wavelengths are shown for the final snapshot to emphasize the periodic geometry. Panel (b) shows the time evolution of the mode amplitude, $A(t)$; the stars indicates the times of the snapshots in (a) and the dotted line shows the linear growth of the normal mode. Panel (c) shows the $x-$average of the distribution $Q(x, y, t)$ for the five snapshots; the dotted is the initial linear gradient.

Note that an overarching feature of our review is the view of the single-wave model and the parent problems from which it descends as partial differential systems; Hamiltonian field theories. An alternative perspective describes the system behaviour at the level of the constitutent particles (which is less suitable for a fluid problem, but certainly relevant for plasma and stellar dynamic applications). Although we largely ignore this alternative viewpoint, one can also consider the single-wave model in the context of such N-body problems (e.g. Antoniazzi et al. (2005); Firpo et al. (2001); Onishchenko et al. (1971); and Tennyson et al. (1994)), in which case one deals with the ordinary differential problem that is equivalent to tracking the characteristics of the system (1)-(3); practically, one truncates the number of particles to arrive at a finite N-body problem.

C. Overview

In Sec. II we describe a large class of Hamiltonian 2+1 field theories that contain the basic ingredients for the phenomena described by the single-wave model. In this section, we also establish our notation and provide examples of specific physical systems, including shear flow from fluid mechanics (§II.C.1), Vlasov theory from plasma physics (§II.C.2), and the XY model from condensed matter physics (§II.C.3). We use, mainly, these three examples to help make our general points throughout the paper. We note that the mean field model with the XY interaction has been called the 'Hamiltonian Mean Field model' by Campa *et al.* (2009) and collaborators. We refrain from this terminology since all of the models treated in this paper are in fact examples of Hamiltonian mean field models. Instead, we will refer to this example as the XY model.

As mentioned above, an essential feature of single-wave dynamics lies in the nature of the linear theory of the parent models. In particular, to understand single-wave phenomena it is necessary to understand the transition to instability that it describes. This transition has been developed and rediscovered independently in many fields, and since this linear dynamics is crucial to our development, we review this in an historical context in Sec. III. We first describe the linear theory for our general class of Hamiltonian models (§III.A) and then consider the early history due to Rayleigh and Kelvin (§III.B), followed by the developments in plasma physics (§III.C), then stellar dynamics and in the XY model (§III.D). A main purpose of producing a normal form theory is to unify discoveries made in disparate fields; the nature and considerable amount of rediscovery and interchange in several areas emphasizes the need for a review of the single-wave model.

As is common in normal form theory, asymptotic calculations must be performed and the situation for the single-wave model is particularly intricate. Thus, in §IV and V we outline the nonlinear dynamics that one must understand to appreciate the single-wave model. In particular, we first demonstrate how conventional weakly nonlinear theory is unable to describe the transition to instability and fails to capture the scale of the nonlinear saturation level except in some very special situations (see §IV.A). That level is referred to as trapping scaling in plasma physics, and we provide a historical commentary on the origin of this scaling (§IV.B), as well as parallel development in fluid mechanics regarding what is termed critical layer theory (§IV.C). These descriptions motivate the asymptotic sequences used in the derivation of the single-wave model.

With the intuition gained from Secs. III and IV, the stage is set for the derivation of the single-wave model, which we do in Sec. V. The derivation involves an asymptotic expansion featuring both the discrete embedded mode and the continuous spectrum. We provide a general derivation that produces the Hamiltonian normal form embodied in the single-wave model. We also observe that, in some specific physical problems, a certain degeneracy occurs that necessitates a degenerate form of the single-wave model, a form shared by some symmetric profiles in the XY model and the plasma and stellar dynamics problems. Thus, in §V.B, we delineate a norm form and a degenerate form of the single-wave model. Next, we discuss the Hamiltonian nature and conservation laws of the single-wave model that are inherited from the Hamiltonian parent model (§V.C). Finally, for later use, we outline the leading-order forms expected for different types of dissipation (§V.D).

The linearized version of the single-wave model is arguably the simplest system capturing the transition to instability of a discrete mode embedded in the continuous spectrum, as well as the disappearance of such a mode and Landau damping. In Sec. VI we describe this linear theory in detail, including the effect of dissipation, so as to address issues of structural stability of our model. Advancing on to the nonlinear dynamics, Sec.s VII and VIII describe the various kinds of patterns captured by the single-wave model. We first discuss the normal form, describing the pattern arising either from linear instability (§VII.A) or from nonlinearly forcing a stable situation (§VII.B). Sec. VIII provides a similar analysis for the degenerate form, considering in detail the XY model. In Sec. IX several variations on the single-wave theme are discussed. Finally, in Sec. X, we conclude and discuss the universality and limitations of the single-wave model.

II. A CLASS OF HAMILTONIAN THEORIES AND SPECIFIC EXAMPLES

We now describe a general class of 2+1 Hamiltonian mean-field theories and outline several specific examples that we discuss in more detail in later sections.

A. A class of Hamiltonian field theories

The class of 2+1 Hamiltonian field theories (Morrison, 2003) possesses a single independent variable, $\zeta(q, p, t)$, which is a density-like variable that depends on the independent phase space variables $z := (q, p)$, coordinates for some phase space $\mathcal{Z}$, as well as time. We suppose the density satisfies a transport equation of the following form:

$$\frac{\partial \zeta}{\partial t} + [\zeta, \mathcal{E}] = 0 \,, \tag{8}$$

where the 'particle' Poisson bracket is defined by the usual expression $[f, g] = f_q g_p - g_q f_p$, where $f_q := \partial f / \partial q$ etc., and the quantity $\mathcal{E}$ is an energy-like quantity that we call the particle energy. If (8) were a Liouville equation, then $\mathcal{E}$ would be a given function of z, and we would have a linear theory. However, we are concerned with mean field theories where $\mathcal{E}$ depends on ζ in a global sense. Thus, our systems are governed by nonlinear (quasilinear) partial integrodifferential equations. Such equations arise, for example, by truncation of BBGKY (Bogoliubov-Born-Green-Kirkwood-Yvon) hierarchies, which results in particular functional dependencies of the particle energy on the density. We do not pursue such an approach, but postulate that the particle energy arises from a total energy (Hamiltonian) functional of the form $H[\zeta] = H_1 + H_2 + H_3 + \dots$, where the one-point energy, H_1, the two-point, H_2, etc. are given as follows:

$$H_1[\zeta] = \int_{\mathcal{Z}} d^2z \, h_1(z) \, \zeta(z, t) \,,$$
$$H_2[\zeta] = \frac{1}{2} \int_{\mathcal{Z}} d^2z \int_{\mathcal{Z}} d^2\hat{z} \, \zeta(z, t) \, h_2(z, \hat{z}) \, \zeta(\hat{z}, t) \,, \tag{9}$$

with the generalizations to H_3, H_4, etc. being obvious. The quantities h_1 and h_2, the interaction kernels, are left unspecified for now. But, we do suppose the two-point interaction possesses the symmetry $h_2(z, \hat{z}) = h_2(\hat{z}, z)$. The particle energy is obtained from the field energy by functional differentiation:

$$\mathcal{E} := \frac{\delta H}{\delta \zeta} = h_1 + \int_{\mathcal{Z}} d^2\hat{z} \, h_2(z, \hat{z}) \, \zeta(\hat{z}, t) \,, \tag{10}$$

where the functional derivative is defined as usual by $\delta H = \int_{\mathcal{Z}} d^2z \, \delta\zeta \, \delta H / \delta\zeta$. It is not difficult to show that $H[\zeta]$ is a constant of motion under the dynamics of (8).

Equation (8) with $\mathcal{E} = \delta H / \delta \zeta$ is a Hamiltonian field theory (Morrison, 2003). However, since there is only one field variable ζ the theory is not of a canonical form, but possesses a noncanonical Lie-Poisson bracket description (for review see, for example, Morrison, 1998 and Marsden and Ratiu, 1999) given by

$$\{F, G\} = \int_{\mathcal{Z}} d^2z \, \zeta \left[\frac{\delta F}{\delta \zeta}, \frac{\delta G}{\delta \zeta} \right] \,. \tag{11}$$

Noncanonical brackets of this form, which depend explicitly upon the variable ζ unlike conventional Poisson brackets that only depend on (functional) derivatives of the canonical variables, express the Hamiltonian form of matter in terms of Eulerian variables. Such noncanonical Poisson brackets were introduced in the context of magnetohydrodynamics in Morrison and Greene (1980), and the specific form of (11) was given for the Vlasov-Poisson system in Morrison (1980) and the two-dimensional Euler equation in Morrison (1982).

Using (11) the equations of motion are obtained in the form

$$\frac{\partial \zeta}{\partial t} = \{\zeta, H\} = -\left[\zeta, \frac{\delta H}{\delta \zeta} \right] = -[\zeta, \mathcal{E}] \,. \tag{12}$$

Associated with the preceding Hamiltonian form are various constants of motion: besides the Hamiltonian $H[\zeta]$ itself, there are the Casimir invariants,

$$C[\zeta] = \int_{\mathcal{Z}} d^2z \, \mathcal{C}(\zeta) \,, \tag{13}$$

where $\mathcal{C}(\zeta)$ is an arbitrary function, which arise from degeneracies in the Poisson bracket.

Other important invariants are momenta, $P[\zeta]$, that are Hamiltonian dependent. Momentum invariants generally arise from translation symmetries that in the present context would be determined by the form of the interaction kernels $h_1, h_2, \ldots$. This is how the strong version of Newton's third law is built into the n-body problem. This idea can be generalized in various ways, but we do so by observing that our system conserves momentum if there exists a canonical transformation of the phase space $\mathcal{Z}$

$$z = (q, p) \longleftrightarrow \bar{z} := (\theta, I)$$

such that in the new particle coordinates $\bar{z} := (\theta, I)$, the interactions h_1, h_2, etc. have upon composition with $z(\bar{z})$ one of the following two forms:

$$h_1 \circ z = \bar{h}_1(I), \qquad h_2 \circ (z, \hat{z}) = \bar{h}_2(I, \hat{I}, |\theta - \hat{\theta}|) \tag{14}$$

or

$$h_1 \circ z = 0, \qquad h_2 \circ (z, \hat{z}) = \bar{h}_2(|I - \hat{I}|, |\theta - \hat{\theta}|). \tag{15}$$

In the first case

$$P[\zeta] = \int_{\mathcal{Z}} d^2 z \, I \, \zeta(z). \tag{16}$$

is conserved, while in the second case we have two kinds of translation invariance and thus two components of the momentum

$$P_1[\zeta] = \int_{\mathcal{Z}} d^2 z \, I \, \zeta(z) \quad \text{and} \quad P_2[\zeta] = \int_{\mathcal{Z}} d^2 z \, \theta \, \zeta(z). \tag{17}$$

All examples treated in this review will be of one of these types and three-point and higher interactions will not be considered.

Associated with each mean-field model is a Hamiltonian n-body problem. This follows by assuming a Klimontovich type of distribution

$$\zeta = \sum_{i=1}^{n} \delta(z - z^i(t)), \tag{18}$$

with $z^i = (q^i, p_i)$, $i = 1, 2, \ldots, n$, and substituting (18) into (8) and seeking a weak solution. Alternatively, the n-body problem arises upon effecting the functional chain rule on $F[\zeta] = f(z^1, z^2, \ldots, z^n)$, where f is defined upon inserting of (18) into F, giving

$$\frac{\partial}{\partial z^i} \left. \frac{\delta F}{\delta f} \right|_{z^i} = \frac{\partial f}{\partial z^i}, \tag{19}$$

to establish a mapping between the canonical and noncanonical Poisson brackets. Both methods yield the Hamiltonian n-body problem

$$\dot{z}^i = [z^i, H], \tag{20}$$

where self-energy terms are removed from H. The existence of this Hamiltonian n-body problem reinforces why our patterns occur in a phase space in the mean-field theory, rather than a configuration space. One consequence of this is that the characteristic equations of the single-wave model possess Liouville's theorem on conservation of phase space volume (here area).

All of the examples treated here arise from equilibria that only depend on I. For this reason we set $\zeta(\theta, I, t) = R(I) + \rho(\theta, I, t)$ and then when a choice of R is made, $\rho(\theta, I, t)$ represents the main dynamical variable. We further assume that θ is an angle-like variable, so that the phase space is periodic in $\theta \in [0, 2\pi]$, and $I \in \mathcal{D}$ with $\mathcal{D}$ equal to $[-1, 1]$ or $(-\infty, \infty)$, depending on the example. Upon substitution of $\zeta = R + \rho$ into $\mathcal{E}$, both of the forms of (14) and (15) can be written as follows:

$$\mathcal{E}[R + \rho] = \mathcal{E}[R] + \mathcal{E}[\rho] =: h(I) + \Phi(\theta, I), \tag{21}$$

with

$$\Phi(\theta, I) = \mathcal{K}\rho := \int_{\mathcal{D}} d\hat{I} \int_0^{2\pi} d\hat{\theta}\, K(I, \hat{I}, |\theta - \hat{\theta}|)\, \rho(\hat{\theta}, \hat{I}, t)\,, \tag{22}$$

where h and K are determined by h_1 and h_2. Thus the governing equations become

$$\rho_t + [R, \Phi] + [\rho, h + \Phi] = 0 \tag{23}$$

or

$$\rho_t + \Omega\rho_\theta - \Phi_\theta \frac{dR}{dI} + [\rho, \Phi] = 0, \tag{24}$$

 where the Poisson bracket is now redefined as $[f, g] = f_\theta g_I - g_\theta f_I$, and $\Omega(I) = dh/dI$. The quantity $h(I)$ corresponds to a Hamiltonian for an integrable system and the coordinates (θ, I) are action-angle coordinates for the characteristics of this system.

Equation (24) will serve as our starting point in subsequent analyses of our examples. In addition for all the examples we consider, the interaction is assumed to have zero mean, i.e.

$$\int_0^{2\pi} d\hat{\theta}\, K(I, \hat{I}, \theta - \hat{\theta}) = 0. \tag{25}$$

Of note is the case where K is independent of I and $\hat{I}$; such a K will be referred to as a *spatial kernel*.

B. Notation

By tradition, different independent and dependent variables have been used in different contexts. For example, in plasma physics, the phase space coordinates, representing position and velocity, are often written as (x, v). In fluid mechanics, both coordinates denote position, just as the example of Sec. I.B used (x, y). To be a little more definite, we will always describe the first independent variable as coordinate-like or angular, while the second will be momentum-like or an action, as for the general independent variables, (q, p) and (θ, I), defined above. Moreover, throughout, we will use

$$[f, g] = f_q\, g_p - f_q\, g_p\,, \quad \text{and} \quad \langle f \rangle = \frac{1}{2\pi} \int_{\mathcal{D}} dp \int_0^{2\pi} dq\, f(q, p)\,, \tag{26}$$

for any 'conjugate' coordinate pair (q, p) (*i.e.* not just for the pair (x, y) as in (4)), and, as above, subscript denotes partial differentiation. When there is a proliferation of subscripts, we will use primes to denote ordinary derivatives and, for example, ∂_x to denote $\partial/\partial x$, and so on. In all cases our coordinate-like variable will be periodic and eventually scaled to be 2π-periodic, while the momentum domain $\mathcal{D}$ is example specific. When $\mathcal{D} = (-\infty, \infty)$ we will denote it by $\mathbb{R}$.

C. Examples

1. Shear flow

Our example of shear flow considers the evolution of disturbances to a channel flow or to perturbations of differentially rotating vortices, as illustrated in Fig. 2(a)-(b) (Drazin and Reid, 1981). Thus, we begin with Euler's equation in two-dimensions, in which case the field ζ corresponds to the scalar vorticity field. In cylindrical geometry the coordinates for $\mathcal{Z}$ would be $(\theta, I) = (\theta, r^2/2)$, the usual polar coordinates; however, we are principally interested in channel flow with a periodic boundary condition and so we adopt $(\theta, I) = (x, y)$, where the spatial coordinate x is equivalent, after a simple scaling, to the "angle" θ. Thus, for shear flow, the action-like coordinate I is equivalent to y, the cross stream coordinate, the equilibrium channel flow speed in the x-direction is $U(y)$, and $\mathcal{K}$ is the inverse of the two-dimensional Laplacian for this geometry. We then set $\zeta = R + \rho = U'(y) + \omega(x, y, t)$, which here physically corresponds to divorcing the
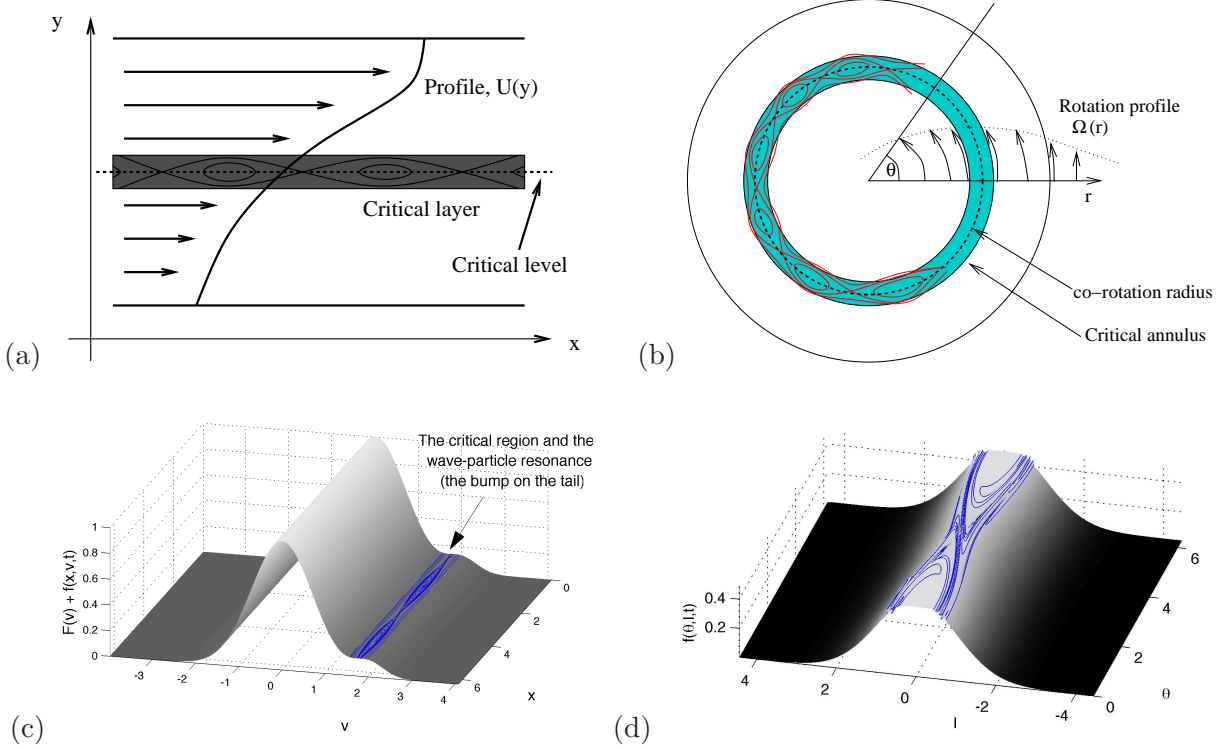
FIG. 2 Sketches of the four main physical problems discussed in this review: in (a), an equilibrium shear flow proceeds in the x-direction, and shears in the y-direction according the profile, $U(y)$. The unstable disturbances considered in this article take the form of weakly unstable modes that have a pronounced effect within a localized "critical layer" (shaded) which surrounds a line (dashed), the "critical level," along which a neutrally stable wave propagates at the same speed as the mean flow. Here, the vorticity distribution twists up into a cat's eye pattern (contours within the shaded critical layer). In (b), the circular variant of the problem is shown: a differentially rotating vortex with equilibrium rotation rate, $\Omega_0(r)$. The critical ring (dashed), or co-rotation radius, now locates the critical region (again shaded and containing an annular cat's eye pattern in the vorticity). The sketch for the plasma problem in (c) displays the total distribution function, $F(v) + f(x, v, t)$, as a surface over the (space,velocity) or (x, v)-plane. In this example, we plot the configuration for the classical bump-on-tail instability, which consists of primary peak at $v = 0$ together with a small bump at $v = v_0 = 2$. The unstable mode is again pronounced within a critical region located by the wave-particle resonance, as shown. Here, the distribution function is wound up by the mode, forming a localized "hole" (contours superposed on the surface). The final example in (d) shows the total distribution function $R(I) + f(\theta, I, t)$ for the XY model, as a surface over the $(\theta, I)-$plane. Now, the equilibrium distribution function, $R(I)$, consists of a single maximum at $I = 0$, which is also the location of the wave-particle resonance and the surrounding critical region. The contours superposed on the surface indicate the cat's eye pattern that develops in the total distribution function due to the appearance of the unstable mode.

background equilibrium flow from an evolving perturbation described by a relative vorticity field $\omega(x, y, t)$. Thus, (24) for this case is

$$\omega_t + U\omega_x - U''\psi_x + [\psi, \omega] = 0\,, \qquad (27)$$

where (22) is equivalent to

$$\omega = \psi_{xx} + \psi_{yy},\tag{28}$$

and $\psi(x, y, t)$, the streamfunction, is identified with Φ. Equations (27)–(28) are dimensionless, the channel width and maximum equilibrium flow speed acting as the relevant units. The flow is bounded by impermeable walls at $y = \pm 1$, and so $\psi(x, \pm 1, t) = 0$, and periodic in $0 \le x < L$, where the domain length is L.

Thus, to summarize, the shear-flow problem is recovered from the system of Sec. II.A by the following identifications:

$$\theta \leftrightarrow x, \ I \leftrightarrow y, \ \Omega(I) \leftrightarrow U(y), \ R(I) \leftrightarrow U'(y),$$
$$\rho \leftrightarrow \omega, \ \text{and (formally)} \ \ K \leftrightarrow \Delta^{-1}.$$

2. The Vlasov-Poisson plasma

In the Vlasov-Poisson system, the plasma is described by an electron distribution function (phase space density) depending on a spatial coordinate, x, and speed, v, with a stationary neutralizing ion background (see Fig. 2(c), which shows the set-up for the classical bump-on-tail instability; Krall and Trivelpiece (1973)). The relevant equilibrium distribution function is spatially homogeneous and determined by a profile, $F(v)$. Disturbances about this equilibrium are described by the perturbation distribution function, $f(x, v, t)$, and electrostatic potential, $\varphi(x, t)$, that satisfy the Vlasov equation,

$$f_t + v f_x + \varphi_x F_v + [\varphi, f] = 0,\tag{29}$$

and Poisson equation,

$$\varphi_{xx} = \int_{\mathbb{R}} \mathrm{d}v\, f(x, v, t) - N_B,\tag{30}$$

where N_B is the neutralizing background (i.e. $N_B = \langle f \rangle$). Here, the electron mass, charge, and an assumed thermal velocity scale are used to nondimensionalize the equations. Thus, lengths are measured in units of Debye length and time in units of the electron plasma frequency. We assume periodic boundary conditions in x, and we demand that f vanish as $v \to \pm\infty$.

Thus, the plasma problem is recovered from the system of Sec. II.A by the following identifications:

$$\theta \leftrightarrow x, \ I \leftrightarrow v, \ \Omega(I) \leftrightarrow v, \ R(I) \leftrightarrow F(v), \ \rho \leftrightarrow f,$$
$$\varphi \leftrightarrow -\Phi, \ \text{and (formally)} \ K \leftrightarrow -\partial_x^{-2} = |x - x'|.$$

3. XY model

Our XY model captures essential features of long-range spin-spin interaction and has been studied in a variety of contexts (Campa *et al.*, 2009; Chaikin and Lubensky, 1995). The phase space coordinates (θ, I) and basic dynamical variable $f(\theta, I, t)$ are equivalent to those for the Vlasov-Poisson system of Sec. II.C.2, and the model differs only by a change in the interaction:

$$f_t + I f_\theta - \Phi_\theta R_I - \Phi_\theta f_I = 0,\tag{31}$$

$$\Phi = -\frac{1}{\pi} \int_{\mathbb{R}} \mathrm{d}I \int_0^{2\pi} \mathrm{d}\hat{\theta}\, f(\hat{\theta}, I, t)\, \cos(\theta - \hat{\theta}).\tag{32}$$

Fig. 2(c) shows a sample configuration in which an instability develops around a singly peaked equilibrium profile, $R(I)$. Thus, the XY model is the system of Sec. II.A with the following identifications:

$$\theta \leftrightarrow \theta, \ I \leftrightarrow, \ \Omega(I) \leftrightarrow I, \ R(I) \leftrightarrow R(I),$$
$$\rho \leftrightarrow f, \ \text{and} \ \ K \leftrightarrow -\pi^{-1} \cos(\theta - \hat{\theta}).\tag{33}$$

4. Other models

There are many models with physical content that fit into the same general Hamiltonian framework described here. One example is the Jeans equation for stellar dynamics (obtained by changing the sign of the interaction in the Vlasov equation and removing the zero net charge condition; *e.g.* Cheng and Gamba (2012); Fujiwara (1981); Ivanov (2001); White (1986); and Yoshikawa *et al.* (2013)). Other examples include various quasi-geostrophic models for describing ocean and atmospheric dynamics (Pedlosky, 1987). In shear flow, the vorticity defect model of Gill (1965) (obtained by simplifying the relationship between the vorticity and the streamfunction; see also Balmforth *et al.* (1997, 2012); and Schamel (2012)) is also applicable. Interesting related examples where the underlying characteristics correspond to integrable n-body problems are the Cologero-Moser system (Illner, 2000; Moser, 1975) and a model introduced by Smereka (1998). Final examples include the Caldeira-Leggett model (Hagstrom and Morrison, 2011a) and the Vlasov-like equations derived by Russo and Smereka (1996) and Smereka (2002) for wave propagation through bubbly liquids.

III. LINEAR THEORY AND HISTORICAL PERSPECTIVE

The linear theory of fluid and plasma systems with continuous spectra has a long history. Here we present a general theory in Sec. III.A for the bifurcation to instability, followed by discussions of the early developments in fluid mechanics in Sec. III.B, plasma physics in Sec. III.C, and other systems in Sec. III.D.

A. General eigenspectra; bifurcation to instability through an embedded neutral mode

We begin by substituting $\rho = \hat{\rho}(I,t)e^{ik\theta}$ (with wavenumber k) into Eqs. (22) and (24) of the general formulation of Sec. II.A. After linearizing the latter in the standard fashion of linear stability theory, we arrive at

$$\hat{\rho}_t = -ik\Omega\hat{\rho} + ikR'\hat{\mathcal{K}}_k\hat{\rho}, \qquad \hat{\mathcal{K}}_k\hat{\rho} = \int_{\mathcal{D}} d\hat{I}\, \hat{K}_k(I,\hat{I})\hat{\rho}(\hat{I},t)\,, \tag{34}$$

and

$$\hat{K}_k(I,\hat{I}) = \int_0^{2\pi} d\theta\, K(\theta,I,\hat{I})e^{ik\theta}\,. \tag{35}$$

Special cases of $\hat{K}_k$ of interest are the following:

shear flow:

$$\hat{K}_k = [k\sinh 2k]^{-1} \times \begin{cases} \sinh[k(I+1)]\sinh[k(\hat{I}-1)], & \text{if } -1 \leq I \leq \hat{I} \\ \sinh[k(I-1)]\sinh[k(\hat{I}+1)], & \text{if } \quad \hat{I} \leq I \leq 1 \end{cases}$$

Vlasov plasma:

$$\hat{K}_k = -k^2\,,$$

XY - interaction:

$$\hat{K}_k = -\delta_{k,1} - \delta_{k,-1}\,,$$

with $\delta_{i,j}$ being the Kronecker delta symbol.

The first term on the right of (34) corresponds to free-streaming motion of fluid elements or particles along each level of I. In the Fourier representation, the free-streaming dynamics is analogous to a continuum of uncoupled oscillators with a range of frequencies $\Omega(I)$ indexed by I. The shearing action of the basic flow

corresponds to phase mixing due to the frequency spread. This can be seen particularly clearly for cases in which the second term on the right of (34) is absent, leading to

$$\rho = \hat{\rho}(I,t)e^{ik\theta} = \hat{\rho}(I,0)e^{ik[\theta - \Omega(I)t]}$$

$$\equiv \hat{\rho}(I,0)\int_{\mathcal{C}} dc\, e^{ik(\theta - ct)}\, \delta(\Omega(I) - c)\,, \tag{36}$$

where $\mathcal{C}$ denotes the range of values of $\Omega(I)$ that correspond to $\mathcal{D}$. This solution models the tilting over of the initial perturbation by differential advection; the lines of constant phase are given by $\theta - \Omega(I)t = const.$ The final piece of (36) further emphasizes how the solution cannot be written in a form that is separable in I and t unless one formulates it as an integral superposition of singular modes of the continuous spectrum with delta-functions for eigenfunctions (Dirac, 1927; Eliassen *et al.*, 1953; van Kampen, 1955). In other words, one can identify the free-streaming operator in the term, $\Omega(I)\rho_\theta$, as creating the continuous spectrum.

The second, interaction term in (34) acts as a perturbation of the free-streaming operator. However, with certain restrictions on the form of $\mathcal{K}_k(I,\hat{I})$, this perturbation of the operator does not change the existence of the continuous spectrum (for rigorous treatments see Degond, 1986; Hagstrom and Morrison, 2011b; Kato, 1966; Morrison, 2003), and only introduces the possibility of additional discrete eigenmodes. This was shown by explicit construction of the solution of the initial-value problem by Case (1960) and Rosencrans and Sattinger (1966).

To find the discrete normal modes introduced by the interaction term, we set $\hat{\rho}(I,t) = \tilde{\rho}(I)e^{-ikct}$, furnishing

$$\tilde{\rho} = \frac{R'\eta}{\Omega - c}, \qquad \eta = \hat{\mathcal{K}}_k\tilde{\rho} \tag{37}$$

and

$$\eta(I) = \int_{\mathcal{D}} d\hat{I}\, \hat{K}_k(I,\hat{I})\frac{R'(\hat{I})\eta(\hat{I})}{\Omega(\hat{I}) - c}\,. \tag{38}$$

If c is complex, this is a regular integral equation. But in the problems of interest, the integral on the right-hand side of (38) becomes singular when c is real, which is symptomatic of the continuous spectrum. Moreover, for $c = c_r + ic_i$ and $c_i \to 0^\pm$, the Plemelj formula (*e.g.* Gakhov (1990)) assists us in writing

$$\eta(I) = \fint_{\mathcal{D}} d\hat{I}\, \hat{K}_k(I,\hat{I})\, \frac{R'(I)\eta(\hat{I})}{\Omega(\hat{I}) - c_r}$$

$$\pm i\pi \sum_j \hat{K}_k(I,I_j)\frac{\eta(I_j)R'(I_j)}{|\Omega'(I_j)|}\,, \tag{39}$$

where $\fint$ means the singularity of the integral is evaluated by taking the Cauchy principal value, and the I_j's denote all values of I for which $\Omega(I) = c_r$. We may satisfy the real and imaginary parts of (39) if we choose $R'(I_j) = 0$ for all the I_j's, and take $\eta(I)$ to be real. This choice is straightforward if $\Omega(I)$ is a monotonic function, as we assume later when we derive the single-wave model. Then, $I_j \to I_*$ and $R'(I_*) = \Omega(I_*) - c_r = 0$. Non-monotonic equilibrium with certain symmetries can also satisfy this condition (such as the jet portrayed below, in Fig. 6, which is symmetrical about the midline). In either circumstance, the special mode that is embedded within the continuum and which is also the limit of the complex eigenmodes as $c_i \to 0^\pm$ is the smooth solution of (39). The distinguished modes are therefore associated with the extrema of the equilibrium profile, $R(I)$ (inflection points of the velocity profile, $\Omega = U(y)$, in the fluid problem).

Note that, if the kernel is independent of the action coordinates, what we call a *spatial kernel*, then $\mathcal{K} \to \mathcal{K}(\theta)$ and the $\mathcal{K}_k$'s and therefore the eigenfunctions η are constants. Hence, (38) reduces to an explicit dispersion relation,

$$D(c,k) = 1 - \mathcal{K}_k \int_{\mathcal{D}} dI\, \frac{R'(I)}{\Omega(I) - c} = 0\,. \tag{40}$$

For the plasma problem, $D(c,k)$ is the plasma dispersion function, and its relatively simple form allows one to extract a number of general criteria for determining the transition to instability, results such as those of

Penrose (1960) (see Sec. III.C). Similar results have recently been outlined for the XY model (Hamiltonian mean field model) by Chavanis and Delfini (2009) as well as vorticity defects by Balmforth *et al.* (1997), although they amount to a minor generalization of those provided by Penrose, which are standard in plasma physics (Krall and Trivelpiece, 1973).

B. Rayleigh's problem

In the late 1800s, Rayleigh explored a variety of fluid stability problems motivated by experiments with smoke jets and flames. As vividly illustrated by cigarettes and chimneys, smoke jets often rise initially uniformly, but then begin tortuous undulations and meanders. Rayleigh's theoretical explanation for the breakdown of the unidirectional shear flow in the jet amounted to a linear stability analysis of (27) and (28). For exponentially growing, wave-like, normal-mode solutions with $\psi \propto e^{ik(x-ct)}$, the system reduces to the so-called "Rayleigh equation,"

$$\psi_{yy} - k^2\psi = \frac{U''\psi}{U - c}\,. \tag{41}$$

This equation follows from (38) on recalling that the kernel is Green's function for the fluid problem, and then recasting this equation in its differential form.

Rayleigh found explicit examples of unstable modes for inviscid shear flows in which $U(y)$ took the form of a sequence of broken lines (corresponding to a stacked set of layers with constant mean vorticity). For such profiles, $U''(y) = 0$ everywhere except at the line breakages, which allows for an explicit closed form solution of (41). His results for these broken-line profiles motivated Rayleigh to continue further to look for a more useful stability criterion for general flow profiles, and he formulated what is now called the "inflection-point theorem": we multiply (27) by ψ^* and integrate across the channel. After a little algebra, involving integration by parts and separation of real and imaginary parts, we arrive at

$$c_i \int_{-1}^{1} dy\, \frac{U''(y)|\psi|^2}{|U - c|^2} = 0. \tag{42}$$

Thus either $c_i = 0$ (and there is no exponentially growing mode), or the integral must vanish, which demands that U'' change sign somewhere within the channel. In other words, a sufficient condition for *stability* is that $U(y)$ have an inflection point. Further results that extended Rayleigh's theorem were presented later by Balmforth and Morrison (1999); Fjørtoft (1950); Howard (1964); and Rosenbluth and Simon (1964). These criteria can be argued to be equivalent to energy stability criteria (Balmforth and Morrison, 2001), akin to Dirichlet's theorem of classical mechanics (see, e.g, Morrison, 1998).

Rayleigh's equation (41) has singular points for real wavespeeds where $U(y) = c_r$. These singularities typically prohibit the construction of neutral waves (e.g. Balmforth and Morrison, 1999), and occur at the so-called "critical levels" for which neutral waves propagate at the same speed as the background flow. These locations play a special role in the single-wave theory described later, and are examples of the resonances mentioned in Sec. I. Note that the critical-level singularities appear only in the normal-mode problem: as is clear from our discussion in Sec. III.A, the linear initial-value problem itself is completely regular, and it is only by forcing solutions into the normal-mode form that one produces the singularity.

The singularities in Rayleigh's equation, and their prohibition of neutral waves led Kelvin to object quite strongly to Rayleigh's theory: "This disturbing singularity vitiates the seeming proof of stability contained in Lord Rayleigh's equations." [1] Kelvin's view was that Rayleigh's singularities reflected a breakdown of linear inviscid theory. At the critical levels, "the motion has a startlingly peculiar character", nonlinearity could not be ignored, and any slight disturbance created "a cat's-eye pattern of elliptic whirls". In fact, Kelvin was convinced that viscous shear flows were linearly stable, as illustrated by his analysis of Couette flow ($U(y) = y$). Kelvin was also probably prejudiced by Reynolds' experiments in pipes, which had been undertaken at roughly the same time, and suggested that there was a finite threshold in the amplitude of perturbations required to generate turbulent motion. Kelvin argued further that inviscid flows were strongly

---

[1] Kelvin and Rayleigh's quotes, as detailed in this section, can be found in the collected works of the two authors (Kelvin, 2001; Rayleigh, 1899).

unstable in the sense that the slightest perturbation would generate cat's eye patterns along any critical levels ("let one or both bounding-surfaces be infinitesimally dimpled in any place and left free to become plane again... Hence the interior disturbance essentially involves elliptic whirls. Thus we see that the given steady laminar motion is *thoroughly* unstable, being ready to break up into eddies in every place, on the occasion of the slightest shock or bump on either plastic plane boundary"). Kelvin evidently felt that there were some fundamental problems with the inviscid formulation.

Despite Kelvin's criticisms, Rayleigh remained convinced that inviscid fluid theory was a useful guide, and that shear flows could be unstable, perhaps guided by his experiments with flames and smoke jets. Rayleigh contended Kelvin's objections by pointing out that the inviscid linear analysis was perfectly valid for exponentially growing modes – in this case c is complex and there are no critical level singularities. However, he did admit that his proof of stability for flows without inflection points only concerned exponentially growing instabilities and did not exclude algebraically growing instability ("Perhaps I went too far in asserting that the motion was thoroughly stable; but it is to be observed that if c be complex, there is no disturbing singularity. The argument, therefore, does not fail, regarded as one for excluding complex values."). In fact, it was not until the 1960s that algebraic instability was to a large degree ruled out for shear flow when researchers followed Landau's Laplace transform treatment of the plasma problem (cf. Sec. III.C) and solved the linear problem as an initial-value problem (Case, 1960; Dikki, 1960; Engevik, 1966; Rosencrans and Sattinger, 1966).

Rayleigh also criticized Kelvin's assumption that viscous flows were stable: "Lord Kelvin arrives at the conclusion that the flow ... is fully stable for infinitesimal disturbances.... Naturally it is with diffidence that I hesitate to follow so great an authority, but I must confess that the argument does not appear to me demonstrative." Nevertheless, some of the inviscid profiles that Rayleigh aimed to establish were unstable to explain unsteady motions in experiments were actually shown to be stable by the inflection-point theorem. Rayleigh's impression was that the theoretical problem lay in taking the inviscid limit ("it is possible that the investigation in which viscosity is altogether ignored is inapplicable to the limiting case of a viscous fluid when the viscosity is supposed infinitely small"). Indeed, as it is now known, the viscous version of the linear stability theory yields the celebrated Orr–Sommerfeld equation, rather than (41), which can have unstable modal solutions even for flow profiles that are stable in inviscid theory (Drazin and Reid, 1981; Landahl, 1986).

C. Plasma oscillations and Landau damping

In the middle of the 20th century the analog of the disturbing singularity discussed by Rayleigh and Kelvin's arose in plasma physics in the context of linear analysis of the Vlasov equation; the singularity now appears at the wave-particle resonance where the particle velocity matches the speed of a neutral plasma wave (oscillation). To observe this directly, let $f = \hat{f}(v)e^{ik(x-ct)} + \text{c.c.}$, and then linearize equations (29) and (30) to obtain

$$f = -\frac{\varphi F'}{v - c}, \qquad \varphi = -\frac{1}{k^2}\int_{\mathbb{R}} dv\, f\,, \tag{43}$$

which clearly presents the singularity at the wave-particle resonance, $v = c$ for $c = c_r$ real. Unlike for Rayleigh's equation the Vlasov problem has a spatial kernel and, thus, we can proceed much further analytically and derive a dispersion relation for the wavespeed c: eliminating $\hat{f}(v)$ yields

$$D(c,k) = 1 - \frac{1}{k^2}\int_{\mathbb{R}} dv\, \frac{F'(v)}{v - c} = 0 \tag{44}$$

(cf. Eq. (40)). Complex conjugate solutions for c can be straightforwardly found from this dispersion relation for certain equilibrium distribution functions, $F(v)$; again, the mode with $c_i > 0$ is unstable. Even without specific choices of $F(v)$, Nyquist methods can be brought to bear on the dispersion relation (44) to construct explicit stability criteria (Penrose, 1960).

The singularity of plasma oscillations is seen in a different way in (44): this dispersion relation contains a singular integral with a branch cut along the real axis of the complex c plane, which again identifies the continuous spectrum (for rigorous spectral theory see Degond, 1986, and Hagstrom and Morrison, 2011b).
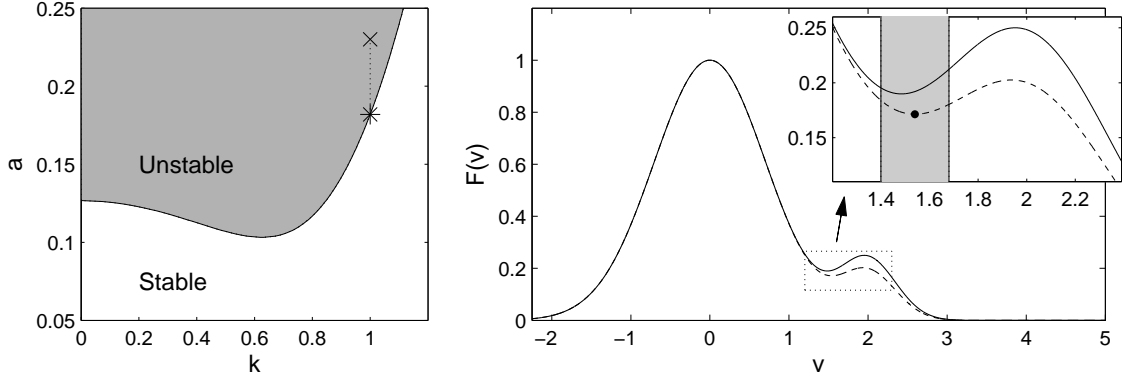
FIG. 3 (a) Stability boundary on the (k, a) plane for parameters values of (46), $\alpha = 4$ and $v_0 = 2$. The star and cross mark the values of a for which the profile is plotted in (b). The star denotes the marginally stable profile for $k = 1$ ($a \approx 0.182$); the cross marks an unstable profile with a slightly larger bump ($a = 0.23$). The inset in (b) shows a magnification of the bump-on-tail region, with the shaded area illustrating the critical region surrounding the minimum of the marginally stable profile over which the distribution function is wound up by the unstable mode. This region is narrower than the velocity spread of the bump.

On using the Plemelj relation (Gakhov, 1990) with $c \to c_* + i0^{\pm}$, we find that

$$F'(c_*) = 0 \qquad \text{and} \qquad 1 - \frac{1}{k^2} \fint_{\mathbb{R}} dv \, \frac{F'(v)}{v - c_*} = 0 \,. \tag{45}$$

In other words, as the equilibrium profile $F(v)$ is adjusted so that the complex conjugate pairs move towards the real axis of the complex c-plane, they limit to a special neutral mode with $c = c_*$. By virtue of the first condition in (45), the special neutral mode is a smooth solution (the singularity of $1/(v - c_*)$ is cancelled by the zero of $F'(v)$ in the numerator of the eigenfunction), even though it is embedded in the continuous spectrum. The embedded mode can be interpreted to lie at a location within the continuous spectrum where the modal "signature" changes sign, consistent with a generalization of Kreĭn's theorem (Hagstrom and Morrison, 2011b; Morrison, 2000) of finite-dimensional Hamiltonian dynamics (Kreĭn, 1950).

For a family of equilibria indexed by a control parameter a, the embedded mode determines the stability boundary on the (k, a)−plane because it is the limit of an unstable complex eigensolution. By way of an example, consider the family of equilibria given by

$$F(v) = e^{-v^2} + a \, e^{\alpha(v - v_0)^2} \,, \tag{46}$$

where α and v_0 are additional parameters. This parameterized family consists of a primary Maxwellian with a superposed "bump-on-tail". Via Penrose's criterion one can establish that there are no distinguished neutral modes associated with the main peak of the distribution near $v = 0$; instability can only arise when the bump on the tail generates further extrema. If the bump amplitude, a, is the main control parameter, the stability boundary is denoted by the curves $a = a(k)$, as illustrated in Fig. 3. The minimum of this boundary ($a \approx 0.103$ for $k \approx 0.62$, $\alpha = 4$ and $v_0 = 2$) occurs when an inflection point first appears in $F(v)$ in the vicinity of the bump, and thereafter splits into two extrema with a further increase of a. However, if the domain is periodic in x, as considered here, there is a minimum value of k determined by the longest spatial wavelength, and so the transition to instability can take place elsewhere on the stability boundary, as illustrated in Fig. 3.

For stable equilibria below the stability boundary, the preceding arguments rule out all regular eigenmodes, and in particular neutral plasma oscillations. This physically unsatisfying conclusion led Landau (1946) to attack the linear initial-value problem using Laplace transforms in order to uncover unambiguously how waves evolved once introduced into the plasma. A direct consequence of Landau's solution was the prediction of the phenomenon that is now called *Landau damping*: the exponential decay of the electric field (or potential $\varphi(x, t)$) that arises due to the phase mixing of particles.

The exponentially decaying contribution to the electic field is often refered to as a *quasi-mode* (or *Landau pole*), as it is not a true normal mode of the linear eigenproblem. To uncover these objects, and the general long-time behavior of the solution, one inverts the Laplace transform solution, which takes the form of a complex integral over the usual Bromwich contour (*e.g.* Krall and Trivelpiece, 1973). The Landau poles can be picked up as the leading-order long-time contributions by deforming the integration contour through the branch cut of the continuous spectrum. One thereby emerges on a different Riemann sheet of the non-analytical dispersion function $D(c, k)$ (which appears in the denominator of the Laplace transform solution), allowing one to encircle and pick up residue contributions from singularities due to zeros of the dispersion relation on a non-physical Riemann sheet. These "fake eigenvalues" are the quasi-modes.

Despite Landau's reputation as one of the eminent theoretical physicists of his day, the relatively mathematical nature of Landau's predictions was not convincing to many plasma physicists. Several questions arose. For example, Landau damping required that the energy contained in the electric field must be removed, which appeared to some to violate energy conservation (but see Morrison, 1994, 2000; Morrison and Pfirsch, 1992 where it is shown explicitly how energy is conserved and energy is transferred). Others argued that the damping effect was a mathematical artifact arising from inconsistencies in the formulation (Allis, 1959; Allis *et al.*, 1963; Ecker and Hoelling, 1963; Weitzner, 1963). On the other hand, in three celebrated papers Bohm and Gross (1949a,b, 1950) argued for the existence of Landau damping outside of Vlasov theory. The issue was not settled until experimental verification of Landau damping was reported by Malmberg and Wharton (1964) (see also Franklin and Braithwaite, 2009; Malmberg *et al.*, 1966), nearly twenty years after Landau's original paper. These authors demonstrated experimentally that the damping vanished when the resonant particles were removed. They did this by removing the tail of the distribution for electrons streaming in one direction but not the other, and observed Landau damping only for the waves propagating in the direction with resonant particles.

From the mathematical perspective the story of Landau damping has continued. Steps toward an early rigorous justification of Landau damping by Backus (1960), who considered the linear limit, were recently extended to the nonlinear regime by Mouhot and Villani (2011). Their proof requires a condition on the initial amplitude in order for the damping to behave essentially like the linear theory. However, as we will see later, the linear results fail for finite amplitude disturbances (see Fig. 10 of Sec. VII.B). The nonlinear arrest of linear Landau damping remains an open problem from a formal mathematical perspective.

D. Violent relaxation, XY model, and phase transitions

Closely connected to Vlasov-Poisson dynamics is the relaxation of stellar systems, which can be described by the Jeans equation (Binney and Tremaine, 2008), which is identical to the Vlasov-Poisson system but for an attracting interaction (the sign of $\mathcal{K}$ is switched) and the removal of the charge neutrality condition. In a famous paper Lynden-Bell (1967) prompted a discussion of this problem by arguing that such relaxation proceeded in two phases: in the first, the ensemble of stars behaves like a continuum, relaxing rapidly from an arbitrary initial condition towards some quasi-steady state (the "violent relaxation"). That state consisted of a structure, or pattern, in phase space characterized by increasingly wound-up filaments. Eventually, the ever decreasing scales precipitate the failure of the continuum approximation, and herald the onset of a second phase in which the discreteness of the system plays an essential role.

More recently, Lynden Bell's violent relaxation was revisited in the context of n-body Hamiltonian dynamics (e.g. Campa *et al.*, 2009) with the XY interaction. Like gravity, this interaction is attractive, and the stellar and XY models has many common features. In addition to the consideration of far-from-equilibrium initial conditions, recent explorations with the XY model also studied equilibrium distributions with low-amplitude perturbations. In particular, stability theories were presented to identify equilibria with linear instabilities (Antoni and Ruffo, 1995; Campa *et al.*, 2009; Inagaki and Konishi, 1993; Yamaguchi *et al.*, 2004), and numerical simulations explored the resulting phase-space patterns. Specific attention was focussed on the nature of the phase transition occuring when the linear instability appeared, and whether statistical techniques could be exploited to predict integral measures of the emerging patterns (such as the magnetization; see Antoniazzi *et al.* (2007); de Buyl *et al.* (2009); Campa *et al.* (2009); and Yamaguchi *et al.* (2004)). Unsurprisingly, the phenomenon of Landau damping was also rediscovered (Campa *et al.*, 2009).

The search for instabilities in the XY model closely follows the Vlasov-Poisson problem: after introducing the normal-mode form, $f(\theta, I, t) = \hat{f}(I)e^{i(\theta - ct)} + $ c.c., into (31) and (32) and linearizing, we arrive at the

explicit dispersion relation,

$$D(c) = 1 + \int_{\mathbb{R}} dI \, \frac{R'(I)}{I - c} = 0 \,, \tag{47}$$

which is the current version of (40) since this problem has a spatial kernel. All Fourier modes with $k \neq \pm 1$ are stable.

Two simple examples for the equilibrium distribution, $R(I)$, that allow further analytical progress are provided by the "top-hat" profile,

$$R(I) = \frac{a}{2} \left[\Theta(I + 1) - \Theta(I - 1) \right], \tag{48}$$

where $\Theta(x)$ represents a Heaviside step function, and the Gaussian,

$$R(I) = \frac{a}{\sqrt{2\pi}} e^{\frac{-I^2}{2}} \tag{49}$$

(cf. Campa *et al.*, 2009; Yamaguchi *et al.*, 2004). For the top-hat profile, R' consists of a pair of delta-functions and so the integral in (47) is performed immediately to furnish

$$D(c) = 1 - \frac{a}{1 - c^2} = 0 \qquad \text{or} \qquad c = \pm \sqrt{\frac{1 - a}{a}}. \tag{50}$$

Thus, when $a > 1$, there is an unstable mode. This example is analogous to the "waterbag" model of the plasma problem (see e.g. Berk and Roberts, 1967). Moreover, both are equivalent to Rayleigh's broken-line profiles. For the Gaussian, the dispersion relation (47) is closely analogous to the plasma dispersion relation with a Maxwellian equilibrium distribution function (Fried and Conte, 1961). The neutral stability condition can be computed on observing that marginally stability occurs for $c = 0$, in which case $a = a_c = 1$. Moreover, once again, for $a > 1$, there is an unstable mode.

Note that the instability of both distributions in (48) and (49) for $a > 1$ is quite different from Vlasov-Poisson theory, for which both equilibrium profiles would be stable. The key difference between the dispersion functions in (44) and (47) is the reversal of the sign of the integral, which arises because the XY interaction is attractive. The sign difference permits the distributions to become unstable in the XY model, a situation that is forbidden in Vlasov-Poisson theory because of the positivity of the distribution function. Likewise, the gravitational attraction of the stellar dynamics problem also reverses the sign of the integral in (44); the instability of a singly peaked distribution that results is a form of the classical Jeans instability, as explored by, for example, Cheng and Gamba (2012); Fujiwara (1981); Ivanov (2001); White (1986); and Yoshikawa *et al.* (2013).

IV. NONLINEAR DYNAMICS: SCALING, SATURATION AND CRITICAL LAYERS

Before proceeding to our derivation of the single-wave in Sec. V, we here motivate the necessity and features of the derivation. In particular, we show why conventional weakly nonlinear analysis fails, and review both the plasma physics and fluid mechanics literature.

A. Conventional weakly nonlinear analysis

The power of bifurcation theory lies in its ability to construct nonlinear states analytically. Conventionally, the center manifold reduction (e.g. Crawford, 1991) is often the method of choice for dissipative systems, whereas Birkhoff normal form theory is applied to Hamiltonian systems (e.g., Bryuno, 1988; van der Meer, 1985).

1. Generalities

Conventional weakly nonlinear theories aim for an amplitude equation that captures the dynamics of the normal mode that bifurcates to instability at a critical threshold in a control parameter. The derivation of the equation can be cast in the form of a regular perturbation expansion, in which one opens with a neutrally stable normal mode balanced on the stability boundary, and then kicks that mode into an unstable action by suitably adjusting the control. The relevant amplitude equation is dictated by the symmetries of the system in question; for the problems of interest here, the equation is a certain Hamiltonian normal form. This bifurcation is characterized by asymptotic scalings for the mode amplitude, the perturbation to the control parameter, and a redefinition of time.

More specifically, and in the general scheme of the full model given at the end of Sec. II.A, the idea is that the equilibrium profile, $R(I)$, is one of a family parameterized by a constant parameter, a. After a suitable choice of domain size and scaling, we focus on the situation in which the normal mode with a wavenumber $k = 1$ is unstable if $a > a_0$, and all the other normal modes are stable. By switching the angular frame of reference we can zero the frequency of that mode (i.e. by transforming coordinates to a frame rotating at the mode's frequency). We then set $a = a_0 + \varepsilon^2 a_2$, where $\varepsilon \ll 1$ is the small parameter that we use to organize the perturbation expansion. The modification to a embodied in $\varepsilon^2 a_2$ creates a change in the equilibrium profile that destabilizes the otherwise neutral mode. Correspondingly, the relatively slow growth of the mode is captured by scaling time. Thus, we set

$$T = \varepsilon t, \quad \frac{\partial}{\partial t} \to \varepsilon \frac{\partial}{\partial T}, \quad \rho(\theta, I, t) \to \rho(\theta, I, T) \quad \text{etc.} \tag{51}$$

The remaining asymptotic scalings are encoded in the following sequences:

$$R(I) = R_0(I) + \varepsilon^2 R_2(I) + \dots, \tag{52}$$

$$\rho = \varepsilon \rho_1(\theta, I, T) + \varepsilon^2 \rho_2(\theta, I, T) + \dots, \tag{53}$$

$$\Phi = \mathcal{K}\rho = \varepsilon \psi_1(\theta, I, T) + \varepsilon^2 \psi_2(\theta, I, T) + \dots, \tag{54}$$

where $\psi_m = \mathcal{K}\rho_m$ for $m = 1, 2, \dots$. The expansion of ρ opens at order ε, even though the equilibrium is modified only at $O(\varepsilon^2)$, which corresponds to the "Hopf scaling" in the terminology of Crawford (see, e.g., Crawford, 1995).

If one substitutes the sequences above into the system (22) and (24), and gathers terms of equal order in ε, one arrives at a hierarchy of equations to solve sequentially for (ρ_m, ψ_m), in the manner of a standard asymptotic expansion (*e.g.* Crawford (1991); Cross and Hohenberg (1993); and Manneville (1995)). The leading-order equations determining (ρ_1, ψ_1) turn out to be the relations satisfied by the distinguished neutral mode. That solution has an undetermined amplitude, $A(T)$. To fix this quantity, we proceed to the next orders. At $O(\varepsilon^2)$ the pair (ρ_2, ψ_2) capture the nonlinear generation of the first harmonic of the neutral mode (with wavenumber $k = 2$) and a correction to the angular average (with wavenumber $k = 0$), but $A(T)$ yet remains unknown. Finally, at $O(\varepsilon^3)$, the requirement that the pair (ρ_3, ψ_3) be bounded and periodic in θ demands that $A(T)$ satisfy a solvability condition, which amounts to the desired amplitude equation. The construction is quite standard, although for the current problems it contains a key flaw. We bring out the nature of this flaw and illustrate the expansion in a slightly simpler setting in Sec. IV.A.2.

2. Weakly nonlinear expansion for spatial kernels

By way of illustration, we perform a weakly nonlinear analysis of the special case of our general model for spatial kernels for which the kernel is independent of the actions, I and $\hat{I}$. As remarked earlier, explicit dispersion relations are available for such kernels (see §II.A and (40)), and both the Vlasov and XY models furnish examples.

For further brevity, we consider the specific situation in which the domain is symmetrical in I, the equilibrium profile $R(I)$ is an even function, and $\Omega(I) := h'(I)$ is an odd function. One can then explore the situation in which an instability arises due to the appearance of a (zero-frequency) normal mode with the form of a standing wave, eliminating any need to transform into the rotating frame of the mode. After the rescaling of time, $T = \varepsilon t$, the governing equations become

$$\varepsilon \rho_T + \Omega \rho_\theta - \Phi_\theta R_I - \Phi_\theta \rho_I = 0 \tag{55}$$

$$\Phi = \int_0^{2\pi} d\hat{\theta} \int_{\mathcal{D}} d\hat{I}\, K(\theta - \hat{\theta})\rho(\hat{\theta}, \hat{I}, T)\,, \tag{56}$$

where recall $\mathcal{D}$ denotes the range of I. It is also convenient to take the angular average,

$$\bar{f} := \frac{1}{2\pi} \int_0^{2\pi} d\theta\, f\,, \tag{57}$$

of the first of these equations:

$$\varepsilon \bar{\rho}_T = (\overline{\Phi \rho_\theta})_I\,. \tag{58}$$

Next, we pose the asymptotic sequences,

$$\begin{aligned} R &= R_0 + \varepsilon^2 R_2\,, \\ \rho &= \varepsilon \rho_1 + \varepsilon^2 \rho_2 + \cdots\,, \\ \Phi &= \varepsilon \Phi_1 + \varepsilon^2 \Phi_2 + \cdots\,, \end{aligned} \tag{59}$$

(cf. (52)–(54)). Introducing these into (55) leads, at order ε to

$$\rho_1 = \frac{R_{0I}\Phi_1}{\Omega}\,, \qquad \Phi_1 = A(T)\mathrm{e}^{i\theta} + c.c.\,, \tag{60}$$

after adopting the marginally unstable mode (with wavenumber $k = 1$) as the leading-order solution. The relation in (56) then gives the marginal stability condition,

$$1 - \hat{K}_1 \int_{\mathcal{D}} dI\, \frac{R_{0I}}{\Omega} = 0 \tag{61}$$

(cf. the dispersion relation (40) with $c = 0$).

At order ε^2, we find

$$\Omega \rho_{2\theta} = R_{0I}\Phi_{2\theta} - \rho_{1T} - \Phi_{1\theta}\rho_{1I}\,. \tag{62}$$

Hence, on introducing (60),

$$\begin{aligned} \rho_2 = \overline{\rho_2} &+ \frac{R_{0I}}{\Omega}\Phi_2 + \frac{R_{0I}}{\Omega^2}\left(iA_T\mathrm{e}^{i\theta} + c.c.\right) \\ &- \frac{1}{2\Omega}\left(\frac{R_{0I}}{\Omega}\right)_I \left(A^2\mathrm{e}^{2i\theta} + c.c.\right). \end{aligned} \tag{63}$$

Substitution of (63) into (56) yields

$$\Phi_2 = \frac{\hat{K}_1 \hat{K}_2 \mathcal{I}}{2(\hat{K}_1 - \hat{K}_2)}\left(A^2\mathrm{e}^{2i\theta} + c.c.\right), \tag{64}$$

where

$$\mathcal{I} = \int_{\mathcal{D}} dI\, \frac{1}{\Omega}\left(\frac{R_{0I}}{\Omega}\right)_I. \tag{65}$$

Here we have used $\hat{K}_0 = 0$ and that the symmetry of $R_0(I)$ and $\Omega(I)$ implies $\int_{\mathcal{D}} dI\, R'_0/\Omega^2 = 0$. In principle, we should also add a second term to this solution with the form, $A_2(T)\mathrm{e}^{i\theta} + c.c$, which denotes a correction to the $k = 1$ neutral mode, but is not needed to determine the amplitude equation for A.

At $O(\varepsilon^2)$ we also arrive at the first non-trivial result from (58):

$$\overline{\rho_2}_T = (\overline{\Phi_{1\theta}\rho_2 + \Phi_{2\theta}\rho_1})_I = \left(\frac{R_{0I}}{\Omega^2}\right)_I (|A|^2)_T\,. \tag{66}$$

To integrate this relation, we must specify an initial condition. If $A(0) = A_0$ and $\overline{f_2}(I, 0) = 0$, corresponding to initializing the system with the equilibrium plus a low-amplitude normal mode, then

$$\overline{\rho_2} = \left(\frac{R_{0I}}{\Omega^2}\right)_I (|A|^2 - |A_0|^2), \tag{67}$$

Finally, we arrive at the $O(\varepsilon^3)$ equation,

$$\rho_{3\theta} = \frac{1}{\Omega}(R_{0I}\Phi_{3\theta} + R_{2I}\Phi_{1\theta} - \rho_{2T} + \Phi_{2\theta}\rho_{1I} + \Phi_{1\theta}\rho_{2I}). \tag{68}$$

Isolating the contribution of the right-hand side to the first Fourier mode, $e^{i\theta}$, and then applying the second relation in (55) leads to the amplitude equation,

$$A_{TT} \int_{\mathcal{D}} dI \frac{R_{0I}}{\Omega^3} = JA + \Gamma|A|^2 A, \tag{69}$$

with

$$J = \int_{\mathcal{D}} dI \frac{R_{2I}}{\Omega} + |A_0|^2 \int_{\mathcal{D}} dI \frac{1}{\Omega}\left(\frac{R_{0I}}{\Omega^2}\right)_{II} \tag{70}$$

and

$$\Gamma = \frac{\hat{K}_1\hat{K}_2\mathcal{I}^2}{2(\hat{K}_1 - \hat{K}_2)} + \int_{\mathcal{D}} dI \frac{1}{\Omega}\left[\left(\frac{R_{0I}}{\Omega^2}\right)_I - \frac{1}{2\Omega}\left(\frac{R_{0I}}{\Omega}\right)_I\right]_I. \tag{71}$$

Note that the integrals that appear in the coefficients of the amplitude equation do not exist unless a number of the derivatives of $R_0(I)$ and $R_2(I)$ vanish at $I = 0$; this is reflective of critical-level singularities in the weakly nonlinear expansion. In fact, as shown by Crawford and Jayaraman (1999), the singularities appear at all orders of the expansion, becoming progressively more severe as one descends through the asymptotic hierarchy. The only instance in which one can justify the asymptotics is if all derivatives of R_0 and R_2 vanish at the wave-particle resonance $I = 0$, which places severe limitations on the equilibrium profile. Notable examples of such situations, however, include Rayleigh's broken-line shear-flow equilibria, the waterbag models of plasma physics, and the top-hat profile of the XY model.

3. Top-hat profile of the XY model

For the XY model with the top-hat equilibrium profile, $\Omega := I$, $\mathcal{D} := \mathbb{R}$, $\hat{K}_1 = -1$, $\hat{K}_2 = 0$ and

$$R_{jI} = \frac{a_j}{2}[\delta(I + 1) - \delta(I - 1)], \tag{72}$$

with $j = 0$ and 2. If we also assume that $|A_0| \ll 1$, the integrals can be evaluated to furnish

$$A_{TT} = a_2 A + \tfrac{1}{2}|A|^2 A. \tag{73}$$

Note that the sign of the second term ensures that nonlinearity is destabilizing in this example. That is, the bifurcation is *subcritical*, and an unstable steady solution branch given by $|A| = \sqrt{-2a_2}$ exists for $a < a_0 = 1$ (where the unpatterned equilibrium state is stable). A similar type of bifurcation arises for broken-line shear-flow profiles in the vorticity defect model of (Balmforth *et al.*, 2012) (where $\hat{K}_k := (2k)^{-1}$).

B. Trapping scaling versus Hopf scaling in the Vlasov problem

In the 1960s and 70s, several attempts were made to continue the analysis of linear electrostatic instability into the nonlinear regime. Some of the key results were obtained by Frieman *et al.* (1963); O'Neil *et al.* (1971); Onishchenko *et al.* (1971); and Simon and Rosenbluth (1976). One of the striking features of these

articles is a disagreement regarding the level of saturation of the instability: the standard way to estimate the saturation level is in terms of the amplitude of the electric field disturbance, A_{sat}, relative to the distance to the stability boundary, as measured by a suitable control parameter, ϵ (such as $\epsilon = a - a_c$, where a_c denotes a point on the stability boundary, for the example of Sec. III.C). Two characteristic scalings were hypothesized: "trapping scaling" (O'Neil $et\ al.$, 1971; Onishchenko $et\ al.$, 1971), for which $A_{\mathrm{sat}} \sim \epsilon^2$, and Hopf scaling (Frieman $et\ al.$, 1963; Simon and Rosenbluth, 1976) with $A_{\mathrm{sat}} \sim \epsilon^{1/2}$, which is the usual saturation level for strongly dissipative instabilities and equivalent to that used above in Sec. IV.A.

Trapping scaling was the essential ingredient in the "single-wave model" of Drummond $et\ al.$ (1970); O'Neil $et\ al.$ (1971); and Onishchenko $et\ al.$ (1971), which was a phenomenologically based theory written down partly using physical arguments. Frieman $et\ al.$ (1963) and Simon and Rosenbluth (1976), on the other hand, championed the Hopf scaling, and attempted amplitude expansions of the kind summarized above. Unfortunately, such expansions are plagued by critical-level singularities which unavoidably haunt the higher-order equations of the expansion, as noted in Sec. IV.A. To avoid this difficulty Frieman $et\ al.$ (1963) and Simon and Rosenbluth (1976) removed the singularities by displacing the poles from the real axis in a regularization procedure that was meant to be equivalent to Landau's solution of the initial-value computation. But the procedure has questionable mathematical validity (strictly speaking, the asymptotics introduces multiple timescales to account for a relatively fast adjustment of the system to the slower growth of the unstable mode; using Landau damping ideas to remove the singularities in the expansion obscures the separation of timescales).

Because neither approach was completely convincing, the effort to distinguish between them fell to numerical simulation and laboratory experiments, which suggested that trapping scaling dictates the saturation level (e.g. Denavit, 1981; Ivanov $et\ al.$, 2005; Tsunoda $et\ al.$, 1987; Valentini $et\ al.$, 2008). Following along parallel lines, (Ivanov, 2001) presents a rediscovery of the trapping scaling in numerical simulations of the Jeans instability. Figs. 4 and 5 display numerical computations of the bump-on-tail instability in the Vlasov problem (for further details of these computations, see Balmforth (2012)); Figure 4 gives an illustration of the nonlinear dynamics occuring during the saturation of an unstable mode. Figure 5 collects together results from a suite of computations that measure the scaling of the saturation level, and confirms trapping scaling.

Relatively recently, two articles have more convincingly demonstrated that the correct scaling is trapping (Crawford, 1995; del-Castillo-Negrete, 1998a,b). Crawford's approach follows the center-manifold route and attempts to derive an amplitude equation for the unstable mode. The approach begins with the Hopf scaling and runs into the technical complications associated with integrals that diverge at the wave-particle resonance as one approaches the point of neutral stability. Rather than treating the singularities with some $ad\ hoc$ rule, Crawford rescaled the mode amplitude with sufficient powers of ϵ in order to counter the divergent integrals. This procedure rescales the mode amplitude back to the trapping scaling and avoids singularity, which formally establishes that trapping is the correct scaling. Unfortunately, Crawford's amplitude equation contains an infinite number of terms of comparable size and cannot be used to explore how the instability saturates.

Del Castillo-Negrete opts for a different approach by transferring results from critical-layer theory of fluid mechanics (Churilov and Shukhman, 1987a, 1996; Goldstein and Hultgren, 1988; Goldstein and Leib, 1988) that exploit matched asymptotic expansions to heal the singularity (see also Pao, 1988). The scaling required in the matched asymptotics is equivalent to trapping scaling, and del Castillo-Negrete thereby derived the single-wave model systematically. This is also the route we follow below in §V, but first we highlight the development of critical layer theory in fluid mechanics.

C. Critical layer theory

The 1960s also saw much development of weakly nonlinear theories in fluid mechanics following advances in describing the onset of fluid convection (e.g. Malkus and Veronis, 1958). The techniques were quickly adapted to viscous shear flow problem by Stuart (1960) and Watson (1960), but they could not be adapted for the corresponding inviscid problem because of the recurring critical-level singularities. Some progress was made by assuming that significant viscosity wiped out the singularity in a slender region surrounding the critical level (Churilov and Shukhman, 1987b; Huerre, 1987; Schade, 1964), an idea dating back to Lin (1945). These insights gave some physical support to the idea that the poles in the asymptotic expansion
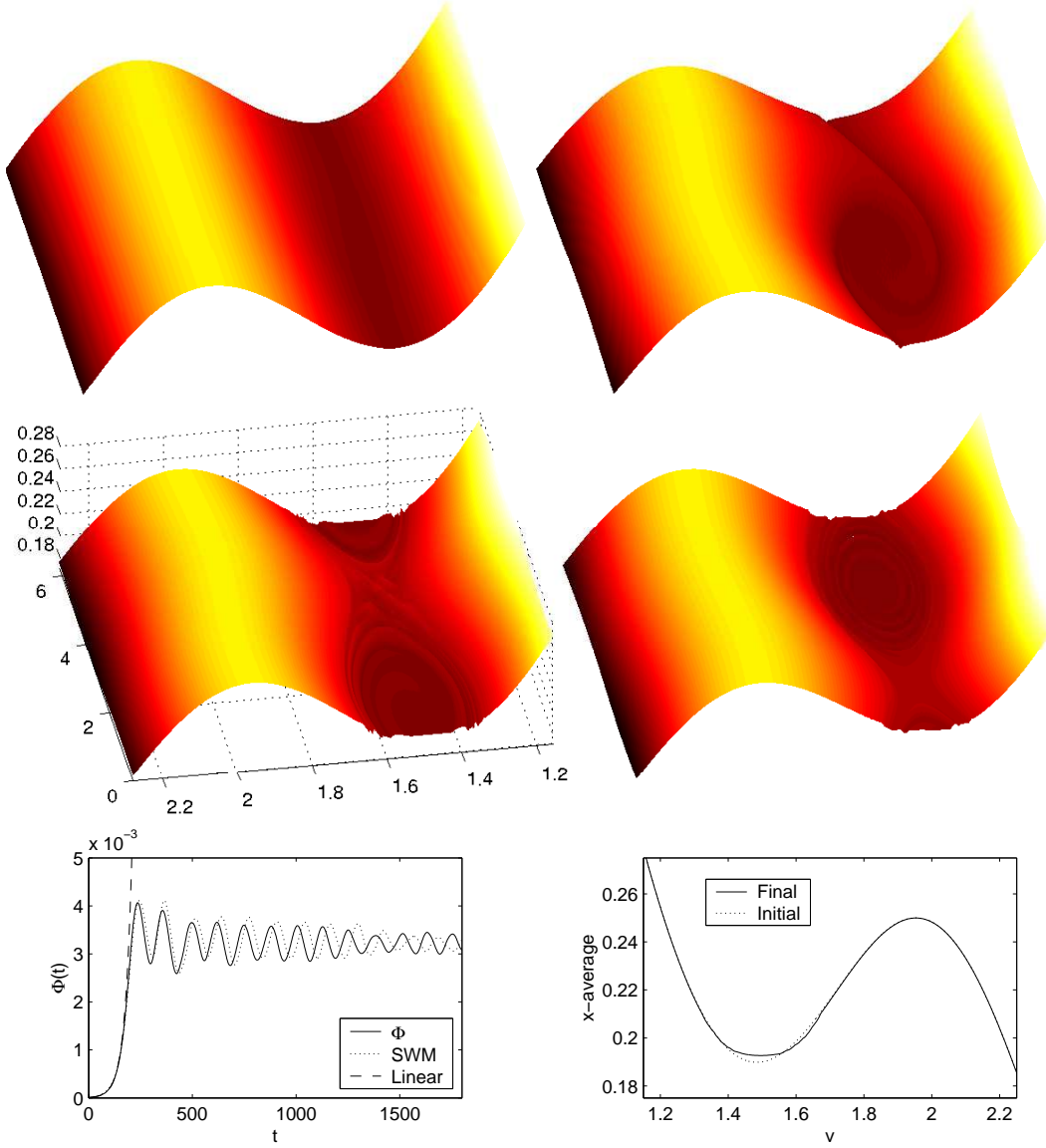
FIG. 4 Simulation of the bump-on-tail instability in the Vlasov problem. The equilibrium is given by (46) with $a = 0.23$ and $v_0 = 2$, and the spatial domain has length $L = 2\pi$. The first four pictures (left to right, top to bottom) show snapshots of the total distribution function, $F(v) + f(x, v, t)$ as surfaces above the (x, v)-plane at the times $t = 140, 200, 400$, and 1800, in the vicinity of the bump (see figure 2(c) for the full surface plot). The penultimate picture shows the amplitude of $\Phi(t) := (\int_0^L \mathrm{d}x \, \varphi^2/L)^{1/2}$; the dashed line shows the expected exponential growth of the unstable mode and the dotted line indicates the prediction of the single-wave model. The final panel shows the spatial average of $F + f$ at the beginning and end of the computation.

could be healed by viscosity. However, viscous effects also inexorably diffuse away from the critical levels, widening the critical layer as time proceeds (Brown and Stewartson, 1978). Overall, this so-called viscous critical-layer theory glosses over the critical-layer dynamics and is not suitable closer to the inviscid limit, the situation of relevance to this review.

The appreciation that the dynamics could be richer led several authors to develop more complicated "critical-layer theories". These theories all proceed by resolving the dynamics of the critical level in detail
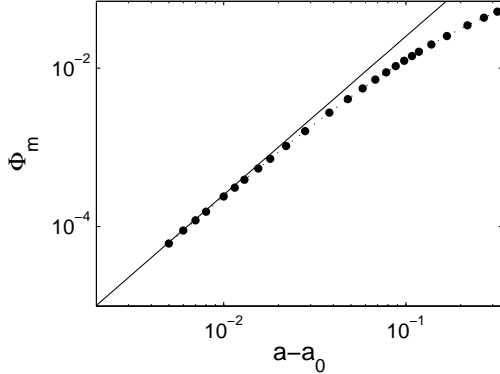
FIG. 5 Numerical data for the saturation measure Φ_m (the first maximum in the amplitude of the potential, $\Phi(t)$), plotted against the distance to the stability boundary, $a - a_0$. The prediction of the single-wave model (based on trapping scaling) is shown by the solid line.

whilst simultaneously including various physical effects to relieve any divergences. For example, Benney and Bergeron (1969) resolved the critical-level singularity by adding nonlinear effects and thereby built steady nonlinear waves (some criticism of their detailed construction was given later by Haberman, 1973 and Brown and Stewartson, 1978). Other theories were those of Stewartson (1978) and Warn and Warn (1978) for forced critical levels that incorporate unsteadiness and nonlinearity. In both examples, a key detail is that nonlinearity first becomes important where the solution is nearly singular, which is over the critical layer, the narrow region surrounding the critical level.

To motivate the critical-layer theory we develop below, we again exploit numerical computations. Figure 6 shows a simulation of instabilities growing on a shear flow in the form of a jet (the background flow is the so-called Bickley jet (Bickley, 1937), with $U(y) = \text{sech}^2 y$, which is popularly used to model the fluid wake behind an obstacle). Both this fluid mechanical example and the Vlasov simulation shown earlier show how the unstable mode grows initially, but then saturates as a result of pronounced nonlinear effects inside a narrow region surrounding the critical level. The principal effect in both examples is the twist up of the background distribution into vortices over the critical layer. Note how the perturbation vorticity distribution is clearly composed of two parts: a global, relatively smooth modal structure, and finely scaled cat's eye patterns emerging around the critical levels that coincide with the inflection points of $U(y)$.

V. THE SINGLE-WAVE MODEL

The stage is now set for a reduction of our general model equations to the single-wave model. From Sec. III we learn that our linear theory has an eigenspectrum that is composed of only the continuum plus a single, distinguished, embedded neutral mode. Examples of such embedded modes include the special plasma oscillations lying on the stability boundary described detailed in Fig. 3. On adjusting a control parameter, and thereby perturbing the equilibrium profile slightly, that mode becomes weakly unstable. The single-wave model describes the ensuing nonlinear development, and an essential ingredient is the trapping scaling discussed in Sec. IV.

A. Derivation

At onset, a distinguished neutral mode is embedded within the continuum and remains regular because its critical level lines up with an extremal point of the equilibrium profile (where $R'(I_*) = 0$). At first sight, this might appear to allow us to proceed with a conventional weakly nonlinear theory as the critical-level singularity then disappears from the leading-order solution (the distinguished mode). However, the continuous spectrum manifests itself at higher order in the asymptotic expansion where the singularity reappears and becomes progressively more severe as one proceeds in the expansion (the core of the difficulty in early expansions for electrostatic instabilities exploiting the Hopf scaling of Sec. IV.B). The cure for the critical-level singularity is to abandon the conventional weakly nonlinear solution over a slender region surrounding the critical level. Within this critical layer, a different solution is needed that varies on a much finer spatial scale. The recipe is therefore a matched asymptotic expansion in which one finds an inner
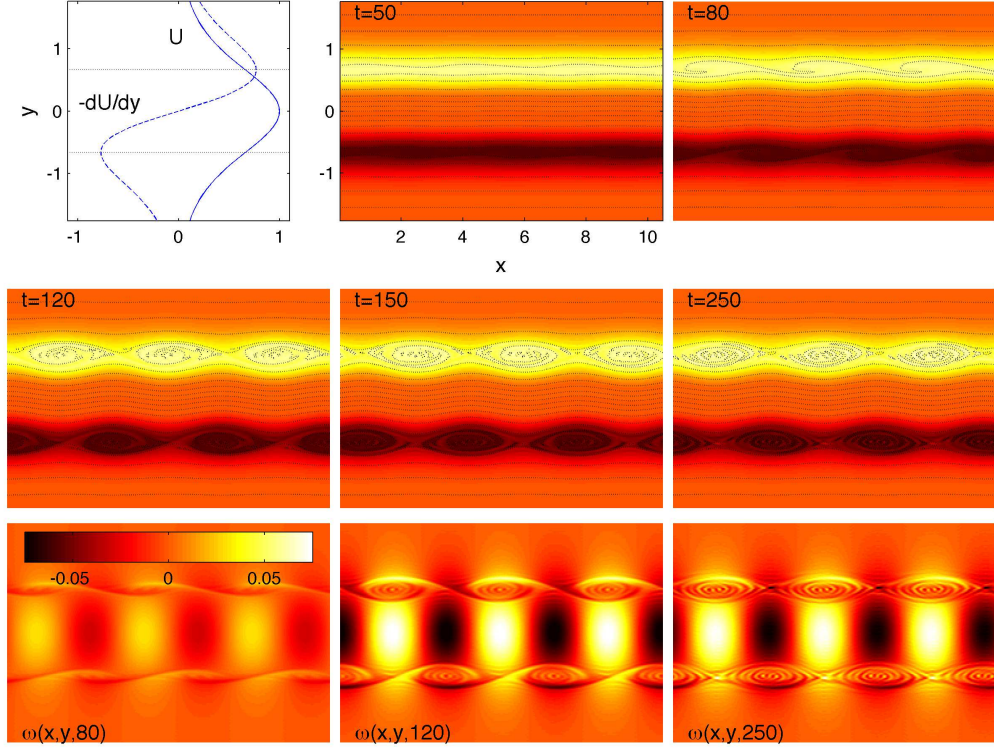
FIG. 6 Computed cat's eye patterns formed from the growth of an unstable mode in a simulation of the Bickley jet (Bickley, 1937). The doubly periodic, computational domain has length $L = 2\pi/k$, with $k = 0.6$, and a pseudo-spectral scheme with an explicit viscosity ($\nu = 3.75 \times 10^{-7}$) is used to numerically solve the equations. The computation is initialized with the third Fourier mode in x, and lower modes excited by round-off errors are explicitly removed. The upper left plot shows the background flow profile, $U(y)$, and the vorticity, $-dU/dy$; the dashed horizontal lines are the critical levels of the unstable mode. Following (left to right, top to bottom) are five snapshots of the vorticity field at the times indicated. Comparison of the vorticity field snapshots with the $-dU/dy$ plot indicates the shading scheme and contour levels. The bottom row of pictures shows the perturbation vorticity field, ω, for three of the snapshots. Further details of these computations can be found in Balmforth and Piccolo (2001).

solution for the critical layer, and then matches to the usual weakly nonlinear solution that remains valid in the 'outer region' further afield. We sketch out this expansion for the general model; additional details can be found in the articles by Balmforth and Piccolo (2001); Churilov and Shukhman (1987a); del-Castillo-Negrete (1998a,b); and Goldstein and Leib (1988).

To ease the discussion, we will take $\Omega(I)$ to be monotonic, implying that there is only a single critical level, and $\Omega' \geq 0$. We also assume that our periodic domain encompasses exactly one wavelength of the distinguished neutral mode and the system has been suitably scaled so that the wavenumber is $k = 1$. In principle, the expansion requires multiple time scales in order to deal with the relatively fast propagation of the neutral mode as well as its much slower growth. However, if we first transform into the frame of the distinguished mode ($\theta \to \theta - \varsigma t$), where ς denotes the frequency of the frame shift, it then suffices to simply rescale and use the slow time, $T = \varepsilon^{-1}t$, where ε is the small parameter that we use to organize the asymptotics. In other words, we begin by introducing the transformation, $\partial_t \to -\varsigma\,\partial_\theta + \varepsilon\,\partial_T$, into the

governing equations (24) and (22), whereupon they become, respectively,

$$\epsilon \rho_T + (\Omega - \varsigma)\rho_\theta - R'\Phi_\theta + [\rho, \Phi] = 0, \tag{74}$$

$$\Phi = \mathcal{K}\rho := \int_{\mathcal{D}} d\hat{I} \int_0^{2\pi} d\hat{\theta}\, K(\theta - \hat{\theta}, I, \hat{I})\, \rho(\hat{\theta}, \hat{I}, t);$$

these equations constitute the starting point for our expansion.

1. Outer regular expansion

Outside the critical layer we assume the asymptotic sequences,

$$R(I) = R_0(I) + \varepsilon R_1(I) + \dots \tag{75}$$

$$\rho = \varepsilon^2 \rho_2(\theta, I, T) + \varepsilon^3 \rho_3(\theta, I, T) + \dots \tag{76}$$

$$\Phi = \mathcal{K}\rho = \varepsilon^2 \psi_2(\theta, I, T) + \varepsilon^3 \psi_3(\theta, I, T) + \dots, \tag{77}$$

where $\psi_m = \mathcal{K}\rho_m$ for $m = 2, 3$. The expansion in (77) opens at order ε^2, which corresponds to the "trapping scaling" of O'Neil et $al.$ (1971) discussed in Sec. IV.B, and the sequence for $R(I)$ incorporates the distortion of the equilibrium profile needed to pass from the marginally stable state to an unstable one (such as by setting $a = a_0 + \varepsilon$ in the parameterized family of equilibria of the plasma problem of Sec III.C, as depicted in Fig. 3).

Upon introducing the sequences into the governing equations and grouping together terms of the same order in ε, we obtain to leading order ε^2,

$$(\Omega - \varsigma)\, \partial_\theta \rho_2 - R_0'\partial_\theta \psi_2 = 0, \tag{78}$$

which can be integrated with respect to θ to obtain

$$\mathcal{L}\rho_2 := \left[1 - \frac{R_0'}{\Omega - \varsigma}\mathcal{K}\right]\rho_2 = 0. \tag{79}$$

The solution to (79) is the embedded neutral mode with $\Omega(I_*) = \varsigma$ and $R_0'(I_*) = 0$:

$$\rho_2(\theta, I, T) = \frac{R_0'\psi_2}{\Omega - \varsigma}, \quad \psi_2(\theta, I, T) = \mathcal{A}(T)\, \eta(I)e^{i\theta} + \text{c.c.}, \tag{80}$$

where $\eta(I)$ is now the relevant ($k = 1$) eigensolution to (38), and the complex amplitude, $\mathcal{A}(T)$, is not yet determined. Note that $e^{-i\theta}\eta(I)$ is also the null vector of $\mathcal{L}^\dagger$, the operator adjoint to $\mathcal{L}$. When evaluated at the critical level $I = I_*$, the solution becomes

$$\rho_2(\theta, I_*, T) = \frac{R_{0*}''}{\Omega_*'}\, \phi(\theta, T), \quad \phi(\theta, T) := \mathcal{A}(T)\, e^{i\theta} + \text{c.c.}, \tag{81}$$

where the subscript '*' notation refers to evaluation at $I = I_*$ and, for later convenience, we have normalized so that $\eta(I_*) = 1$.

Proceeding to order ε^3 we obtain

$$(\Omega - \varsigma)\, \partial_\theta \rho_3 - R_0'\partial_\theta \psi_3 = R_1'\partial_\theta \psi_2 - \partial_T \rho_2, \tag{82}$$

which when integrating with respect to θ and dividing through by $(\varsigma - \Omega)$ yields

$$\mathcal{L}\rho_3 = \rho_3 - \frac{R_0'\psi_3}{\Omega - \varsigma}$$

$$= \frac{R_1'\psi_2}{\Omega - \varsigma} + \frac{R_0'}{(\Omega - \varsigma)^2}\left(i\mathcal{A}_T\, \eta\, e^{i\theta} + \text{c.c.}\right). \tag{83}$$

In general, although $R'(I)$ vanishes at the critical level, neither $R''(I)$ nor $R_1'(I)$ will vanish. Thus, the right-hand side of (83) is singular, which impedes us from multiplying by the adjoint $e^{-i\theta}\eta(I)$ and integrating to eliminate ρ_3 to find the desired equation for $\mathcal{A}(T)$. To avoid this stumbling block, we resolve the critical-layer dynamics by using an inner solution. The scaling of the inner region is determined by noting that the asymptotic sequence, $\varepsilon^2\rho_2 + \varepsilon^3\rho_3$ becomes disordered as I tends to I_*. In fact, because $\rho_2 \sim O(1)$ and $\rho_3 \sim O(I - I_*)^{-1}$ as $I \to I_*$, the asymptotic solution breaks down within a slender layer of thickness ε surrounding the critical level. This is where we must search for the inner, critical-layer solution.

2. Inner critical layer solution

For the critical layer, we define a stretched coordinate $Y := (I - I_*)/\varepsilon$ and a new variable, $\zeta(\theta, Y, t)$, (not to be confused with the general $\zeta(q, p, t)$ of Sec. II.A), such that

$$\rho = \varepsilon^2 \zeta(\theta, Y, T) + \varepsilon^2 \rho_2^{\text{outer}}(\theta, I_*, T). \tag{84}$$

Because $\Phi = \mathcal{K}\rho$ is an integral transform of ρ which smoothes that variable, there is no critical-layer structure in Φ at leading order (cf. Sec. V.A.4), and therefore $\Phi \sim \varepsilon^2 \psi_2(\theta, I_*, T) = \varepsilon^2 \phi(\theta, T)$ over this region. Given these variables, the relation $\partial_I = \varepsilon^{-1} \partial_Y$, and Eq. (24), the equation for ζ becomes, to leading order,

$$\partial_T \left(\zeta + \frac{R_{0*}''}{\Omega_*'} \phi \right) + \Omega_*' Y \zeta_\theta - \left(R_{1*}' + \zeta_Y \right) \phi_\theta = 0, \tag{85}$$

where $\phi(\theta, T)$ is given by (81).

Equation (85) is a fully nonlinear evolution equation for the critical-layer dynamics and offers no further simplification. The problem cannot be solved in closed form and must be approached numerically in general. Thus, the problem still boils down to the solution of a partial differential equation, and the single-wave model remains of infinite dimension.

3. Matching

Expressed in terms of Y, the inner limit of the outer solution can be written in the form,

$$\rho \sim \epsilon^2 \frac{R_{0*}'' \phi}{\Omega_*'} + \epsilon^2 \frac{R_{1*}' \phi}{Y \Omega_*'} + \epsilon^2 \frac{R_{0*}'' \phi_{T\theta}}{Y \Omega_*'^2} + O(\epsilon^3), \tag{86}$$

provided $\psi_3 = \mathcal{K}\rho_3$ does not diverge faster than $(I - I_*)^{-1}$ as $I \to I_*$, which is the case for the $\mathcal{K}$-operators of interest here. On the other hand, the inner solution has an outer limit given by

$$\rho \sim \epsilon^2 \zeta + \epsilon^2 \frac{R_{0*}'' \phi}{\Omega_*'}, \tag{87}$$

with the second term being the outer contribution to the inner solution. The two leading-order solutions can therefore be successfully matched provided $\zeta \to 0$ for $Y \to \pm\infty$, which requires consideration the initial condition, $\zeta(\theta, Y, 0)$. In particular, we take $\zeta(\theta, Y, 0) = 0$, which corresponds to kicking the system into action by introducing the discrete mode at a low amplitude, $\mathcal{A}(0) = \mathcal{A}_0$ with $|\mathcal{A}_0| \ll 1$, without further rearranging the equilibrium distribution within or outside the critical layer. The large $|Y|$ limit of (85) then implies that

$$\zeta \sim \frac{R_{1*}' \phi}{Y \Omega_*'} + \frac{R_{0*}'' \phi_{T\theta}}{Y \Omega_*'^2} + O(Y^{-2}). \tag{88}$$

Thus, $\zeta \sim O(Y^{-1})$ for $|Y| \gg 1$, ensuring the match.

4. Solvability

The final step is to apply a solvability condition on ρ_3 to determine $\mathcal{A}(T)$. To accomplish this task, first consider

$$\mathcal{K}\rho = \int_0^{2\pi} d\hat{\theta} \int_{\mathcal{D}} d\hat{I} \, K(\theta - \hat{\theta}, I, \hat{I}) \, \rho(\hat{\theta}, \hat{I}, T). \tag{89}$$

We break the integral over $\mathcal{D}$ into three pieces: $[I_L, I_* - \Delta]$, $(I_* - \Delta, I_* + \Delta)$ and $[I_* + \Delta, I_R]$, where $[I_L, I_R]$ denotes the full integration over $\mathcal{D}$ and $\varepsilon \ll \Delta \ll 1$. The breakages in the integral therefore extend into the

matching region where both the outer and inner solutions remain valid. For the integral in I over $\mathcal{D}$ of (89), we then obtain

$$\varepsilon^2 \int_{\mathcal{D}} d\hat{I}\, K(\theta - \hat{\theta}, I, \hat{I})\, \rho_2(\hat{\theta}, \hat{I}, T)$$

$$+ \varepsilon^3 \fint_{\mathcal{D}} d\hat{I}\, K(\theta - \hat{\theta}, I, \hat{I})\, \rho_3(\hat{\theta}, \hat{I}, T) + \varepsilon^3 K(\theta - \hat{\theta}, I, I_*) \int_{-\Delta/\epsilon}^{\Delta/\epsilon} dY\, \zeta(\hat{\theta}, Y, T) + O(\epsilon^4)\,,$$

where we now use the notation,

$$\fint_{\mathcal{D}} dI\, f(I) := \int_{I_L}^{I_* - \Delta} dI\, f(I) + \int_{I_* + \Delta}^{I_R} dI\, f(I)\,. \tag{90}$$

Hence,

$$\psi_2 = \varepsilon^2 \int_{\mathcal{D}} d\hat{I}\, K(\theta - \hat{\theta}, I, \hat{I})\, \rho_2(\hat{\theta}, \hat{I}, T) \tag{91}$$

throughout $\mathcal{D}$, which is therefore free of critical-layer structure as remarked earlier, and

$$\psi_3 = \int_0^{2\pi} d\theta \fint_{\mathcal{D}} d\hat{I}\, K(\theta - \hat{\theta}, I, \hat{I})\, \rho_3(\hat{\theta}, \hat{I}, T) \tag{92}$$

$$+ \int_0^{2\pi} d\theta\, K(\theta - \hat{\theta}, I, I_*) \int_{-\Delta/\epsilon}^{\Delta/\epsilon} dY\, \zeta(\hat{\theta}, Y, T)\,.$$

Now we multiply Eq. (83) by $\eta(I)e^{-i\theta}$, integrate θ over $[0, 2\pi]$, and I over the ranges $[I_L, I_* - \Delta]$ and $[I_* + \Delta, I_R]$. The left-hand side of (83) becomes,

$$\int_0^{2\pi} d\theta \fint_{\mathcal{D}} dI \left(\rho_3 - \frac{R_0'\psi_3}{\Omega - \varsigma} \right) e^{-i\theta}\, \eta \tag{93}$$

$$= -\int_0^{2\pi} d\theta \int_{-\Delta/\varepsilon}^{\Delta/\varepsilon} dY\, e^{-i\theta}\, \zeta(\theta, Y) + O(\Delta)\,, \tag{94}$$

on introducing ψ_3 from (92) and using the following properties of η: $\mathcal{L}^\dagger \eta = 0$, $\eta e^{-i\theta} = \mathcal{K}[R_0'\eta e^{-i\theta}/(\Omega - \varsigma)]$ and $\eta_* = 1$. The right-hand side of (83), on the other hand, becomes

$$2\pi i\, \mathcal{A}_T \fint_{\mathcal{D}} dI\, \frac{R_0'\eta^2}{(\Omega - \varsigma)^2} + 2\pi \mathcal{A} \fint_{\mathcal{D}} dI\, \frac{R_1'\eta^2}{\Omega - \varsigma}\,. \tag{95}$$

Thence,

$$i\, \mathcal{A}_T \fint_{\mathcal{D}} dI\, \frac{R_0'\eta^2}{(\Omega - \varsigma)^2} + \mathcal{A} \int_{\mathcal{D}} dI\, \frac{R_1'\eta^2}{\Omega - \varsigma} \tag{96}$$

$$= -\frac{1}{2\pi} \int_0^{2\pi} d\theta \int_{-\Delta/\epsilon}^{\Delta/\epsilon} dY\, e^{-i\theta}\, \zeta(\theta, Y, t) + O(\Delta)\,.$$

Finally, we take the limits $\Delta \to 0$ and $\Delta/\varepsilon \to \infty$. This turns the integrals over I in (96) into standard principal-value integrals, and the integral over Y into another principal-value integral, this time at its infinite limits.

B. Normal and degenerate forms

Gathering together the results of Sec. V.A, we rewrite Eqs. (81), (85), and (96) compactly as

$$\phi(\theta, T) = \mathcal{A}(T)\, e^{i\theta} + \mathcal{A}(T)^*\, e^{-i\theta}\,, \tag{97}$$

$$\mathcal{Q}_T + [\mathcal{Q}, \mathfrak{E}] = 0\,, \tag{98}$$

$$i\varpi\,\mathcal{A}_T + \nu\,\mathcal{A} = -\left\langle \zeta\, e^{-i\theta} \right\rangle\,, \tag{99}$$

where

$$\mathcal{Q}(\theta, Y, T) := \zeta + \frac{R_{0*}''}{\Omega_*'}\,\phi + \frac{R_{0*}''}{2}\,Y^2 + R_{1*}'\, Y\,, \tag{100}$$

$$\mathfrak{E}(\theta, Y, T) := \frac{\Omega_*'}{2}Y^2 + \phi(\theta, T)\,, \tag{101}$$

$$\varpi := \fint_{\mathbb{R}} dI\, \frac{R_0'\eta^2}{(\Omega - \varsigma)^2}\,, \qquad \text{and} \qquad \nu := \int_{\mathbb{R}} dI\, \frac{R_1'\eta^2}{\Omega - \varsigma}\,. \tag{102}$$

These equations can be simplified further by scaling, which we do in the next section to obtain the normal form. Before setting about this task, we briefly recall the origin of some of the quantities appearing in the system: the variable $\mathcal{Q}$ corresponds to the limit of the total distribution, $\zeta = R(I) + \rho$, the Hamiltonian system of Sec. II.A within the critical layer. The equilibrium distribution, $R(I)$, contributes the coefficients, R_{0*}'' and R_{1*}' (the leading-order curvature and the first-order slope), to the definition of $\mathcal{Q}$. Featuring in (101) is the leading-order 'shear' at the critical level, $\Omega_*' \equiv h''(I_*)$, determined from the one-particle piece of the Hamiltonian. The integral quantities, ϖ and ν, depend on the shape of the eigenfunction of the embedded mode.

1. Normal

To place the system into a simpler form, we introduce a characteristic timescale τ, a scale for action μ, and rescaling of the distribution, b. We then define the new variables,

$$t := \frac{T}{\tau}\,, \quad x = \theta + \mu\, t\,, \quad y := \Omega_*'\tau Y + \mu\,, \tag{103}$$

$$\varphi := -\Omega_*'\tau^2\phi\,, \quad A := -\Omega_*'\tau^2 \mathcal{A}\, e^{-i\mu t}\,, \tag{104}$$

$$\check{\zeta} := b\zeta\,, \quad Q = b\mathcal{Q} - \tfrac{1}{2}\mu^2\kappa + \mu\gamma\,, \tag{105}$$

where

$$\kappa := -\frac{bR_{0*}''}{(\tau\Omega_*')^2}\,, \qquad \gamma := \mu\kappa + \frac{bR_{1*}'}{\tau\Omega_*'}\,. \tag{106}$$

If $\varpi \neq 0$, we may then make the selections,

$$b = \frac{\tau^2}{\varpi}\,, \quad \mu := \tau\frac{\nu}{\varpi}\,, \tag{107}$$

where ϖ and ν are given in (102); the "degenerate" case, with $\varpi = 0$ will be dealt with separately in Sec. V.B.2. Substituting these forms into Eqs. (97), (98), and (99), and then dropping the '$\check{}$' on ζ leads to

$$\varphi(x, t) = A e^{ix} + A^* e^{-ix}\,, \tag{108}$$

$$Q_t + [Q, \mathcal{E}] = 0 \tag{109}$$

$$iA_t = \left\langle \zeta\, e^{-ix} \right\rangle\,, \tag{110}$$

where

$$Q(x,y,t) := \zeta + \kappa\varphi - \frac{\kappa}{2}y^2 + \gamma y \tag{111}$$

$$\mathcal{E}(x,y,t) := \frac{y^2}{2} - \varphi(x,t). \tag{112}$$

An alternative form of Eq. (109) is

$$\zeta_t + y\zeta_x + \varphi_x\zeta_y = -\kappa\varphi_t - \gamma\varphi_x. \tag{113}$$

The initial and boundary conditions are

$$A(0) = A_0, \qquad \zeta(x,y,0) = 0,$$
$$\zeta \sim y^{-1}(\kappa\varphi_{xt} - \gamma\varphi) \quad \text{for } |y| \gg 1, \tag{114}$$

where A_0 is the initial mode amplitude. Note that the relatively weak decay of ζ with y does not interfere with the construction of $\langle\zeta\,\mathrm{e}^{-\mathrm{i}x}\rangle$ because the integral over y is interpreted using the principle value at its limits (*cf.* (96)). Similarly, one can eliminate the variable ζ entirely in favor of Q by observing that

$$\langle Q\mathrm{e}^{-\mathrm{i}x} - \kappa A\rangle = \langle(Q - \kappa\varphi)\,\mathrm{e}^{-\mathrm{i}x}\rangle$$
$$= \left\langle\left(\zeta - \frac{\kappa}{2}y^2 + \gamma y\right)\mathrm{e}^{-\mathrm{i}x}\right\rangle$$
$$= \langle\zeta\mathrm{e}^{-\mathrm{i}x}\rangle, \tag{115}$$

provided the potentially divergent integral involving $\frac{1}{2}\kappa y^2\mathrm{e}^{-\mathrm{i}x}$ is dealt with by first performing the x-average.

Equations (108)–(112) are what we call the normal form of the single-wave model. Crucially, the absence of dissipation in the problem has the unappealing consequence that no dimensional reduction occurs as part of the asymptotic analysis, and the single-wave model retains a partial differential form. Of course, no dimensional reduction can be expected here, since at the onset of instability, the distinguished neutral mode is arbitrarily close to an infinite number of singular continuum modes with comparable wavespeeds; the two equations composing the single-wave model describe the interaction between the distinguished mode and a superposition of locally resonant continuum modes within the critical layer.

Note that one further simplification is possible: since τ has not yet been specified, we may exploit this timescale to set $\gamma = \pm 1$. The parameter γ is built from the correction to the equilibrium profile, R_1, and, as shown below, acts as the trigger for instability. After scaling, the two choices, $\gamma = \pm 1$, refer to whether the system is displaced from marginality into the unstable ($\gamma = -1$) or stable ($\gamma = +1$) regimes. Aside from the initial amplitude A_0, this leaves a single parameter in the problem, namely κ, which is related to R_{0*}'', the curvature of the leading-order equilibrium profile at the critical level. This parameter encodes information regarding the position of the embedded mode along the stability boundary: at the minimum of the stability boundary where all wavenumbers are stable, $R_{0*}'' = 0$ (see Sec. III.C) and so $\kappa = 0$; elsewhere on the stability boundary, κ does not vanish (and the danger of additional unstable modes is removed by suitably choosing the length of the periodic domain).

The normal form as given by (108), (110), and (113) was derived for various types of fluid shear flows by Balmforth (1999); Balmforth *et al.* (2001a); Balmforth and Piccolo (2001); Churilov and Shukhman (1987a); Goldstein and Leib (1988); and Shukhman (1989). The system is similar, though not identical, to the original single-wave model proposed for unstable electrostatic waves (O'Neil *et al.*, 1971; Tennyson *et al.*, 1994) and nonlinear Landau damping (Imamura *et al.*, 1969). In the original single-wave model, the right-hand side of (113) did not appear (i.e., $\kappa \equiv \gamma \equiv 0$) and instability was introduced into the system via a suitable initial condition, $\zeta(x,y,0) \neq 0$. O'Neil *et al.* (1971) used a beam-like distribution (a delta-function at a fixed velocity); Onishchenko *et al.* (1971) and Imamura *et al.* (1969) used a linear profile, equivalent to the $\kappa \equiv 0$ case. del-Castillo-Negrete (1998a,b) derived the single-wave model above, but then elected to drop the parameters γ and κ and follow the route of O'Neil *et al.* (1971) to instability by selecting a suitable initial condition. However, when viewed as the weakly nonlinear description of the distinguished mode on the stability boundary, there is no freedom in the choice of initial condition; only the position on the stability boundary (and therefore κ) is a free parameter.

2. Degenerate

It may transpire that $\varpi = 0$. When this happens, the scaling leading to the normal form of Sec. V.B.1 is precluded because we cannot make the selections in (107). Upon examination of (102), it is evident that $\varpi = 0$ is unlikely unless there is a simplicity or symmetry to the problem, which turns out to be the case for some physical examples. A case in point is that of the XY model introduced in Sec. II.C.3. For this case, $\Omega = I$ and the interaction has a spatial kernel $(-\pi^{-1}\cos(\theta - \hat{\theta})$ is independent of action I) so η is constant (see Sec. III.A). Moreover, for equilibrium profiles like the Gaussian of Sec. III.D, $R_0'(I)$ is odd in I, the embedded mode has $\varsigma = 0$, and $\varpi = 0$ follows immediately. We will treat this example in detail in Sec. VIII, while here we work out the general degenerate form. From Eq. (99) it is clear that the mode amplitude for the degenerate form will no longer be governed by a differential equation, but by an integral constraint.

Instead of (107), we now make the selections

$$b = \frac{\tau}{\nu}, \quad \mu = -\frac{R_{1*}'}{\nu\Omega_*'} \tag{116}$$

With these choices, $\gamma = 0$ and Eqs. (97), (98), and (99) now become

$$\varphi(x,t) = A\mathrm{e}^{\mathrm{i}x} + A^*\mathrm{e}^{-\mathrm{i}x}, \tag{117}$$

$$Q_t + [Q, \mathcal{E}] = 0 \tag{118}$$

$$A = \left\langle \zeta\,\mathrm{e}^{-\mathrm{i}x} \right\rangle, \tag{119}$$

where

$$Q(x,y,t) := \zeta + \kappa\varphi - \frac{\kappa}{2}y^2. \tag{120}$$

$$\mathcal{E}(x,y,t) := \frac{y^2}{2} - \varphi(x,t). \tag{121}$$

Finally, we are again free to choose τ, and thereby scale out a parameter. The only parameter remaining explicitly is κ, and so we choose

$$\tau = \frac{1}{(\Omega_*')^2}\left| \frac{R_{0*}''}{\nu} \right| \tag{122}$$

so that $\kappa \equiv -\mathrm{sgn}(R_{0*}''/\nu) = \pm 1$. With this selection, as demonstrated in Sec. VI, we find that the system is unstable when $\kappa = -1$ (and stable if $\kappa = 1$). Note that, because the mode amplitude is no longer a dependent variable, but given by the integral constraint (119), the initial amplitude of the mode does not appear as an independent parameter, and the initial state of the system remains to be specified. One option is to initialize using the linear normal mode of Sec. VI. Alternatively, a more convenient method in practice is to kick the system into action by adding a transient forcing term to (119) that smoothly switches on the dynamics.

C. Hamiltonian structure and conservation laws

1. Normal Hamiltonian structure

Both the normal and degenerate forms of the single-wave model of Sec. V.B inherit the structure of their Hamiltonian parent models, discussed in Sec. II. For the normal form of the model, the Hamiltonian is given by

$$H_n = \int_{\mathbb{R}} dy \int_0^{2\pi} dx \left(\mathcal{E}Q + \kappa\,|A|^2 \right). \tag{123}$$

The two terms in (123) are reminiscent of the particle kinetic energy and the electrostatic energy for the Vlasov-Poisson system (see Sec. II). This Hamiltonian together with the Poisson bracket of (7) gives the single-wave model. To see this we compute the derivatives,

$$\frac{\delta H_n}{\delta Q} = \mathcal{E} \quad\text{and}\quad \frac{\partial H_n}{\partial A^*} = -2\pi \left\langle Q\mathrm{e}^{\mathrm{i}x} - \kappa A \right\rangle, \tag{124}$$

where Q, A, and A^* are independent variables, and insert them into (7) to obtain

$$Q_t = \{Q, H_n\} = -[Q, \mathcal{E}],$$
$$A_t = \{A, H_n\} = -i\left\langle Qe^{-ix} - \kappa A\right\rangle \tag{125}$$

and similarly $A_t^* = (A_t)^*$. This Hamiltonian structure is the continuum version of that derived in Tennyson *et al.* (1994) (see also Mynick and Kaufman, 1978; Smith and Pereira, 1978).

Showing that (123) exists requires some care, of the type commented upon in Sec. V.B.1, since the second term of H_n is divergent. To show that Hamiltonian (energy) H_n is in fact finite we return to (113) and analyze more carefully the large $|y|$ behavior of ζ, obtaining

$$\zeta \sim \frac{1}{y}(\kappa\varphi_{xt} - \gamma\varphi) + \frac{1}{y^2}(\kappa|A|^2 - \kappa\varphi_{tt} - \gamma\varphi_{xt}) + \dots . \tag{126}$$

The x-independent, $O(y^{-2})$ term in (126) follows upon averaging (113) over x, and is sufficient to cancel the divergent second piece of H_n, leaving a convergent double integral.

Given the Hamiltonian structure, it is natural to look for invariants. Since both the single wave and the medium can carry momentum we expect a total momentum of the following form to be conserved (cf. Tennyson *et al.* (1994)):

$$P = 2\pi|A|^2 - \int_{\mathbb{R}} dy \int_0^{2\pi} dx\, y\, \zeta\,, \tag{127}$$

where the first term of (127) will shortly be identified with the wave action, while the second has the familiar form of the (relative) x-component of the momentum in vortex dynamics (e.g. Flierl and Morrison, 2011). It can be shown that P commutes with H_n, i.e. $\{P, H_n\} = 0$, or directly that this is equivalent to

$$P_t = \left(\langle y\zeta\rangle - |A|^2\right)_t = 0\,.$$

An immediate consequence of the Poisson bracket of (7) is the existence of the following infinite family of Casimir invariants (see e.g. Morrison, 1998):

$$C = \int_{\mathbb{R}} dy \int_0^{2\pi} dx\, \mathcal{C}(Q)\,, \tag{128}$$

where $\mathcal{C}$ is an arbitrary function of Q. An important Casimir is the 'enstrophy'

$$C_2 := \int_{\mathbb{R}} dy \int_0^{2\pi} dx\, Q^2\,. \tag{129}$$

With some manipulation this can be shown to be equivalent to

$$C_2 = \int_{\mathbb{R}} dy \int_0^{2\pi} dx\, \zeta^2 - 2\kappa H_n + 2\gamma\left(2\pi|A|^2 - P\right)\,. \tag{130}$$

Since H_n and P are constants of motion, this also implies the further invariant,

$$I = \int_{\mathbb{R}} dy \int_0^{2\pi} dx\, \zeta^2 + 4\pi\gamma|A|^2\,. \tag{131}$$

From (131) we obtain a stability condition, viz., for $\gamma = +1$ in the vicinity of the equilibrium state $A = \zeta = 0$, the invariant I provides a norm for bounding solutions to an infinitesimal neighborhood of this equilibrium. Also, with the initial conditions $\zeta(x, y, 0) = 0$ and $A(0) = A_0$ we have

$$\gamma|A|^2 + \frac{1}{2}\langle\zeta^2\rangle = \gamma|A_0|^2\,. \tag{132}$$

Thus, for $\gamma = +1$, we have the finite amplitude bounds $|A|^2 \leq |A_0|^2$ and $\langle\zeta^2\rangle \leq 2|A_0|^2$. This amounts to energy-Casimir stability for this example (see e.g. Morrison, 1998).

To show that $\mathcal{J} = 2\pi |A|^2$ is equivalent to the wave action, we introduce the coordinate change,

$$A = \sqrt{\frac{\mathcal{J}}{2\pi}} \, e^{i\Psi} \qquad \text{and} \qquad A^* = \sqrt{\frac{\mathcal{J}}{2\pi}} \, e^{-i\Psi} \, . \tag{133}$$

The bracket of (7) becomes

$$\{F, G\} = \left(\frac{\partial F}{\partial \Psi} \frac{\partial G}{\partial \mathcal{J}} - \frac{\partial G}{\partial \Psi} \frac{\partial F}{\partial \mathcal{J}} \right)$$
$$+ \int_{\mathbb{R}} dy \int_0^{2\pi} dx \, Q \left[\frac{\delta F}{\delta Q}, \frac{\delta G}{\delta Q} \right] \, , \tag{134}$$

where now Ψ and $\mathcal{J}$ are a genuine canonically conjugate pair of wave variables for the wave. In terms of these variables the potential φ is given by

$$\varphi = \sqrt{\frac{2\mathcal{J}}{\pi}} \cos(x + \Psi)$$

and Eq. (110) is replaced by the following two real-valued equations:

$$\dot{\Psi} = \frac{\partial H_n}{\partial \mathcal{J}} = - \left\langle \sqrt{\frac{2\pi}{\mathcal{J}}} \, Q \, \cos(x + \Psi) - \kappa \right\rangle$$
$$\dot{\mathcal{J}} = -\frac{\partial H_n}{\partial \Psi} = -2 \left\langle \sqrt{2\pi\mathcal{J}} \, Q \, \sin(x + \Psi) \right\rangle \, . \tag{135}$$

2. Degenerate Hamiltonian structure

It is evident from Sec. V.C.1 that divergences associated with system size must be treated with some delicacy; e.g., observing that $\langle \varphi \rangle$ vanishes requires integration over x, giving zero because of periodicity, before integration over y, which would give a divergent result, as discussed in obtaining Eq. (115). Such system size divergences are common for two-dimensional theories such as vortex dynamics, quasigeostropy, etc., which possess infinite kinetic energy for unbounded domains. For this reason, relative energies and momenta are often used (see, e.g., Flierl and Morrison, 2011 for an example of numerically tracking such quantities), but for our presentation of the Hamiltonian form for the degenerate case, we find it convenient to introduce a system size so that $\langle 1 \rangle = \mathcal{D}$. The need for this artifice is compounded by the fact that for the degenerate form, the theory is written entirely in terms of the variable Q - the amplitude being determined by Eq. (119), which is a constraint equation. Tools for handling such constraints are now well-developed (Chandre *et al.*, 2013, 2012; Tassi *et al.*, 2009), but we will present the Hamiltonian structure for this degenerate case in a manner akin to that for the Vlasov-Poisson system (Morrison, 1980), which has a bracket of the form of (12).

Using (117) and (119) it is evident that the constraint amounts to φ being functionally dependent on ζ, i.e.,

$$\varphi(x) = 2\langle \zeta \cos(x - x') \rangle =: \underline{\varphi}[\zeta](x) \tag{136}$$

where the underline will be used to denote φ as an operator. Upon introducing the linear operator

$$\mathcal{L}_\kappa := \mathcal{I} + \kappa \underline{\varphi} \, ,$$

where $\mathcal{I}$ is the identity operator, the equation of motion (118) becomes

$$\mathcal{L}_\kappa[\zeta_t] = -y \, \zeta_x - \underline{\varphi}[\zeta]_x \, \zeta_y \tag{137}$$

and thus it is necessary to assume $\mathcal{L}_\kappa[\zeta_t]^{-1}$ exists, which we write as

$$\mathcal{L}_\kappa^{-1} = \frac{1}{\mathcal{I} + \kappa \underline{\varphi}} = \mathcal{I} - \kappa \underline{\varphi} + \kappa^2 \underline{\varphi}^2 - \dots \, . \tag{138}$$

Various properties of the operators $\underline{\varphi}$ and $\mathcal{L}_\kappa$ will be needed, and so we present them now. Observe, both operators are formally self-adjoint, e.g,

$$\langle g \, \underline{\varphi}[h] \rangle = \langle h \, \underline{\varphi}[g] \rangle$$

for functions $g, h(x, y)$, and we have the following:

$$\mathcal{E} = y^2/2 - \underline{\varphi}[\zeta] \tag{139}$$

$$Q = \mathcal{L}_\kappa[\zeta] - \kappa y^2/2 \tag{140}$$

$$\zeta = \mathcal{L}_\kappa^{-1}[Q + \kappa y^2/2] \,. \tag{141}$$

Also, by periodicity, $\underline{\varphi}[1] = \underline{\varphi}[g(y)] = 0$, where g is a function of y alone. A short calculation gives

$$\underline{\varphi}\left[\underline{\varphi}[\zeta]\right] = \mathcal{D}\underline{\varphi}[\zeta] \;\Rightarrow\; \underline{\varphi}^n[\zeta] = \mathcal{D}^{n-1}\underline{\varphi}[\zeta] \,. \tag{142}$$

Thus, upon making use of (138) we obtain

$$\mathcal{L}_\kappa^{-1}[y^2/2] = y^2/2 \,,$$

$$\mathcal{L}_\kappa^{-1}\left[[\underline{\varphi}[\zeta]\right] = \frac{1}{1 + \kappa\mathcal{D}} \, \underline{\varphi}[\zeta] \,, \tag{143}$$

and a functional chain rule calculation (e.g. Morrison, 2013) yields

$$\frac{\delta F}{\delta \zeta} = \mathcal{L}_\kappa\left[\frac{\delta F}{\delta Q}\right] \quad \text{or} \quad \frac{\delta F}{\delta Q} = \mathcal{L}_\kappa^{-1}\left[\frac{\delta F}{\delta \zeta}\right] \,, \tag{144}$$

which we will find convenient.

Now, the Hamiltonian of (123) for the normal form suggests a Hamiltonian for the degenerate case with terms as follows:

$$\begin{aligned}
H_d[\zeta] = {} & \frac{1}{2} \int_\mathcal{D} dy \int_0^{2\pi} dx \; y^2 \, \zeta \\
& - \frac{(1 + \kappa\mathcal{D})}{2\pi} \int_\mathcal{D} dy \int_0^{2\pi} dx \int_\mathcal{D} dy' \int_0^{2\pi} dx' \\
& \times \zeta(x, y)\zeta(x', y') \cos(x - x') \,,
\end{aligned} \tag{145}$$

which has a form reminiscent of the Hamiltonian for the Vlasov-Poisson system. Evidently,

$$\begin{aligned}
\frac{\delta H_d}{\delta \zeta} &= \frac{y^2}{2} - \frac{(1 + \kappa\mathcal{D})}{\pi} \int_\mathcal{D} dy' \int_0^{2\pi} dx' \; \zeta(x', y') \cos(x - x') \\
&= \frac{y^2}{2} - (1 + \kappa\mathcal{D})\underline{\varphi}[\zeta]
\end{aligned} \tag{146}$$

Making use of (146), (144), and (146) gives

$$\frac{\delta H_d}{\delta Q} = \frac{y^2}{2} - \underline{\varphi} = \mathcal{E} \,; \tag{147}$$

whence, we obtain

$$Q_t = \{Q, H_d\} = -[Q, \mathcal{E}] \,, \tag{148}$$

the equation of motion of (118). This Hamiltonian structure is similar to that given in Bachelard *et al.* (2009) for the XY model.

D. Dissipative effects within the critical layer

Depending on the physics under consideration, the Hamiltonian forms described in Sec. V.C can be amended by adding terms that describe dissipative effects. In particular, dissipation terms can be included on the right-hand side of the critical-layer equation (113), corresponding to various kinetic theory transport processes:

$$\zeta_t + y\,\zeta_x + \varphi_x\zeta_y + \kappa\varphi_t + \gamma\varphi_x = (\lambda\zeta_y)_y\,. \tag{149}$$

The dissipative term corresponds to viscous dissipation in the fluids context, where λ is sometimes refered to as the Haberman parameter (*e.g.* (Goldstein and Hultgren, 1988; Shukhman, 1998a)). In the kinetic theory context, the term descends from the approximation of a Fokker-Planck operator (*e.g.* Ng *et al.* (1999, 2006); and Pao (1988)), in which case λ may depend on the coordinate y.

The inclusion of such dissipative terms within the ordering scheme of Sec. V.A requires justification. In each case, there needs to be a distinguished scaling that ensures the term enters at the same order as the other physical effects inside the critical layer, whilst simultaneously not affecting the outer solution. We do not pursue this here in generality, and mention only that for the fluid problem the kinematic viscosity ν of the parent model, which provides a term $\nu(\omega_{xx} + \omega_{yy})$ on the right-hand side of Eq. (27), must be scaled as $\nu = \varepsilon^3\nu_3$, and λ is then a suitably scaled version of ν_3 (cf. Churilov and Shukhman, 1987a; Goldstein and Hultgren, 1988). Pao (1988) provides the analogous result for the Vlasov equation with a Fokker-Planck collision operator. Note that if $\lambda \gg 1$, one can perform some additional reductions of the model to furnish simpler amplitude equations (see Churilov and Shukhman, 1987a, 1996; Goldstein and Hultgren, 1988), but here we focus on the less viscous cases with λ order unity or smaller.

VI. LINEAR SINGLE-WAVE DYNAMICS

We now explore the linear theory of the single-wave model, focussing mostly on the normal form of Sec. V.B.1. On discarding the nonlinear term, $\varphi_x\zeta_y$, the system can be written as

$$\zeta_t + y\,\zeta_x + \kappa\varphi_t + \gamma\varphi_x = (\lambda\zeta_y)_y\,, \tag{150}$$

$$\mathrm{i}A_t = \left\langle \zeta\,\mathrm{e}^{-\mathrm{i}x} \right\rangle, \qquad \varphi = A\mathrm{e}^{\mathrm{i}x} + \mathrm{c.c.}\,, \tag{151}$$

where we have included the dissipative terms of Sec. V.D. These equations can be solved analytically for both normal modes and the initial-value problem. As a result of the latter, we arrive at one of the simplest examples of a system exhibiting Landau damping.

A. Normal modes

We consider first the ideal case where the dissipative terms of Sec. V.D are set to zero (i.e. $\lambda = 0$), and then we investigate what happens when we include them.

1. Ideal

Assuming that nondissipative normal modes have the dependencies, $\zeta \propto e^{\mathrm{i}(x - c_1 t)}$ and $A \propto e^{-\mathrm{i}c_1 t}$ (recall our single-wave has wavenumber $k = 1$), where c_1 is the (complex) wavespeed, Eqs. (150) and (151) reduce to

$$\zeta = \frac{\kappa c_1 - \gamma}{y - c_1}\,A\mathrm{e}^{\mathrm{i}x} + c.c. \tag{152}$$

and

$$c_1 A = (\kappa c_1 - \gamma)A \int_{\mathbb{R}} dy\,\frac{1}{y - c_1} = \mathrm{i}\pi(\kappa c_1 - \gamma)A\,\mathrm{sgn}(c_{1i})\,. \tag{153}$$

The second equality of (153) is valid for all $c_{1i} \neq 0$; it is easily obtained by closing the contour with a semicircle in the upper or lower half plane, depending on the sign of c_{1i}, and using Cauchy's theorem. Solving (153) for c_1 gives

$$c_1 = \frac{\pi\gamma}{1 + \pi^2\kappa^2}\left[\pi\kappa - \mathrm{i}\,\mathrm{sgn}(c_{1i})\right], \tag{154}$$

Thus, $c_{1i} = -\pi\gamma\,\mathrm{sgn}(c_{1i})/(1 + \pi^2\kappa^2)$, which is inconsistent unless $\gamma < 0$. Since we have normalized $\gamma = \pm1$, this indicates that the system is unstable when $\gamma = -1$. However, if $\gamma = +1$, there is no consistent solution for c_{1i}, and so there are no normal modes and the system is stable.

The factor of $\mathrm{sgn}(c_{1i})$ in (153) arises because the integral has a branch cut along the real axis of the complex c_1-plane, which as noted in Sec. III reflects the continuous spectrum lying along the contour of integration. If we start from the consistent unstable solution with $c_{1i} > 0$ ($\gamma = -1$) we can follow Landau and analytically continue c_1 into the lower have plane by deforming the contour of integration so as to capture the pole. This gives

$$\int_{\frown} dz\, \frac{1}{z - c_1} = i\pi$$

where the symbol on the integral is selected to show the contour is deformed so as to enclose the descending pole. This procedure of Landau amounts to analytically continuing through the branch cut and onto a different Riemann sheet with $c_{1i} < 0$. Thus, the analytic continuation of the dispersion relation in (154), which would appear in the long time limit of the Laplace transform solution of the initial-value problem (as in Landau's classical analysis), has no $\mathrm{sgn}(c_{1i})$. The damped solutions one obtains in this case for $\gamma > 0$ correspond to the quasi-modes discussed in Sec. III.C.

Following suite for the degenerate normal form of Sec. V.B.2, we find that the normal-mode solutions satisfy

$$\zeta = \frac{\kappa c_1}{y - c_1}\, A\mathrm{e}^{\mathrm{i}x} + c.c. \tag{155}$$

and

$$A = \kappa c_1 A \int_{\mathbb{R}} dy\, \frac{1}{y - c_1} = \mathrm{i}\pi\kappa c_1 A\, \mathrm{sgn}(c_{1i})\,. \tag{156}$$

That is,

$$c = \mathrm{i}c_i, \qquad |c_i| = -\frac{1}{\pi\kappa}\,. \tag{157}$$

Hence, there are normal modes and the system is unstable if $\kappa = -1$.

2. Dissipative

Assuming that λ is constant, the dissipative modes satisfy the following equation:

$$\lambda\zeta_{yy} - \mathrm{i}(y - c_1)\zeta = \mathrm{i}(\gamma - \kappa c_1)\varphi\,. \tag{158}$$

Equation (158) can be solved by using Airy functions or Fourier transforms (*e.g.* Balmforth, 1998; Benney and Bergeron, 1969):

$$\zeta = \mathrm{i}(\kappa c_1 - \gamma)\varphi\, \mathcal{J}(y, c_1; \lambda_0, \lambda_1, \lambda_2), \tag{159}$$

where

$$\mathcal{J} := \int_0^\infty dq\, \mathrm{e}^{-\lambda q^3/3 + -\mathrm{i}q(y - c_1)}\,.$$
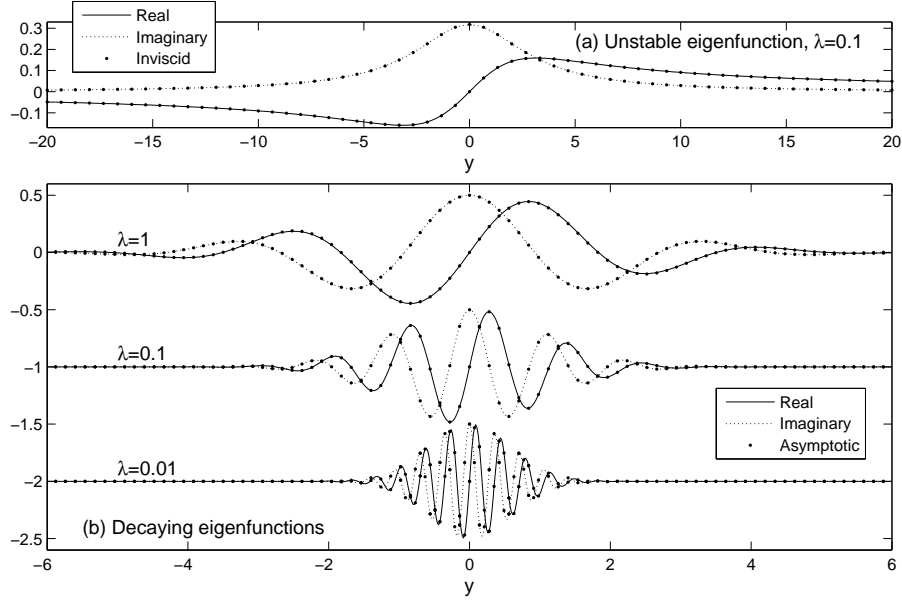
FIG. 7 Eigenfunctions for $\kappa = 0$. Panel (a) shows the unstable mode for $\lambda = 0.1$ and 0, and panel (b) the decaying modes for $\lambda = 1$, 0.1 and 0.01. Also shown in (b) is the asymptotic result of Eq. (161).

Upon inserting (159) into (151), and then interchanging the order of integration, we obtain $\delta(q)$ for the integral over y. Using this to evaluate the integral over q gives the eigenvalue,

$$c_1 = \frac{\pi\gamma}{1 + \pi^2\kappa^2}(\pi\kappa - \mathrm{i}). \tag{160}$$

Equation (160) is identical to the inviscid result, save that $\mathrm{sgn}(c_{1i})$ no longer appears. Thus, if $\gamma = -1$, the system is unstable, and the inviscid and viscous growth rates coincide. But when $\gamma = +1$, there is a decaying viscous normal mode with no inviscid counterpart. However, it does correspond to the fake eigenvalue (quasi-mode) obtained by analytical continuation of the inviscid dispersion relation.

The eigenfunctions associated with the unstable and decaying eigenvalues are illustrated in Fig. 7. The unstable viscous mode has a regular shape and smoothly limits to the inviscid eigenfunction. However, the decaying viscous modes oscillate spatially with a wavelength that becomes ever shorter as the viscous parameter λ is decreased. For $\lambda \ll 1$, the approximate shape of the decaying eigenfunctions can be found using the method of stationary phase on the integral in (159):

$$\zeta \sim \frac{\sqrt{\pi}(\kappa c_1 - \gamma)\varphi}{\lambda^{1/4}(y - c_1)^{1/4}} \exp\left[\frac{5\mathrm{i}\pi}{8} - \frac{2}{3}\mathrm{e}^{\mathrm{i}\pi/4}\sqrt{\frac{(y - c_1)^3}{\lambda}}\right]. \tag{161}$$

Clearly, this viscous mode has no regular inviscid limit.

B. The initial-value problem and Landau damping

The solution of the initial-value problem for ζ can be written in the form,

$$\zeta = -\mathrm{e}^{\mathrm{i}x}\int_0^t [\kappa A_s(s) + \mathrm{i}\gamma A(s)]\mathrm{e}^{-\mathrm{i}y(t-s) - \lambda(t-s)^3/3}\,\mathrm{d}s + \text{c.c.} \tag{162}$$

Again, the integral over y generates a delta-function, allowing the mode amplitude to be found,

$$A = A_0 \mathrm{e}^{\Gamma t}, \qquad \Gamma = \frac{\pi\gamma}{(\mathrm{i}\pi\kappa - 1)}, \tag{163}$$

where Γ is the viscous normal-mode eigenvalue. The complete solution is then given by

$$\zeta = \frac{A_0 e^{\Gamma t + ix}}{i\pi\kappa - 1} \int_0^t e^{-\Gamma s - iys - \lambda s^3/3} \, ds + \text{c.c.} . \tag{164}$$

For $\lambda \to 0$, Eq. (164) reduces to

$$\zeta = \frac{i\gamma A_0 e^{ix}(e^{\Gamma t} - e^{-iyt})}{\pi\gamma - \pi\kappa y - iy} + \text{c.c.}, \tag{165}$$

Alternatively, for $t \gg 1$, we may replace the upper limit of the integral in (164) by infinity to leading order, recovering the viscous eigenfunction in (159). Thus, if the system is unstable, the solution of the initial-value problem converges to the inviscid or viscous normal mode. When the system is stable, on the other hand, the initial-value solution converges to an exponentially decaying disturbance which is equivalent to the decaying viscous mode. In the inviscid problem, the decaying disturbance corresponds to a Landau pole or quasi-mode. It is clear from (165) that the quasi-mode has a form which is not separable in space and time (the combination $i(x - yt)$ appears), and consequently it cannot be a true normal mode. Moreover, the quasi-mode is evidently the inviscid limit of the decaying mode, as found in some related problems (Balmforth, 1998; Stewartson, 1981).

Mathematically, Landau damping results from phase mixing in integral superpositions of modes of the continuous spectrum. The solution in (163) and (165) is, in fact, one such superposition. In (165), we observe the non-decaying, non-separable factor, $\exp i(x - yt)$, reflective of the basic advection and the continuous spectrum (see Sec. III.A). This non-separable structure of the superposition is also directly responsible for Landau damping: the long-time limit of integrals of the form,

$$\int_{\mathbb{R}} dy \, \hat{F}(y) e^{i(x-yt)} ,$$

vanishes according to the Riemann-Lebesgue lemma (Stein and Weiss, 1971), provided $|F(y)|$ is integrable. Moreover, in the case where $F(y)$ is analytic in a strip containing the real y axis (as is the case for (165)), the decay is exponential, and this the mathematical essence of Landau damping.

Physically, the non-separable superposition of continuum modes describes how a perturbation in the plasma or fluid tilts over as a result of the action of particles orbiting at different speeds or from the shearing flow of fluid elements. A tilting, initially periodic, disturbance then evolves into an increasingly crenellated (phase mixed) structure as shown in Fig. 8. There is no decay in the tilting process: the plasma distribution function or fluid vorticity is simply re-arranged. However, integral averages of these quantities, such as the electric field or streamfunction, do decay as a result of increasing cancellations. This does not imply that energy dissipation takes places; merely that energy is transfered between the various components of the energy as shown in Balmforth and Morrison (2001) and Morrison and Pfirsch (1992).

Note that, although exponential decay dominates the decay of the streamfunction in the single-wave model, shear tilting normally leads to algrabraic decay in fluid shear flows (e.g. Brown and Stewartson, 1980). A full solution of the linear initial-value problem for shear flow does indeed uncover both algebraic and exponential behavior (Briggs et al., 1970). The former disappears in the single-wave expansion because it lies at higher order in the asymptotic scheme. Thus, small disturbances to stable flows would decay exponentially for a period, as the quasi-modes appear and subside, but ultimately a slower, more protracted algebraic decay sets in. This behavior is seen both in solutions of the linear initial-value problem for differentially rotating vortices, and in electron plasma experiments designed to imitate them (Schecter et al., 2000).

VII. NORMAL FORM PATTERN FORMATION

We now consider the nonlinear patterns described by the single-wave model; we first consider the unstable case ($\gamma = -1$), and then discuss the stable case ($\gamma = 1$).
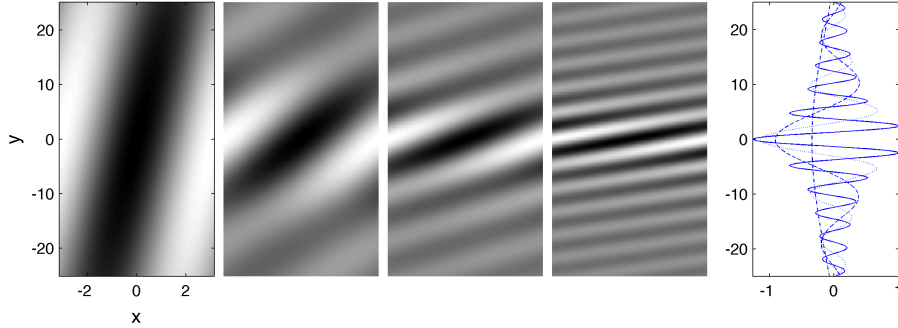
FIG. 8 Snapshots of the solution to the linear version of the single-wave model at the times, $t = 0.1$, 0.4, 0.75, and 1.5, showing the tilting of a initially periodic disturbance in a stable flow ($\gamma = 1$ and $\kappa = 0$). The right-hand picture shows the increasingly crenellated (phase mixed) distribution along $x = 0$ for the same times.

A. Pattern formation via unstable modes

A typical example of the nonlinear evolution of an unstable mode is shown in Fig. 9, computed numerically (for a description of the scheme, and more details of the computational solutions, see Balmforth *et al.*, 2001a and Balmforth and Piccolo, 2001). Initially, $A(t)$ grows exponentially as predicted by linear theory. However, when the mode amplitude reaches order one values, that growth is interrupted and the linear instability saturates. The saturation occurs when the mode twists up the total critical-layer distribution Q of (111) into a localized pattern. Beyond saturation, the mode continues to wind up the distribution, creating a well-defined cats-eye structure in Q that corresponds to vortices in the fluid and electron holes in the plasma. The final x-averaged Q in Fig. 9 shows a suppression of the original equilibrium gradient at the center of the critical region. Thus, saturation occurs when the mode removes the unstable mean gradients surrounding its critical level. Importantly, the flattened equilibrium distribution is contained well within the critical layer, and therefore occupies a much narrower region that the area spanned by the unstable gradients of the equilibrium (e.g. the bump in the plasma problem; see also Tsunoda *et al.* (1987)). A complete suppression of those gradients requires much more extensive re-arrangements, which could only be achieved if the mode amplitude saturated at a level dictated by the Hopf scaling.

Overall, the dynamics culminating in the formation of the localized structures matches that seen with full simulations. The electron hole formation displayed in Fig. 4 is ubiquitous in Vlasov-Poisson simulations of unstable equilibria (see also, e.g., Cheng and Knorr, 1976; Heath *et al.*, 2012 and references therein). Similarly, the cat's eye structures seen in Fig. 6 are a common pattern that forms in simulations of unstable shear flow. A benefit of the single-wave model is the attainment of finer resolution with equivalent computational cost.

Saturation also does not produce a steady mode amplitude. In fact, aperiodic "trapping" oscillations ensue (as they are often called by plasma physicists, since they reflect oscillations in the population of particles that are resonantly trapped in the potential created by the wave). The initial trapping oscillations are connected to the first overturns of the level sets of Q. These oscillations subside as the localized structure (the cat's eye) becomes well developed. The persistent trapping oscillations that occur much later appear to correspond to the sporadic formation of secondary structures within the localized structure that are sometimes called "macro-particles" (del-Castillo-Negrete and Firpo, 2002; Tennyson *et al.*, 1994). Unfortunately, numerical computations with finite resolution are unable to determine the ultimate fate of the system and its trapping oscillations. Phase mixing ideas (cf. Goldstein and Leib, 1988; Killworth and McIntyre, 1985; O'Neil, 1965) suggest that the secondary structures eventually become sheared out and disappear to leave a smooth, steady cat's eye. However, numerical simulations do not show much sign of the expected algebraic decay and numerical diffusion obscures the true dynamics (Balmforth and Piccolo, 2001).

In fact, explicit dissipation like the viscous term in (149) has an especially destructive effect on the cat's
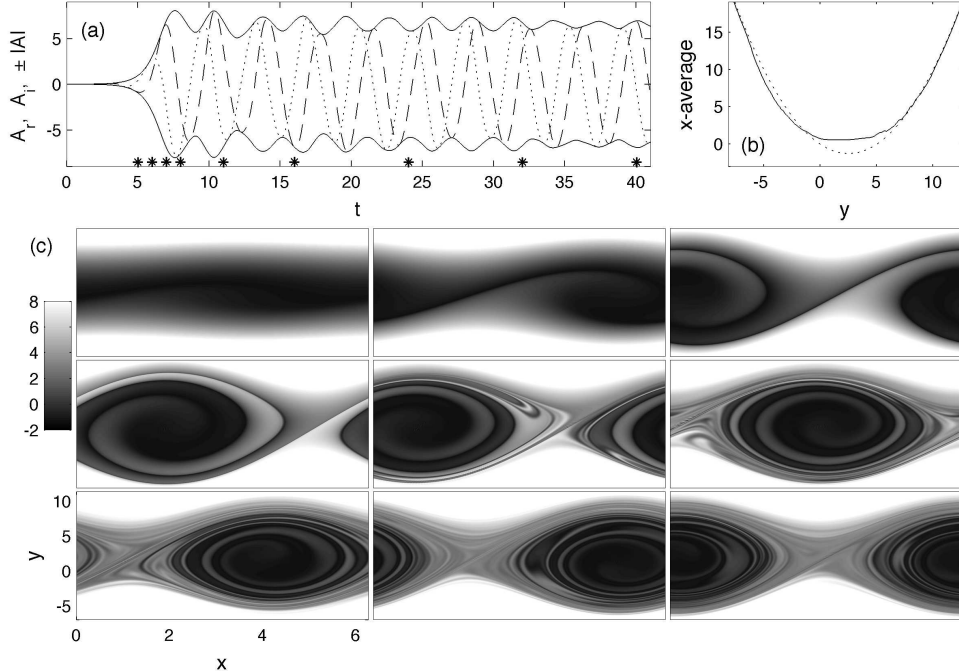
FIG. 9 Computation of an unstable mode in the single-wave model for $\gamma = -1$ and $\kappa = -0.4$. (a) shows a time series of A_r (dashed), A_i (dotted) and $\pm|A|$ (solid), and (b) shows the initial (dotted) and final (solid) x-averages of the total critical-layer distribution, $Q = -\kappa y^2/2 + \gamma y + \kappa \varphi + \zeta$. The stars in (a) denote the times at which snapshots of q are shown in (c) as densities on the (x, y)-plane,

pattern: when one adds viscosity, the rearrangements of the distribution within the critical region begin to diffuse outwards. Consequently, the cat's eyes spread and the critical layer thickens continually with time. This allows the mode to access fresh, unstable equilibrium gradients, prompting a secular growth in $A(t)$; asymptotic estimates and numerical computations indicate that $A \sim t^{2/3}$ over long times (Balmforth and Piccolo, 2001; Churilov and Shukhman, 1987a; Goldstein and Hultgren, 1988). Secular growth continues until the system passes out of the the single-wave regime. In this situation, the single-wave model only captures an initial transient and the trapping scaling is eventually broken.

B. Pattern formation in stable systems; nonlinear quasi-modes

In dissipative systems, the occurrence of instability and the resulting dynamics is usually the most interesting problem; stable systems relax back to equilibrium exponentially quickly and the only complication that can occur is if there are multiple possible end-states that "frustrate" the evolution of the system. Nondissipative systems like the pendulum, on the other hand, have an infinite number of possible periodic orbits adjacent to the stable equilibrium position, a general property of finite-dimensional Hamiltonian systems (see, e.g., Moser, 1976), and the Darwinian choice amongst them is determined by the energy of the initial condition. Stable ideal plasmas and inviscid shears also support an infinite number of adjacent wave-like nonlinear states. For Vlasov plasmas, the explicit construction of such states (the so-called BGK modes) dates back to Bernstein et al. (1958); in shear flows, Kelvin-Stuart cat's eye patterns (Drazin and Reid, 1981) are other examples. Nevertheless, despite this wealth of equilibria and the absence of dissipation, linear theory predicts that stable ideal plasma and inviscid shear flow relax through Landau damping. However, using the single-wave model, we now illustrate how sufficiently nonlinear perturbations do not continually decay.

Numerical solutions of the nonlinear initial-value problem with $\gamma = +1$ and $\kappa = 0$ and differing initial amplitudes are shown in Fig. 10 (Balmforth et al., 2001a). When the initial amplitude is sufficiently low, the numerical solutions do indeed display increasing crenellation of the distribution and the mode amplitude de-
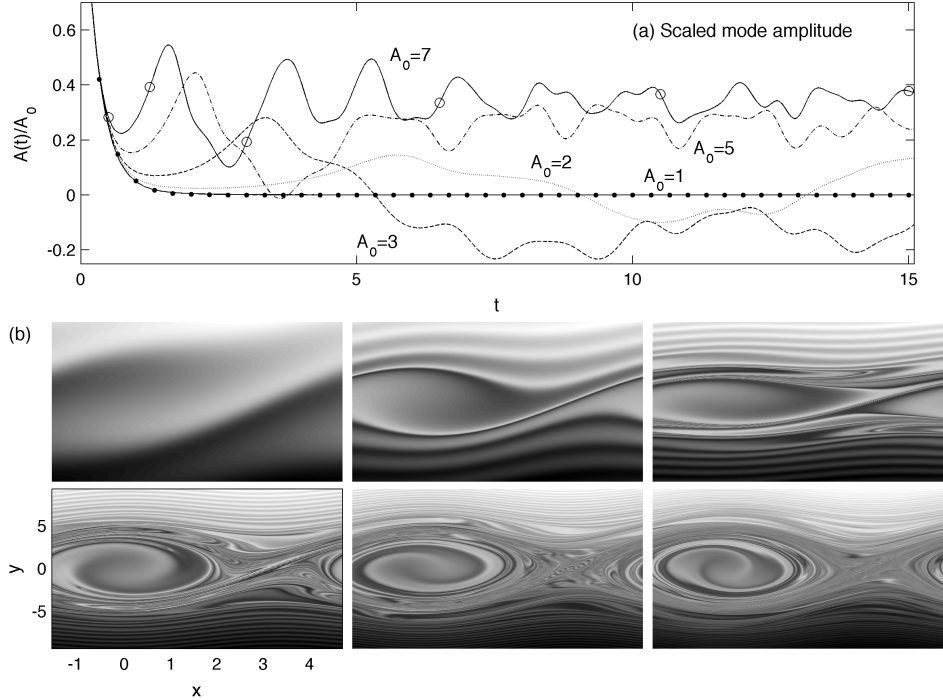
FIG. 10 Computation of a stable mode in the single-wave model for $\gamma = +1$ and $\kappa = 0$. Panel (a) shows scaled mode amplitudes, $A(t)/A_0$, for perturbations with different initial amplitude, A_0. The dots show the trend of Landau damping. Panel (b) shows the evolving cat's eye pattern for $A(0) = 7$ at the times indicated by the circles in (a). In the particular case $\kappa = 0$, the single-wave model possesses solutions with a real mode amplitude, $A(t)$, and the reflection symmetry, $y \to -y$, $x \to -x$, and $\zeta \to -\zeta$.

cays as predicted by linear theory. However, for larger initial amplitudes, the damping becomes interrupted, and the mode amplitude returns to larger values where it fluctuates unsteadily in a sequence of aperiodic trapping oscillations.

The interruption of Landau damping corresponds to the creation of another cat's eye pattern. Thus, sufficiently strong nonlinear perturbations realize Kelvin's objections (see Sec. III.B) to inviscid shear flow dynamics. The critical threshold in A_0 below which Landau damping continues unabated occurs for initial amplitudes of about unity. However, this threshold does not provide a clean criterion for the formation of a cat's eye because for slightly larger initial amplitudes (e.g. $A_0 = 2$ and 3 in Fig. 10), the mode amplitude repeatedly switches sign. This implies that the mode twists up the distribution in one direction for a period, but then the sense of overturning switches and the mode unwinds the twisted background; it is not clear whether a coherent cat's eye ever forms. Only for somewhat larger initial amplitudes ($A_0 = 5$ and 7 in Fig. 10) does the mode amplitude remain of one sign and the critical-layer distribution winds up continually into a cat's eye.

In the plasma context, the interruption of Landau damping has been observed in many computations with the Vlasov equation and in experiments (e.g., Brunetti *et al.*, 2000; Danielson *et al.*, 2004; Feix *et al.*, 1994; Franklin *et al.*, 1972; Ivanov and Cairns, 2006; Ivanov *et al.*, 2004; Lancelotti and Dorning, 2003; Manfredi, 1997; Sugihara and Kamimura, 1972). However, although the nonlinear structures are often assumed to converge to steady BGK modes, persistent trapping oscillations again render unclear the ultimate fate of the system, as for the unstable problem and illustrated by the solutions in Fig. 10, Recent computations with the Vlasov equation have also suggested that the nonlinear arrest of Landau damping depends sensitively on the type of initial distribution and may not always occur (Hui and Zhengming, 2012; Raghunathan and Ganesh, 2013; Valentini, 2005). Some mathematical considerations on the problem are offered by Lin

and Zeng (2011), and (Sedláček, 2005) provides a complementary discussion of the dynamics in Fourier-transformed velocity space. Concerns over the failure of the continuum limit in the long-time limit have also been raised Carbone *et al.* (2007) and Galeotti and Califano (2005), following on from similar, earlier considerations for the single-wave model (Firpo *et al.*, 2001).

With a simple reinterpretation of variables, the single-wave model can be applied to problems in polar coordinates (cf. Sec. II.C.1). Thus, thresholds observed in the single-wave model apply to the formation of nonlinear structures in desymmetrized vortices, both in numerical computations (Bassom and Gilbert, 1998; Bernoff and Lingevitch, 1994; Möller and Montgomery, 1999; Rossi *et al.*, 1997) and in non-neutral plasma experiments (Driscoll and Fine, 1990; Schecter *et al.*, 2000). The interest in these thresholds was sparked off by the idea that Landau damping (or, more generally, "continuum" damping, which includes algebraically decaying perturbations) could act to cause disturbed vortices to return to axisymmetry, rationalizing the preponderance of almost circular vortices in two-dimensional turbulence, and explaining the circularity and vertical alignment of hurricanes (Martinez *et al.*, 2010; Montgomery and Kallenbach, 1996; Schecter and Montgomery, 2004; Schecter *et al.*, 2002)). However, if the vortex is too distorted, then it does not return to axisymmetry, a cat's eye develops and a multipolar vortex forms. Two numerical simulations of the two-dimensional Euler equations, showing the evolution of an elliptically distorted, Gaussian vortex are shown in Fig. 11. The more weakly distorted vortex displays sub-threshold axisymmetrization, whereas the larger distortion creates a multipole. By modeling the disturbance as the response of a weakly nonlinear quasi-mode and then deriving an appropriate version of the single-wave model to describe the dynamics, Balmforth *et al.* (2001a) predicted that the critical amplitude threshold translates to an initial aspect ratio of about 1.1 (a ten percent departure from circularity); the two simulations in Fig. 11 do indeed straddle this value. Turner *et al.* (2008); Turner and Gilbert (2007, 2008) present a much more thorough analysis of the threshold for desymmetrized vortices, and some further applications are described by Turner *et al.* (2009). Le Dizes (2000) offers a complementary discussion of the problem in the limit that the critical layer is dominated by viscosity, and three-dimensional aspects of the problem are considered by Maslowe and Nigam (2008).

VIII. XY MODEL; PATTERNS OF DEGENERATE FORM

As noted in Sec. V.B.2 the XY model (also called the *Hamiltonian mean field model* by Campa *et al.* (2009) and others) provides an example of the degenerate form of the single-wave model; in this section we explore the pattern formation described by both the XY model and its degenerate single-wave form near onset. For the task, we consider the Gaussian family of equilibrium profiles,

$$R = \frac{a}{\sqrt{2\pi}} \exp\left(-\tfrac{1}{2}I^2\right) = R_0 + \varepsilon R_1 = \frac{1 + \varepsilon a_1}{\sqrt{2\pi}} \exp\left(-\tfrac{1}{2}I^2\right). \tag{166}$$

For this profile, $I_* = 0$, $R'_{1*} = 0 \Rightarrow \hat{\gamma} = 0$. Moreover, $\Omega'_* = 1$ and (because this example has a spatial kernel) $\eta = 1$, indicating

$$\nu = \fint_{\mathbb{R}} \mathrm{d}I \, \frac{R'_1}{I} = a_1. \tag{167}$$

The degenerate form of the equations of the single-wave model for this problem is therefore

$$\zeta_t + y\zeta_x + \varphi_x \zeta_y = -\kappa \varphi_t, \qquad A = \langle e^{-\mathrm{i}x}\zeta \rangle, \tag{168}$$

where $\kappa = -\mathrm{sgn}(\nu/R''_{0*})$.

In Sec. VI, we established that the system is unstable when $\kappa = -1$, and the growth rate is π^{-1}, or $-\Omega'_*\nu/(\pi R''_{0*}) \longrightarrow (a-1)\sqrt{2/\pi}$, in terms of the original variables. When $\kappa = +1$, the system is linearly stable and small perturbations decay through Landau damping; again, the exponent is $(a-1)\sqrt{2/\pi}$ for the original variables. Note that, except for the two choices, $\kappa = \pm 1$, determining the stability of the system, the degenerate form of the single-wave model of (168) has no free parameters.
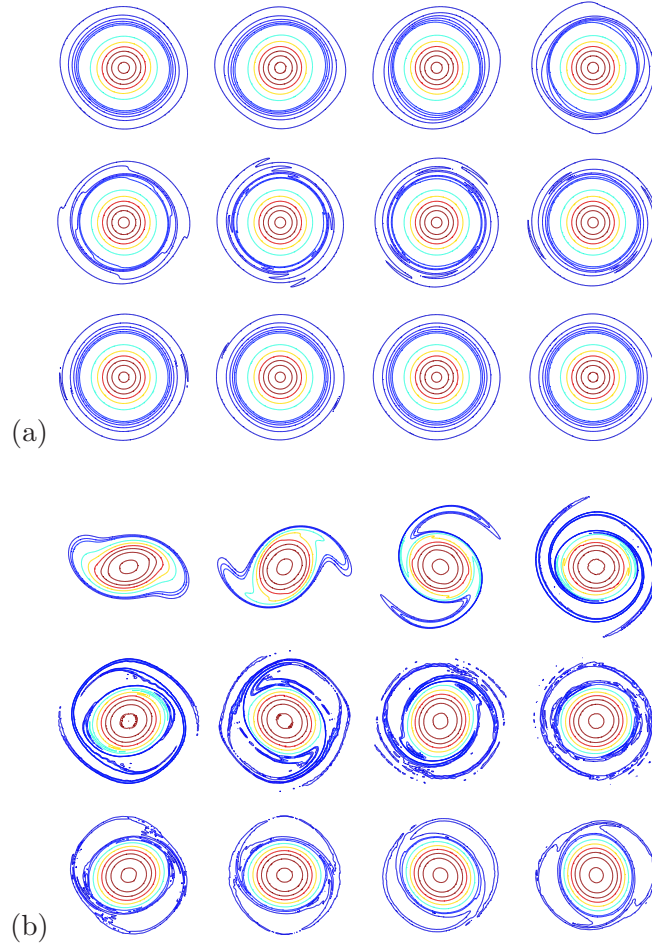
FIG. 11 Simulation results of elliptical perturbations to a stable (Gaussian) vortex. Shown are contours of constant vorticity. In panel (a) the perturbation is small and the vortex axisymmetrizes, while in panel (b) the perturbation is above a threshold for the formation of a multipole state.

A. Unstable modes and degenerate phase-space patterns

Consider now patterns that occur in the XY model with the Gaussian equilibrium profile by increasing the amplitude parameter a through unity to trigger instability. We first solve the XY model numerically by using the operator splitting scheme of Cheng and Knorr (1976). We begin the simulation by kicking the equilibrium state by adding the forcing, $10^{-4}te^{-10t^2}\cos\theta$, to the potential Φ in (32). This procedure prepares an initial condition for the dynamics after the forcing term decays to zero. Such prepared initial conditions, were called *dynamically accessible* in Morrison and Pfirsch (1989, 1990, 1992), where they were advocated because they preserve phase space constraints.

Figure 12 shows results for such a kick-started simulation with $a = 1.2$. Specifically, Fig. 12(a) displays the temporal behavior of the amplitude, $\mathcal{A}(t)$, of the potential, defined in

$$\Phi = \mathcal{A}(t)e^{i\theta} + c.c., \tag{169}$$

along with the behavior of linear growth (dashed line), for the Gaussian equilibrium depicted in Fig. 12(b). Figure 12(a) shows the solution initially following the linear growth, followed by oscillations in $\mathcal{A}(t)$ that are symptomatic of the twist-up of $\rho(\theta, I, t)$ into a cat's eye pattern around the peak of the distribution. In Fig. 12(c) we see that the corresponding average in θ of the total distribution $R(I) + \rho(\theta, I, t)$ is thereby flattened, suggesting how the instability is able to saturate itself nonlinearly. Not surprisingly, beyond
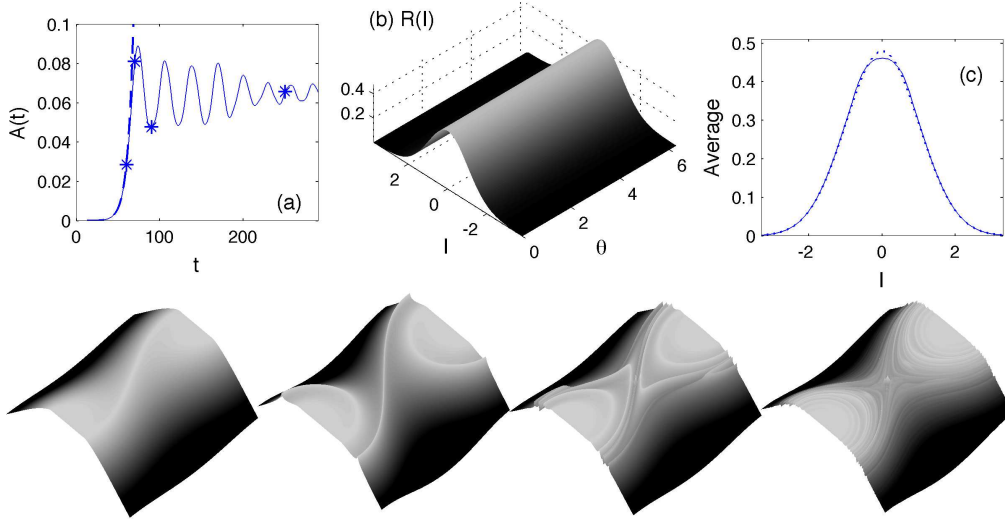
FIG. 12 Kicked (dynamically accessible) solution of the XY model of (168) for the Gaussian equilibrium distribution of (49) with $a = 1.2$. Panel (a) shows the mode amplitude, $\mathcal{A}(t)$, along with the expected linear growth (dashed line). Panel (b) shows the equilibrium distribution as a surface over the (θ, I)-plane. Panel (c) shows the initial and final θ-averages of the total density. The stars in (a) indicate the times of the snapshots of the total density $R(I) + \rho(\theta, I, t)$ shown in the lower row as surfaces over the (θ, I)-plane, focussing on the central maximum.

saturation, trapping oscillations continue in $\mathcal{A}(t)$. Figure 12(d) depicts snapshots of the total distribution at the times indicated by the stars in Fig. 12(a), and shows how cat's eyes develop during saturation.

Figure 13(a) shows scaling data obtained from a suite of computations of the type depicted in Fig. 12; the first maximum of $\mathcal{A}(t)$ is plotted (cf. Fig. 12(a)) against the control parameter a. This figure verifies the trapping scaling of the saturation level.

The remaining two panels of Figure 13 show the numerical solution of the degenerate form of the single-wave model in (117)–(121). The system is again kicked into action by suitably forcing the potential φ. The unstable mode grows and saturates in a similar manner to the dynamics seen for the full XY model in Fig. 12. The mode amplitude, $A(t)$, peaks first for $A_m \approx 0.52$, which leads to a prediction for the first maximum of $\mathcal{A}(t)$ in terms of the original variables: $\mathcal{A}_{max} \approx 2\pi A_m(a-1)^2$. This prediction is included in Fig. 13(a); the scaling data for the amplitude maxima from the full XY model computations converge satisfyingly to the prediction. Note that trapping scaling means that the rearrangment of $\rho(\theta, I, t)$ is unable to suppress the distribution to the point where the θ-average shown in Fig. 12(c) corresponds to a linearly stable equilibrium.

B. Patterns in stable systems; nonlinear Landau damping in the XY model

The parallels between the XY model and the Vlasov equation, together with the fact that both can be reduced to the single-wave model in the vicinity of onset, suggests that the XY dynamics should also display pattern formation even when $a < 1$, provided the system is forced with sufficient strength. That is, the XY model should display a nonlinear arrest of Landau damping akin to that discussed in Sec. VII.B. To confirm this expectation we once more solve the initial-value problem for the full XY model, again initiating the computations by applying a suitable kick to the potential.

Figure 14 shows a computation in which a stable Gaussian equilibrium with $a = 0.9$ is forced by adding to $\Phi(\theta, t)$ the external potential,

$$\Phi_e = 2\mathcal{A}_0 t e^{-10t^2} \cos\theta. \tag{170}$$

In Fig. 14(a) a plot of the logarithm of $\mathcal{A}$ vs t is shown for a drive amplitude $\mathcal{A}_0 = 0.5$. This plot shows
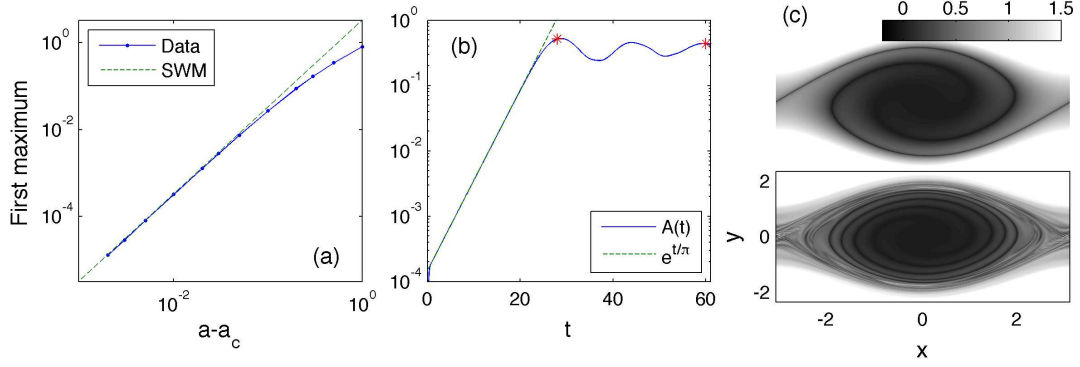
FIG. 13 Numerical results for the XY model with Gaussian equilibrium and kick start (cf. Fig. 12). Panel (a) shows scaling data for the XY model, with the height of the first maximum in $\mathcal{A}(t)$, the amplitude of the potential, plotted against the control parameter $a-1$. Also shown is the trapping scaling prediction of the single-wave model (SWM, dashed line). Panels (b) and (c) show the numerical solution of the degenerate single-wave model: panel (b) shows the mode amplitude, $A(t)$, vs. time, t, along with the expected linear growth (dashed line); the stars of this panel mark times for the snapshots of the solution, $Q = \frac{1}{2}y^2 + \zeta - \varphi$, shown as densities on the (θ, I)-plane in panel (c).

how the initial decay becomes interrupted for a sufficiently large initial perturbation, as in Vlasov-Poisson simulations (e.g., Cheng and Knorr, 1976; Heath *et al.*, 2012). Fig. 14(c) displays plots of the total density at the times indicated by the stars in Fig. 14(a); the interruption of Landau damping is caused by trapping and the emergence of the nonlinear quasi-modes visible in these images. These cat's eye structures are symmetrically displaced about the maximum of the original equilibrium profile at $I = 0$. Reducing the amplitude of the initial kick as in Fig. 14(b) prolongs the transient in which the system decays through Landau damping, but we have not attempted to compute any threshold below which that damping continues unabated. Further explorations of nonlinear Landau damping in the XY model are presented by Barré and Yamaguchi (2009).

C. Smoothing the top-hat profile

The XY model is convenient for exploring the differences between the dynamics underlying trapping and Hopf scaling. In this section we explore these differences in detail by considering the instabilities of a family of equilibrium profiles in which we smooth out the discontinuities of the top-hat profile of (31), As discussed in Sec. III.D, the top-hat profile (analogous to a broken-line shear flow or "water-bag" Vlasov equilibria) has a bifurcation to instability at $a = 1$ with $c = 0$, much like the Gaussian profile. However, we argued earlier (Sec. IV.A), the instabilities of the top-hat profile are expected to be affected by nonlinearity at strengths characterized by the Hopf scaling and be *subcritical*. In other words, the transition to instability for the top-hat profile is quite different from that for a smooth equilibrium profile like the Gaussian.

The family of equilibrium profiles we adopt are given by

$$R = \frac{a}{4}\left[\tanh\left(\frac{I+1}{\Upsilon}\right) - \tanh\left(\frac{I-1}{\Upsilon}\right)\right], \tag{171}$$

where Υ is a parameter controlling the narrowness of the hyperbolic tangent functions. When Υ is decreased from order one values, the steps in the profile at $I = \pm 1$ sharpen, and for $\Upsilon \to 0$ limit to the discontinuities of the top-hat. Using these profiles, we again conduct suites of initial-value problems; as for the Gaussian examples above, we begin these computations with $\rho(\theta, I, 0) = 0$ and kick the system into action by adding the forcing (170) to the potential, $\Phi(\theta, t)$, with $\mathcal{A}_0$ taken to be small (10^{-4}), at least initially.
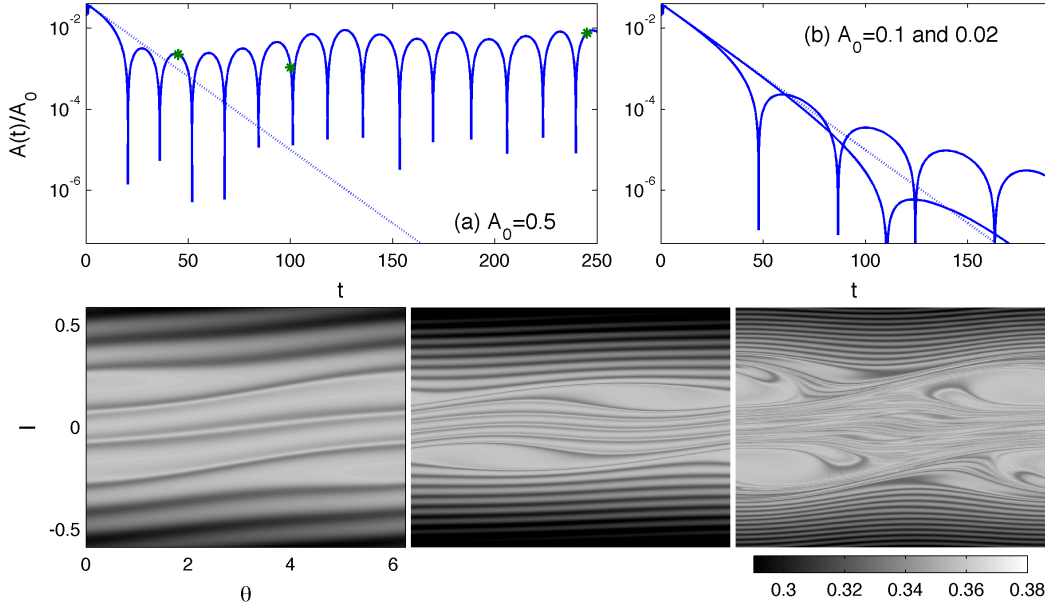
FIG. 14 Solutions to the nonlinear XY model for $a = 0.9$, initiated by adding the external forcing (170) to the potential $\Phi(\theta, t)$. In panel (a) $\mathcal{A}_0 = 0.5$, and the stars indicates the times at which snapshots of $\rho(\theta, I, t)$ are shown below in panel (c) as densities on the (θ, I)-plane. In panel (b), the smaller values of $\mathcal{A}_0 = 0.1$ and 0.02 are used, and longer intervals of Landau damping are observed. The dotted lines in (a) and (b) indicate the solution to the linear problem.

Figure 15 displays scaling data for the smoothed top-hat profiles of (171). For $\Upsilon > 1/4$, the first maximum, $\mathcal{A}_*$, follows the trapping scaling predicted by the single-wave model sufficiently close to the stability boundary (see panel (b)). However, as the profile becomes sharper, the trapping prediction for $\mathcal{A}_*$ increases exponentially quickly (with $\mathcal{A}_*$ proportional to $(R_{0*}'')^{-2} \propto \Upsilon^2 \cosh^4(1/\Upsilon)$), and the system is unable to remain in the trapping regime much beyond onset. Instead, the saturation level flattens off quickly beyond the trapping regime and $\mathcal{A}_*$ approaches a different scaling that we interpret to be more like that for a genuine top-hat profile (e.g. $\Upsilon = 0.28$). Indeed, for the lowest values of Υ (e.g. $\Upsilon = 1/8$), the trapping regime is no longer observed and $\mathcal{A}_*$ remains finite as $a \to a_c$, which is consistent with the subcritical bifurcation of the top hat profile.

The detection of a finite-amplitude branch of solutions for $a \geq a_c$ with low Υ suggests that an unstable subcritical branch is born in the bifurcation at $a = a_c$, and that this branch subsequently turns around at smaller values of a, That is, there must be a second, saddle-node bifurcation for $a < a_c$, which generates the larger-amplitude stable solutions that return to higher a and provide the end-states of the initial-value computations. Thus, for the top-hat profile, or its relatively sharp smooth relatives of (171) with $\Upsilon \ll 1$, the instability has an abrupt onset.

For intermediate values of Υ (e.g. $\Upsilon = 1/4$), the system first follows the trapping scaling and, therefore, initially shows a relatively smooth transition. However, the branch's amplitude subsequently increases quickly and becomes vertical. The branch then disappears (no doubt by turning back on itself), leaving the system to grow to higher amplitudes and achieve a first maximum closer to that of the corresponding top-hat solution. The amplitude data in Fig. 15(b) is thereby rendered discontinuous. In other words, although the profile with $\Upsilon = 1/4$ initially suffers a second-order phase transition following the trapping scaling, the transition can appear to become first-order if the system is pushed too far beyond the single-wave regime.

Because we begin the initial-value computations from a weakly perturbed equilibrium profile parameterized by a, the solutions do not converge to any finite amplitude solutions for $a < a_c$, but Landau damp back to the unpatterned equilibrium. Nevertheless, it is possible to initialize computations with stronger kicks in this parameter regime (i.e. perturb the system with larger values for $\mathcal{A}_0$). The resulting initial-value problems then display a clear threshold behavior, as illustrated in Fig. 16: for lower values of $\mathcal{A}_0$, the system executes regular, weakly decaying oscillations with an amplitude set by $\mathcal{A}_0$, as seen for the cases with
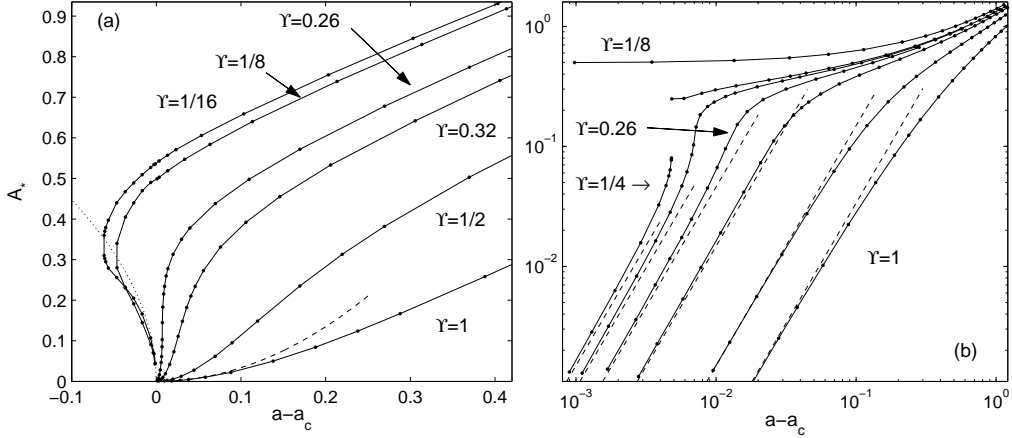
FIG. 15 Scaling data for the first maximum, $\mathcal{A}_*$, plotted against distance to the stability boundary, $a - a_c$, for the smoothed top-hat profiles of (171) for various values of the smoothing parameter, Υ. Panel (a) shows data for $\Upsilon = 1/16$, 1/8, 0.26, .32, 1/2 and 1. Panel (b) plots the same data logarithmically (omitting $\Upsilon = 1/16$), and includes additional data for $\Upsilon = 0.25$ and 0.28. The dashed lines indicate the prediction of the single-wave model, and the dotted curve in (a) is the subcritical weakly nonlinear solution expected for the top-hat.
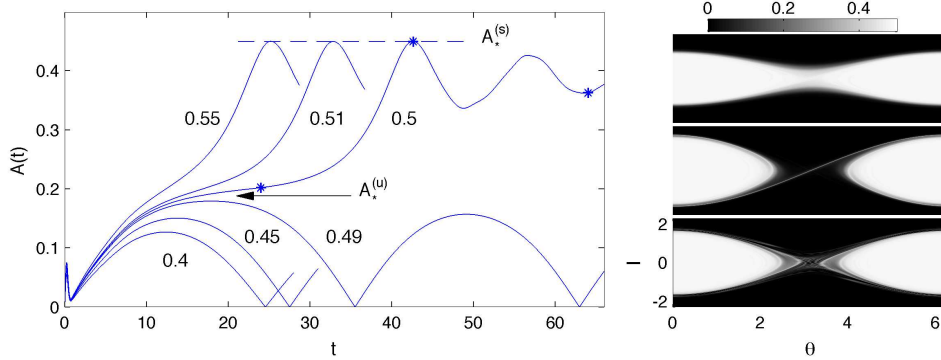

FIG. 16 Panel (a) depicts $\mathcal{A}(t)$, for $a = 0.96 < a_c \approx 0.986$ and $\Upsilon = 1/8$, for computations kicked with different amplitudes $\mathcal{A}_0$ for the forcing (170) added to $\Phi(\theta, t)$. The values of $\mathcal{A}_0$ are as shown and the "stable" and "unstable" first maxima, $\mathcal{A}_*^{(s)}$ and $\mathcal{A}_*^{(u)}$, are also indicated. For $\mathcal{A}_0 = 0.5$, the stars indicate the times of the three snapshots of $\rho(\theta, T, t)$ shown in panel (b) to the right.

$\mathcal{A}_0 = 0.4$, 0.45 and 0.49 in Fig. 16. Simultaneously, $\rho(\theta, I, t)$ develops no persistent phase-space pattern. Larger forcings, however, trigger a growth of the mode amplitude upto a level, $\mathcal{A}_*^{(s)}$, that is otherwise independent of $\mathcal{A}_0$, as seen for $\mathcal{A}_0 = 0.5$ and higher in the figure. The system subsequently executes trapping oscillations and $\rho(\theta, I, t)$ develops a cat's eye pattern much like the end states generated in the linearly unstable regime.

The threshold forcing amplitude $\mathcal{A}_0$ corresponds to a first maximum, $\mathcal{A}_*^{(u)}$ that we assume is characteristic of the unstable subcritical nonlinear state. On the other hand, the nonlinear states identified by $\mathcal{A}_*^{(s)}$, are plausibly the stable solutions on the upper branch. By recording the two first maxima, $\mathcal{A}_*^{(u)}$ and $\mathcal{A}_*^{(s)}$, we are therefore able to continue the scaling data of Fig. 15 to $a < a_c$ for the cases with sharper equilibrium profiles ($\Upsilon = 1/16$ and 1/8). As expected, the data for $\mathcal{A}_*^{(s)}$ continue the original results for the first maxima from $a > a_c$ into the linearly stable regime. Moreover, this stable branch eventually terminates at lower a by colliding with the unstable branch characterized by $\mathcal{A}_*^{(u)}$. As illustrated in Fig. 15(a), the latter converge

towards the weakly nonlinear solution branch predicted for a true top-hat profile (as given by the weakly nonlinear theory of Sec. IV.A.3 which, after a translation of $|A| = \sqrt{-2a_2}$ back into the original unscaled variables, furnishes $\mathcal{A}_*^{(u)} = \sqrt{2(1-a)}$).

In summary, top-hat (or broken-line and water-bag) equilibrium profiles display a very different nonlinear dynamics at onset to that of smooth profiles. The differences between the two in linear theory is well appreciated: the linear eigenspectra of smooth, stable profiles are characterized purely by the continuous spectra, which leads to Landau damping (or, more generally, to "continuum damping" for shear flows, for which algebraic decay also appears), whereas piecewise linear profiles support persistent discrete waves riding on the interfaces of the equilibrium. That the weakly nonlinear states are also very different is not, however, so well acknowledged.

IX. VARIANTS AND DEVIANTS

So far we have seen several examples of single-wave model dynamics, viz., the patterns that form when equilibrium gradients inside the critical layer are wound up to saturate an unstable mode or arrest Landau damping. We next mention a number of variations on this single-wave theme.

A. Long-wave theories and subharmonic instability

An important ingredient in our derivation of the single-wave model is the imposition of periodicity in x, which leads to a wave-like global mode with a critical layer. Different boundary conditions would imply a different global mode structure in x and furnish a "single-mode" theory near the onset of instability. Alternatively, in spatially extended systems entire bands of wavenumber become unstable, rather than a distinguished neutral mode. In asymptotic analysis, one accounts for a finite bandwidth by introducing multiple lengthscales, with the long length scale describing the spatial modulation of unstable patterns.

For systems suffering a long-wave instability the situation is more straightforward, since then one retains only a single, long length scale. When the unstable system also suffers critical-level singularities, the global mode amplitude depends on both the slow time and the long length scale, and the resulting weakly nonlinear theory couples familiar nonlinear wave equations to the critical-layer dynamics. Following this route in shear flows, Balmforth and Young (1997) and Stewartson (1981) coupled critical layers to the nonlinear Schrödinger equation and Boussinesq equations, respectively. More recent developments are provided by Shagalov *et al.* (2009).

When the unstable wavenumber is finite, an alternative to solving the full multiple scale theory is to reconstitute the two spatial variables back into a single one. A single-wave-like model is then recovered, but contains additional spatial derivatives capturing larger-scale spatial modulations of the wave patterns. This route has been followed by Shagalov *et al.* (2010).

Models with spatial modulation incorporate a key physical effect: the subharmonic secondary instability of a chain of cat's eyes that can lead to pairings of the vortices or plasma holes (e.g. Flierl *et al.*, 1987; Winant and Browand, 1974 and Feix *et al.*, 1994; Shoucri, 2008, respectively). This instability is easily illustrated for the simulation of a jet pictured earlier in Fig. 6. In that simulation, the third Fourier mode in x is unstable and grows to create the cat's eye pattern displayed in the figure; the lower overtones initially had zero amplitude, and any round-off errors that might otherwise excite these modes were deliberately suppressed. Once those lower overtones are allowed to develop, on the other hand, we arrive at the evolution shown in Fig. 17, in which a pairing instability of the cat's eyes emerges to destroy the pattern. This dynamics is not captured by the single-wave description, and is one of its main limitations. In plasma physics, the breakdown of the single-wave model in describing unstable plasma waves as a result of subharmonic instability has been well studied, both theretically and experimentally (*e.g.* Dimonte and Malmberg (1978); Hartmann and Driscoll (2001); Matsiborko *et al.* (1973); Shoucri (1980); and Wharton *et al.* (1968)), with a view towards understanding the progression to the regime of quasi-linear theory (Krall and Trivelpiece, 1973). There has also been recent interest in the question of whether subharmonic instability always impact BGK-type equilibria, like those appearing in the single-wave model, or if stable multi-hole solutions can exist in some spatial domains (Balmforth, 2012; Guo and Strauss, 1995; Lin, 2001, 2005; Manfredi and Bertrand, 2000).
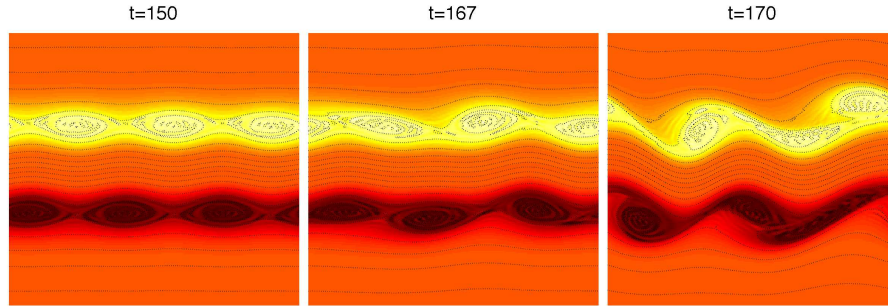
FIG. 17 Subharmonic instability in an unstable jet. The panels show the late evolution of the jet after an unstable mode with x-wavenumber three grows to create a symmetrically placed pair of cat's eye patterns. In contrast to Fig. 6, the lower overtones were allowed to be excited by round-off error during the earlier parts of the computation, resulting in a subharmonic, vortex pairing instability.

B. Modified single-wave models and forced critical layers

The instability in the single-wave model results from the equilibrium gradients within the critical layer; once these gradients are twisted up by the global mode, the instability saturates (unless it can be reactivated by viscous diffusion). In other situations, the global mode can be rendered unstable by a different mechanism, and the instability competes with Landau damping in a critical layer (Balmforth and Young, 2002; see also Esler and Willcocks, 2012; Warn and Gauthier, 1989; Willcocks and Esler, 2012). The weakly nonlinear theory describing this situation is much like the single-wave model (with $\gamma = +1$), except that the amplitude equation for $A(t)$ contains a linear growth term. However, the unstable mode is not then able to saturate: as the mode grows, it twists up the critical-layer distribution into cat's eyes, removing the stabilizing equilibrium gradients that damp the mode. Consequently, the mode amplifies even faster, twisting up an ever wider critical layer until the trapping scaling is broken.

The opposite physical situation arises when the mode is driven by unstable equilibrium gradients within the critical layer, but damped globally (such as in the two-species plasma model with disparate ion masses explored by Balmforth and Kerswell (2002)). Then, the amplitude equation contains a linear decay term, and saturation again arises when the destabilizing equilibrium gradients in the critical layer are twisted up into cat's eyes. However, the global damping is unaffected by those critical layer rearrangements and continues to damp the mode beyond saturation, forcing a subsequent decline in mode amplitude. The ultimate decay of the mode appears to be halted by the migration of the cat's eye across the critical region, which allows the mode to access fresh equilibrium gradients (Balmforth and Kerswell, 2002).

Another natural variation on the theme is to couple more waves in the outer region with the critical layer, furnishing multi-wave models. In fluid mechanics this has been done for coupled Rossby waves (Vanneste, 1996), wind-excited water waves (Alexakis et al., 2004; Reutov, 1980), over-reflectional instabilities in shallow-water and compressible shear flows (Balmforth, 1998), and even-odd mode interactions in jets (Leib and Goldstein, 1989). In plasma physics, additional waves were included in extensions of the original single-wave model to explore subharmonic instability and the transition to the quasi-linear regime (Besse et al., 2011; Dimonte and Malmberg, 1978; Matsiborko et al., 1973; Volokitin and Krafft, 2012; Zaslavsky et al., 2008). More recently, multiple waves have been added in relativistic beam-plasma systems (Evstatiev et al., 2003, 2005) and in models of plasma turbulence (Cary et al., 1992; Doxas and Cary, 1997). Other problems that could be attacked in this way (but have not yet been) include ion acceleration in the central plasma sheet of the Earth's geotail (Padhye and Horton, 1999) and the instability of inviscid flow over compliant walls (Benjamin, 1963; Landahl, 1962).

In these examples, the wave dynamics is, by itself, linear, and the nonlinearity of the problem arises from the twisting-up of the critical layer, as in the standard single-wave model. A slightly different version of the multi-wave problem is the so-called beat-wave resonance of plasma theory (Crawford et al., 1986; Crawford and O'Neil, 1987), which has also been applied to vortex dynamics (Ait et al., 2011; Friedland and Shagalov,

2002; Mattor *et al.*, 2006; Mitchell and Driscoll, 1994) and astrophysical disks (Mattor and Mitchell, 1996). Here, two regular wave modes are coupled through a triad nonlinear resonance to a singular mode with a critical layer. Conventional beat-wave theory treats the critical-layer dynamics in a purely linear fashion, adding the Landau damping of the singular mode. Depending on the degree of re-arrangements inside the critical layer, however, one can envision situations in which the nonlinear critical-layer dynamics may become important, which calls for a generalization of the theory along the lines of the development of the single-wave model.

A more complicated extension of the single-wave model arises in shear flows with either density strat-ification or embedded magnetic fields. In such situations, one must add more dynamically evolving fields inside the critical layer to capture the evolution of the fluid density or the magnetic field; the result is a modal amplitude equation coupled to a pair of partial differential transport equations describing the critical layer (Shukhman, 1998a; Shukhman and Churilov, 1997). Miller (2004) presents a related example arising in the analysis of viscoelastic shear instability.

The critical layer in the single-wave model is rearranged due to the growth of a global mode. In other problems, there is no such mode and the critical layer is directly forced by an external perturbation. Models describing these situations contain a critical-layer equation in which the potential or streamfunction, φ, is determined not by an evolution equation but directly from the integral critical-layer distribution and the global forcing (as in the degenerate form of the single-wave model; Sec. V.B.2). The classic example of such a problem in fluid mechanics is the forced Rossby wave critical layer where waves excited by a uneven boundary enter a shear flow and impinge on the critical level (Redekopp, 1977; Stewartson, 1978; Warn and Warn, 1978). However, the theory has also been applied to a differentially rotating accretion disk perturbed by a forming planet (Balmforth and Korycansky, 2001), which is key in modeling angular momentum exchange and the migration of extra-solar planets (Goldreich and Tremaine, 1979; Papaloizou and Terquem, 2006). A novelty of forced critical layers is that the global potential or streamfunction contains a richer wavenumber content than the single-wave model. As a result, the filamentation of the critical layer distribution can suffer secondary instability (Killworth and McIntyre, 1985), with the filaments rolling up into smaller vortices and generating more filamentation. A cascade ensues, leading to what Haynes (1985) has coined "critical-layer turbulence".

All of the critical-layer models described above have the common feature that inside the critical region, the differential advection in y is locally linear. Theories that consider a critical layer located at the tip of a fluid jet where the flow is locally parabolic (Balmforth *et al.*, 2001b; Brunet and Haynes, 1995; Brunet and Warn, 1990) lead to a shearing term with quadratic form $y^2 \zeta_x$. Disturbances in the linear initial-value problem are then found to decay algebraically as well as exponentially. Thus Landau damping is supplemented by a weaker form of continuum damping near the shearless point of the velocity profile. Moreover, the phase-space patterns that are generated can show a richer topology (see del-Castillo-Negrete and Morrison, 1993), taking the form of either stacked cat's eyes or other kinds of patterns (Balmforth *et al.*, 2001b).

C. Singular neutral modes

Another key feature of the single-wave model is that the distinguished neutral mode that we perturb off the stability boundary is smooth. However, the distinguished mode need not be regular. For example, although symmetrical jets like that illustrated in Fig. 6 have smooth neutral modes, when the profile is made asymmetrical it generally becomes impossible to satisfy the condition, $U''(y_*) = U(y_*) - c_r = 0$, at both critical levels simultaneously. The neutral modes on the stability boundary then become singular, and the inner expansion for the critical layer is needed in the leading order of the asymptotics. Other examples include instabilities of Rossby waves (Hickernell, 1984), stratified, compressible, magnetized or three-dimensional shear flow (Churilov, 2009, 2011; Churilov and Shukhman, 1994, 1995; Churilov, 1999; Goldstein and Choi, 1989; Goldstein and Leib, 1989; Shukhman, 1998b), and two-species plasmas (Balmforth and Kerswell, 2002; Berk *et al.*, 1996, 1999; Crawford and Jayaraman, 1996, 1999).

Because one has to re-order the asymptotic expansion for singular distinguished modes, the trapping scaling is no longer the relevant measure of the mode amplitude. It turns out that nonlinearity first be-comes important at the level $\epsilon^{5/2}$. This conclusion was reached by Crawford and Jayaraman, 1996, 1999, using center-manifold methods, but once more this formal analysis does not furnish a convenient amplitude

equation. Again matched asymptotics rescues the situation, although the expansion must be taken to much higher order than in the single-wave case. The results of the expansion are also quite different, with the analysis eventually predicting a delay-differential equation for the mode amplitude (Balmforth and Kerswell, 2002; Berk *et al.*, 1996, 1999; Churilov, 2009, 2011; Churilov and Shukhman, 1994, 1995; Churilov, 1999; Goldstein and Choi, 1989; Goldstein and Leib, 1989; Hickernell, 1984; Shukhman, 1998b). Unfortunately, that equation predicts that nonlinearity is destabilizing: beyond the initial phase of linear growth, the nonlinear terms promote an explosive growth of the mode amplitude. As a result, the mode rapidly leaves the "singular scaling" and only a transient is described by the model, unless there is a significant dissipation which can halt the divergence (*e.g.* Berk *et al.* (1996); Churilov (1999); and Goldstein and Leib (1989)).

X. CONCLUDING REMARKS

For a pattern theorist, the single-wave model could be regarded as unsatisfactory because it offers no reduction in the dimension of the problem. Yet despite the lack of dimensional reduction, the single-wave model has several virtues over the original equations. First, mathematically, the model equations offer some simplifications over the full problem, but nevertheless captures the important dynamical behavior, such as the creation of cat's eyes. Second, the model appears in a wide range of different problems, and therefore provides a universal description of pattern formation in a variety of systems with continuous spectra.

Given this universality, it is worthwhile emphasizing the key properties of the original problem that are required for the single-wave model to emerge as the weakly nonlinear description in the vicinity of onset. As we have outlined, the single-wave model requires periodic boundary conditions in the direction of the equilibrium streaming or flow, and a regular neutral mode lying on the stability boundary to open the expansion of asymptotic theory. However, by themselves these properties are not sufficient to lead to the single-wave model: the so-called "Kuramoto model" describes a population of coupled oscillators with fixed amplitude and varying phase and natural frequency that is coupled through a mean field (Kuramoto, 1975; Strogatz, 2000). The continuum limit of this model furnishes a partial differential system that possesses equilibrium solutions corresponding to populations with randomly distributed phases. The associated linear problem has a continuous spectrum, stable populations exhibit Landau damping, and instabilities arise when a distinguished neutral mode detaches from the continuum (Crawford and Davies, 1999; Strogatz *et al.*, 1992). However, the nonlinear dynamics of the instability, and the phase-synchronized population patterns that form, are quite different from the cat's eyes of our fluid and plasma problems (Balmforth and Sassi, 2000). The similarity in the linear problem is therefore misleading, and simply the presence of a distinguished mode bifurcating from the continuum is not sufficient to anticipate the single-wave model.

In fact, a key difference between the Kuramoto model and our plasma and fluid problems is that the former does not possess a Hamiltonian structure. An underlying Hamiltonian structure undoubtedly impacts any weakly nonlinear description. Nevertheless, the complete classification of models for which the single-wave model is an appropriate normal form has not been performed, and an underlying Hamiltonian structure may be neither necessary nor sufficient. There is, however, a Hamiltonian interpretation of the bifurcations to instability of the single-wave model. For example, the normal from case can be viewed a a continuum version of the Hamiltonian-Hopf bifurcation, which generalizes the discrete Kreĭn (Kreĭn, 1950) transition that is known to occur in a variety of fluid and plasma systems (e.g., Cairns, 1979; Casti *et al.*, 1998; Kueny and Morrison, 1995; MacKay and Saffman, 1986; Morrison and Kotschenreuther, 1990; Sturrock, 1958; Tassi and Morrison, 2011; Tassi *et al.*, 2008). This will be the subject of a future publication (Hagstrom and Morrison, 2013).

Some other open questions are as follows. First, the single-wave model describes the saturation of an unstable mode that twists up the destabilizing equilibrium gradients in its critical layer. However, in the single-wave scaling, the critical layer is much thinner than the range of unstable gradients, and saturation occurs when the background equilibrium has been flattened over only a small fraction of that range. Why does the mode not continue to grow and feed off the unstable gradients outside the narrow critical region? The answer surely lies in the fact that the system is constrained by the need to conserve the infinite number of Casimir invariants of Sec. II.A. Also, when dissipation is added to the system, the mode begins to grow secularly beyond saturation. Thus, the saturated single-wave system looks very much like a negative energy state of a finite-dimensional Hamiltonian problem with dissipation-induced instability (Krechetnikov and Marsden, 2007; Morrison, 1998; Morrison and Kotschenreuther, 1990).

Second, as mentioned earlier, it is not clear what is the ultimate fate of the unstable mode. Beyond saturation, aperiodic trapping oscillations occur that attenuate somewhat with time. However, one cannot decide whether the oscillations persist, or if the system relaxes to a steady BGK mode. One often observes the intermittent creation and subsidence of secondary structures, or macroparticles, which contribute to the aperiodic motion (Tennyson *et al.*, 1994), albeit possibly with a dominant frequency. If the trapping oscillations continue indefinitely, then the critical region is in a constant state of agitation, and prolonged chaotic mixing occurs across the cat's eyes (del-Castillo-Negrete, 2000).

ACKNOWLEDGMENTS

REFERENCES

Ait, A. H., K. Siddiqui, G. H. Vatistas, M. Fayed, and H. D. Ng, 2011, Physical review. E, Statistical, nonlinear, and soft matter physics **83**(5 Pt 2), 056319.

Alexakis, A., R. Rosner, and Y.-N. Young, 2004, J. Fluid Mech. **503**, 171.

Allis, W. P., 1959, in *Electrons, Ions, and Waves, Selected Works of William Phelps Allis*, edited by S. C. Brown (MIT Press, Cambridge Massachuetts), volume 1, pp. 269–279.

Allis, W. P., S. J. Buchsbaum, and A. Bers, 1963, *Waves in anisotropic plasmas* (MIT Press, Cambridge, Massachuetts).

Antoni, M., and S. Ruffo, 1995, Phys. Rev. E **52**, 2361.

Antoniazzi, A., G. De Ninno, D. Fanelli, A. Guarino, and S. Ruffo, 2005, in *Journal of Physics: Conference Series* (IOP Publishing), volume 7, p. 143.

Antoniazzi, A., D. Fanelli, S. Ruffo, and Y. Y. Yamaguchi, 2007, Phys. Rev. Lett. **99**, 040601.

Bachelard, R., C. Chandre, A. Ciani, D. Fanelli, and Y. Y. Yamaguchi, 2009, Phys. Lett. A **373**, 4239.

Backus, G., 1960, J. Math. Phys. **1**, 178.

Balmforth, N., 2012, Communications in Nonlinear Science and Numerical Simulation **17**(5), 1989.

Balmforth, N. J., 1998, J. Fluid Mech. **357**, 199.

Balmforth, N. J., 1999, J. Fluid Mech. **387**, 97.

Balmforth, N. J., D. del-Castillo-Negrete, and W. R. Young, 1997, J. Fluid Mech. **333**, 197.

Balmforth, N. J., and R. R. Kerswell, 2002, J. Plasma Phys. **68**(2), 87.

Balmforth, N. J., and D. Korycansky, 2001, Mon. Not. Roy. Astron. Soc. **326**, 833.

Balmforth, N. J., S. G. Llewellyn Smith, and W. R. Young, 2001a, J. Fluid Mech. **426**, 95.

Balmforth, N. J., and P. J. Morrison, 1999, Stud. Applied Math. **102**, 309.

Balmforth, N. J., and P. J. Morrison, 2001, in *Large-Scale Atmosphere-Ocean Dynamics 2: Geometric Methods and Models*, edited by J. Norbury and I. Roulstone (Cambridge University Press, Cambridge, U.K.).

Balmforth, N. J., and C. Piccolo, 2001, J. Fluid Mech. **449**, 85.

Balmforth, N. J., C. Piccolo, and M. Umurhan, 2001b, J. Fluid Mech. **449**, 115.

Balmforth, N. J., A. Roy, and C. P. Caulfield, 2012, J. Fluid Mech. **694**, 292.

Balmforth, N. J., and R. Sassi, 2000, Physica D **143**, 21.

Balmforth, N. J., and W. R. Young, 1997, Phys. Rev. Lett. **79**, 4155.

Balmforth, N. J., and Y.-N. Young, 2002, J. Fluid Mech. **450**, 131.

Barré, J., and Y. Y. Yamaguchi, 2009, Phys. Rev. E **79**, 036208.

Bassom, A. P., and A. D. Gilbert, 1998, J. Fluid Mech. **371**, 109.

Benjamin, T. B., 1963, J. Fluid Mech. **16**, 436.

Benney, D. J., and R. F. Bergeron, 1969, Stud. Appl. Math. **48**, 181.

Berk, H., B. Breizman, and M. Pekker, 1996, Physical review letters **76**(8), 1256.

Berk, H. L., B. N. Breizmann, J. Candy, M. Pekker, and N. V. Petviashvili, 1999, Phys. Plasmas **6**, 3102.

Berk, H. L., and K. V. Roberts, 1967, Phys. Fluids **10**, 1595.

Bernoff, A. J., and J. Lingevitch, 1994, Phys. Fluids **6**, 3717.

Bernstein, I. B., J. M. Greene, and M. D. Kruskal, 1958, Phys. Rev. **108**, 546.

Besse, N., Y. Elskens, D. F. Escande, and P. Bertrand, 2011, Plasma Physics and Controlled Fusion **53**(2), 025012.

Bickley, W. C., 1937, Philos. Mag. **23**, 727.

Binney, J., and S. Tremaine, 2008, *Galactic Dynamics* (Princeton University Press, Princeton, N. J.), second edition.

Bohm, D., and E. P. Gross, 1949a, Phys. Rev. **75**, 1851.

Bohm, D., and E. P. Gross, 1949b, Phys. Rev. **75**, 1864.

Bohm, D., and E. P. Gross, 1950, Phys. Rev. **79**, 992.

Briggs, R. J., J. D. Daugherty, and R. H. Levy, 1970, Phys. Fluids **13**, 421.

Brown, S. N., and K. Stewartson, 1978, Geophys. Astrophys. Fluid Dyn. **10**, 1.

Brown, S. N., and K. Stewartson, 1980, J. Fluid Mech. **100**, 811.

Brunet, G., and P. H. Haynes, 1995, J. Atmos. Sci. **52**, 464.

Brunet, G., and T. Warn, 1990, J. Atmos. Sci. **47**, 1173.

Brunetti, M., F. Califano, and F. Pegoraro, 2000, Physical Rev. E **62**, 4109.

Bryuno, A. D., 1988, Russian Math. Surveys **43**, 25.

de Buyl, P., D. Fanelli, R. Bachelard, and G. D. Ninno, 2009, Phys. Rev. Special Topics - Accelerators and Beams **12**, 060704.

Cairns, R. A., 1979, J. Fluid Mech. **92**, 1.

Campa, A., T. Dauxois, and S. Ruffo, 2009, Phys. Repts. **480**, 57.

Carbone, V., R. De Marco, F. Valentini, and P. Veltri, 2007, EPL (Europhysics Letters) **78**(6), 65001.

Cary, J. R., I. Doxas, D. F. Escande, and A. D. Verga, 1992, Phys. Fluids B **4**.

Case, K. M., 1960, Phys. Fluids **3**, 143.

Casti, A., P. J. Morrison, and E. A. Spiegel, 1998, Annals of the New York Academy of Sciences **867**, 93.

Chaikin, P. M., and T. C. Lubensky, 1995, *Principles of condensed matter physics* (Cambridge U. Press, Cambridge).

Chandre, C., L. de Guillebon, A. Back, E. Tassi, and P. J. Morrison, 2013, J. Phys. A .

Chandre, C., P. J. Morrison, and E. Tassi, 2012, Phys. Lett. A **376**, 737.

Chavanis, P. H., and L. Delfini, 2009, Euro. Phys. J. B **69**, 389.

Cheng, C. Z., and G. Knorr, 1976, J. Comp. Phys. **22**, 330.

Cheng, Y., and I. M. Gamba, 2012, Communications in Nonlinear Science and Numerical Simulation **17**(5), 2052.

Churilov, S., 2009, Physics of Fluids **21**, 074101.

Churilov, S., 2011, Physics of Fluids **23**(11), 114101.

Churilov, S., and I. Shukhman, 1994, Journal of Fluid Mechanics **281**, 371.

Churilov, S., and I. Shukhman, 1995, Journal of Fluid Mechanics **291**, 57.

Churilov, S. M., 1999, J. Fluid Mech. **392**, 233.

Churilov, S. M., and I. G. Shukhman, 1987a, Geophys. Astrophys. Fluid Dyn. **38**, 145.

Churilov, S. M., and I. G. Shukhman, 1987b, Proc. Roy. Soc. A **409**, 351.

Churilov, S. M., and I. G. Shukhman, 1996, J. Fluid Mech. **318**, 189.

Crawford, J. D., 1991, Rev. Mod. Phys. **63**, 991.

Crawford, J. D., 1995, Phys. Plasmas **2**, 97.

Crawford, J. D., and K. T. R. Davies, 1999, Physica D **125**, 1.

Crawford, J. D., and A. Jayaraman, 1996, Phys. Rev. Lett **77**, 3549.

Crawford, J. D., and A. Jayaraman, 1999, Phys. Fluids **6**, 666.

Crawford, J. D., A. N. Kaufman, C. Oberman, and S. Johnston, 1986, Phys. Fluids **29**, 3219.

Crawford, J. D., and T. O'Neil, 1987, Physics of Fluids **30**, 2076.

Cross, M. C., and P. C. Hohenberg, 1993, Rev. Mod. Phys. **65**, 851.

Danielson, J. R., F. Anderegg, and C. F. Driscoll, 2004, Phys. Fluids **92**, 245003.

Degond, P., 1986, Trans. Am. Math. Soc. **294**, 435.

del-Castillo-Negrete, D., 1998a, Phys. Lett. **241**, 99.

del-Castillo-Negrete, D., 1998b, Phys. Plasmas **5**, 3886.

del-Castillo-Negrete, D., 2000, Chaos **10**, 75.

del-Castillo-Negrete, D., and M. C. Firpo, 2002, Chaos **12**, 496.

del-Castillo-Negrete, D., and P. J. Morrison, 1993, Phys. Fluids A **5**, 948.

Denavit, J., 1981, Phys. Fluids **28**, 2773.

Dikki, L. A., 1960, Sov. Phys. Doklady **135**, 1179.

Dimonte, G., and J. Malmberg, 1978, Physics of Fluids **21**, 1188.

Dirac, P., 1927, Z. Physik **44**, 585.

Doxas, I., and J. Cary, 1997, Phys. Plasmas **4**, 2508.

Drazin, P. G., and W. H. Reid, 1981, *Hydrodynamic Stability* (University Press, Cambridge).

Driscoll, C. F., and K. S. Fine, 1990, Phys. Fluids B **2**, 1359.

Drummond, W. E., J. H. Malmberg, T. M. O'Neil, and J. R. Thompson, 1970, Phys. Fluids **13**, 2422.

Ecker, G., and J. Hoelling, 1963, Phys. Fluids **6**, 70.

Eliassen, A., E. Høiland, and E. Riis, 1953, Institute for Weather and Climate Res. Oslo, Sweden, Pub. No. **1**.

Eliasson, B., and P. K. Shukla, 2007, Phys. Reports **442**, 225.

Engevik, L., 1966, Dept. Applied Math. Bergen, Norway, Pub. No. **11**.

Esler, J., and B. Willcocks, 2012, Geophysical & Astrophysical Fluid Dynamics **106**(3), 320.

Evstatiev, E. G., P. J. Morrison, and W. Horton, 2003, Phys. Plasmas **10**, 4090.

Evstatiev, E. G., P. J. Morrison, and W. Horton, 2005, Phys. Plasmas **12**, 072198.

Feix, M. R., P. Bertrand, and A. Ghizzo, 1994, in *Advances in kinetic theory and computing*, edited by B. Perthame (World Scientific, Singapore), pp. 44–81.

Firpo, M., F. Doveil, Y. Elskens, P. Bertrand, M. Poleni, and D. Guyomarc, 2001, Physical Review E **64**(2), 026407.

Fjørtoft, R., 1950, Geofys. Publ. **17**, 1.

Flierl, G. R., P. Malanotte-Rizzoli, and N. J. Zabusky, 1987, J. Phys. Ocean. **17**, 1408.

Flierl, G. R., and P. J. Morrison, 2011, Physica D **240**, 212.

Franklin, R., and N. S. J. Braithwaite, 2009, Plasma Sources Science and Technology **18**(1), 014019.

Franklin, R. N., S. M. Hamberger, and G. J. Smith, 1972, Phys. Rev. Lett. **29**, 914.

Fried, B. D., and S. D. Conte, 1961, *The plasma dispersion function* (Academic Press, London).

Friedland, L., and A. Shagalov, 2002, Physics of Fluids **14**, 3074.

Frieman, E., S. Bodner, and P. Rutherford, 1963, Phys. Fluids **6**, 1298.

Fujiwara, T., 1981, Publ. Astron. Soc. Japan **33**, 531.

Gakhov, F., 1990, *Boundary Value Problems* (Dover, New York).

Galeotti, L., and F. Califano, 2005, Physical review letters **95**(1), 015002.

Gill, A. E., 1965, J. Fluid Mech. **21**, 503.

Goldreich, P., and S. Tremaine, 1979, Astrophys. J. **233**, 857.

Goldstein, M., and S.-W. Choi, 1989, Journal of Fluid Mechanics **207**, 97.

Goldstein, M. E., and L. S. Hultgren, 1988, J. Fluid Mech. **197**, 259.

Goldstein, M. E., and S. J. Leib, 1988, J. Fluid Mech. **191**, 481.

Goldstein, M. E., and S. J. Leib, 1989, J. Fluid Mech. **207**, 73.

Guo, Y., and W. A. Strauss, 1995, Communications on Pure and Applied Mathematics **48**(8), 861.

Haberman, R., 1973, Stud. Appl. Math. **51**, 139.

Hagstrom, G. I., and P. J. Morrison, 2011a, Physica D **240**, 1652.

Hagstrom, G. I., and P. J. Morrison, 2011b, Trans. Theory and Stat. Phys. **39**, 466.

Hagstrom, G. I., and P. J. Morrison, 2013, in *Spectral Analysis, Stability and Bifurcations in Modern Nonlinear Physical Systems*, edited by O. Kirrilov (Springer-Verlag, Berlin).

Hartmann, D., and C. Driscoll, 2001, Physics of Plasmas **8**, 3457.

Haynes, P. H., 1985, J. Fluid Mech. **161**, 493.

Heath, R. E., I. M. Gamba, P. J. Morrison, and C. Michler, 2012, J. Comp. Phys. **231**, 1140.

Hickernell, F. J., 1984, J. Fluid Mech. **142**, 431.

Howard, L. N., 1964, J. de Mécanique **3**, 433.

Huerre, P., 1987, Proc. Roy. Soc. A **409**, 369.

Hui, X., and S. Zhengming, 2012, Plasma Science and Technology **14**(3), 181.

Illner, R., 2000, Fields Inst. Comm **27**, 98.

Imamura, T., R. Sugihara, and T. Taniuti, 1969, J. Phys. Soc. Japan **27**, 1623.

Inagaki, S., and T. Konishi, 1993, Publ. Astron. Soc. Japan **45**, 733.

Ivanov, A., and I. H. Cairns, 2006, Physical review letters **96**(17), 175001.

Ivanov, A., I. H. Cairns, and P. Robinson, 2004, Physics of plasmas **11**, 4649.

Ivanov, A., S. Vladimirov, and P. Robinson, 2005, Physical Review E **71**(5), 056406.

Ivanov, A. V., 2001, The Astrophysical Journal **550**(2), 622.

van Kampen, N. G., 1955, Physica **21**, 949.

Kato, T., 1966, *Perturbation Theory for Linear Operators* (Springer-Verlag, Berlin).

Kelvin, W. T. B., 2001, *Mathematical and Physical Papers, by Sir William Thomson. Collected from Different Scientific Periodicals from May, 1841, to the Present Time* (University of Michigan Library, Ann Arbor, MI).

Killworth, P. D., and M. E. McIntyre, 1985, J. Fluid Mech. **161**, 449.

Krall, N. A., and A. W. Trivelpiece, 1973, *Principles of Plasma Physics* (New York: McGraw-Hill).

Krechetnikov, R., and J. E. Marsden, 2007, Rev. Mod. Phys. **79**, 519.

Kreĭn, M., 1950, Dokl. Akad. Nauk SSSR A **73**, 445.

Kueny, C. S., and P. J. Morrison, 1995, Phys. Plasmas **2**, 1926.

Kuramoto, Y., 1975, in *International symposium on mathematical problems in theoretical physics*, edited by H. Araki (Springer-Verlag, New York), number 39 in Lecture Notes in Physics, pp. 420–422.

Lancelotti, C., and J. J. Dorning, 2003, Phys. Rev. E **68**, 026406.

Landahl, M., 1962, J. Fluid Mech. **13**, 607.

Landahl, M., 1986, in *1986 Summer Study Program in Geophysical Fluid Dynamics at Woods Hole: Order and Disorder in Turbulent Shear Flow*, edited by M. Stern (Woods Hole, MA: Woods Hole Oceanographic Institution), volume WHOI-86-45, pp. 44–50.

Landau, L. D., 1946, J. Phys. (Moscow) **10**, 25.

Le Dizes, S., 2000, Journal of Fluid Mechanics **406**(1), 175.

Leib, S. J., and M. E. Goldstein, 1989, Phys. Fluids A **1**, 513.

Lin, C. C., 1945, Quart. App. Maths. **3**, 117.

Lin, Z., 2001, Mathematical Research Letters **8**(4), 521.

Lin, Z., 2005, Communications on pure and applied mathematics **58**(4), 505.

Lin, Z., and C. Zeng, 2011, Communications in Mathematical Physics **306**(2), 291.

Lynden-Bell, D., 1967, Mon. Not. R. astr. Soc. **136**, 101.

MacKay, R. S., and P. G. Saffman, 1986, Proc. R. Soc. Lond. A **406**, 115.

Malkus, W. V. R., and G. Veronis, 1958, J. Fluid Mech. **4**, 225.

Malmberg, J. H., and C. B. Wharton, 1964, Phys. Rev. Lett. **17**.

Malmberg, J. H., C. B. Wharton, and W. E. Drummond, 1966, in *Plasma Physics and Controlled Nuclear Fusion Research* (International Atomic Energy Agency, Vienna), volume 1.

Manfredi, G., 1997, Phys. Rev. Lett. **79**, 2815.

Manfredi, G., and P. Bertrand, 2000, Physics of Plasmas **7**, 2425.

Manneville, P., 1995, *Dissipative structures and weak turbulence* (Springer).

Marsden, J. E., and T. S. Ratiu, 1999, *Introduction to Mechanics and Symmetry* (Springer-Verlag, New York, NY).

Martinez, Y., G. Brunet, and M. Yau, 2010, Journal of the Atmospheric Sciences **67**(11), 3559.

Maslowe, S., and N. Nigam, 2008, SIAM Journal on Applied Mathematics **68**(3), 825.

Matsiborko, N., I. Onishchenko, I. FAINBERG, V. Shapiro, and V. Shevchenko, 1973, Soviet Physics-JETP **36**, 460.

Mattor, N., B. Chang, and T. Mitchell, 2006, Physical review letters **96**(4), 45003.

Mattor, N., and T. B. Mitchell, 1996, Astrophys. J. **472**, 532.

van der Meer, J. C., 1985, *The Hamiltonian Hopf bifurcation*, Lecture Notes in Mathematics 1160 (Springer-Verlag, Berlin).

Miller, J. C., 2004, 2003 Program of Study Non-Newtonian Geophysical Fluid Dynamics , 191.

Mitchell, T. B., and C. F. Driscoll, 1994, Phys. Rev.Lett. **73**, 2196.

Möller, J. D., and M. T. Montgomery, 1999, J. Atmos. Sci. **56**, 1674.

Montgomery, M. T., and R. J. Kallenbach, 1996, Quart. J. Roy. Meteorol. Soc. **122**, .

Morrison, P. J., 1980, Phys. Lett. A **80**, 383.

Morrison, P. J., 1982, in *Mathematical Methods in Hydrodynamics and Integrability in Dynamical Systems*, edited by M. Tabor and Y. Treve (American Inst. Phys.), volume 88, pp. 13–46.

Morrison, P. J., 1994, Phys. Plasmas **1**, 1447.

Morrison, P. J., 1998, Rev. Mod. Phys. **70**, 467.

Morrison, P. J., 2000, Trans. Theory and Stat. Phys. **29**, 397.

Morrison, P. J., 2003, in *Nonlinear Processes in Geophysical Fluid Dynamics*, edited by O. U. Velasco Fuentes, J. Sheinbaum, and J. Ochoa (Kluwer, Dordrecht), pp. 53–69.

Morrison, P. J., 2013, Phys. Plasmas **20**, 012104.

Morrison, P. J., and J. M. Greene, 1980, Phys. Rev. Lett. **45**, 790.

Morrison, P. J., and M. Kotschenreuther, 1990, in *Nonlinear World: IV International Workshop on Nonlinear and Turbulent Processes in Physics*, edited by V. G. Baryakhtar, V. M. Chernousenko, N. S. Erokhin, A. B. Sitenko, and V. E. Zakharov (World Scientific, Singapore), pp. 910–932.

Morrison, P. J., and D. Pfirsch, 1989, Phys. Rev. A **40**, 3898.

Morrison, P. J., and D. Pfirsch, 1990, Phys. Fluids B **2**, 1105.

Morrison, P. J., and D. Pfirsch, 1992, Phys. Fluids **4B**, 3038.

Moser, J., 1975, Adv. Math. **16**, 197.

Moser, J., 1976, Comm. Pure App. Math. **29**, 727.

Mouhot, C., and C. Villani, 2011, Acta Math. **207**, 9.

Mynick, H. E., and A. Kaufman, 1978, Phys. Fluids **21**, 653.

Ng, C., A. Bhattacharjee, and F. Skiff, 1999, Physical review letters **83**(10), 1974.

Ng, C., A. Bhattacharjee, and F. Skiff, 2006, Physics of plasmas **13**, 055903.

O'Neil, T. M., 1965, Phys. Fluids **8**, 2255.

O'Neil, T. M., J. H. Winfrey, and J. H. Malmberg, 1971, Phys. Fluids **14**, 1204.

Onishchenko, I. N., A. R. Linetskii, N. G. Matsiborko, V. D. Shapiro, and V. I. Shevchenko, 1971, Soviet Phys. JETP. **11**, 281.

Padhye, N., and W. Horton, 1999, Phys. Plasmas **6**.

Pao, Y.-p., 1988, Physics of Fluids **31**, 302.

Papaloizou, J. C., and C. Terquem, 2006, Reports on Progress in Physics **69**(1), 119.

Pedlosky, J., 1987, *Geophysical Fluid Dynamics* (Springer-Verlag).

Penrose, O., 1960, Phys. Fluids **3**, 258.

Raghunathan, M., and R. Ganesh, 2013, Physics of Plasmas **20**, 032106.

Rayleigh, J. W. S., 1899, *Scientific Papers 1869–1881* (Cambridge University Press, Cambridge).

Redekopp, L. G., 1977, J. Fluid Mech. **82**, 725.

Reutov, V. P., 1980, Izvestiya, Atmosph. Oceanic Phys. **16**, 938.

Rosenbluth, M. N., and A. Simon, 1964, Phys. Fluids **7**, 557.

Rosencrans, S. I., and D. H. Sattinger, 1966, J. Math. and Phys. **45**, 289.

Rossi, L. F., J. F. Lingevitch, and A. J. Bernoff, 1997, Phys. Fluids **9**, 2329.

Russo, G., and P. Smereka, 1996, SIAM Journal on Applied Mathematics **56**(2), 327.

Schade, H., 1964, Phys. Fluids **7**, 623.

Schamel, H., 2012, Phys. Plasmas **19**(2), 02xxxx.

Schecter, D. A., D. H. E. Dubin, A. C. Cass, C. F. Driscoll, I. M. Lansky, and T. M. O'Neil, 2000, Phys. Fluids **12**, 2397.

Schecter, D. A., and M. T. Montgomery, 2004, Physics of Fluids **16**, 1334.

Schecter, D. A., M. T. Montgomery, and P. D. Reasor, 2002, Journal of the atmospheric sciences **59**(2), 150.

Sedláček, Z., 2005, Transport Theory and Statistical Physics **34**(1-2), 63.

Shagalov, S. V., V. P. Reutov, and G. V. Rybushkina, 2009, Izvestiya Atmospheric and Oceanic Physics **45**, 629.

Shagalov, S. V., V. P. Reutov, and G. V. Rybushkina, 2010, Izvestiya Atmospheric and Oceanic Physics **46**, 95.

Shoucri, M., 1980, Physics of Fluids **23**, 2030.

Shoucri, M., 2008, Communications in Nonlinear Science and Numerical Simulation **13**(1), 174.

Shukhman, I., 1998a, Journal of Fluid Mechanics **369**, 217.

Shukhman, I., 1998b, Physics of Fluids **10**, 1972.

Shukhman, I., and S. Churilov, 1997, Journal of Fluid Mechanics **343**(1), 197.

Shukhman, I. G., 1989, J. Fluid Mech. **200**, 425.

Simon, A., and M. Rosenbluth, 1976, Phys. Fluids **19**, 1567.

Smereka, P., 1998, Physica **124D**, 104.

Smereka, P., 2002, Journal of Fluid Mechanics **454**, 287.

Smith, G. R., and N. Pereira, 1978, Phys. Fluids **21**, 2253.

Stein, E. M., and G. Weiss, 1971, *Introduction to Fourier analysis on Euclidean spaces* (Princeton University Press, Princeton, New Jersey).

Stewartson, K., 1978, Geophys. Astrophys. Fluid Dyn. **9**, 185.

Stewartson, K., 1981, IMA J. Applied Math. **27**, 133.

Strogatz, S. H., 2000, Physica D **143**, 1.

Strogatz, S. H., R. E. Mirollo, and P. C. Matthews, 1992, Phys. Rev. Lett. **68**, 2730.

Stuart, J. T., 1960, J. Fluid Mech. **9**, 353.

Sturrock, J. A., 1958, Phys. Rev. **112**, 1488.

Sugihara, R., and T. Kamimura, 1972, J. Phys. Soc. Japan **33**, 206.

Tassi, E., C. Chandre, and P. J. Morrison, 2009, Phys. Plasmas **16**, 082301.

Tassi, E., and P. J. Morrison, 2011, Phys. Plasmas **18**, 032115.

Tassi, E., P. J. Morrison, F. L. Waelbroeck, and D. Grasso, 2008, Plasma Phys Cont. Fusion **50**, 085014.

Tennyson, J. L., J. D. Meiss, and P. J. Morrison, 1994, Physica D **71**, 1.

Tsunoda, S., F. Doveil, and J. Malmberg, 1987, Physical review letters **59**, 2752.

Turner, M., A. D. Gilbert, and A. P. Bassom, 2008, Physics of Fluids **20**, 027101.

Turner, M. R., A. P. Bassom, and A. D. Gilbert, 2009, Journal of Fluid Mechanics **638**, 49.

Turner, M. R., and A. D. Gilbert, 2007, J. Fluid Mech. **593**, 255.

Turner, M. R., and A. D. Gilbert, 2008, J. Fluid Mech. **614**, 381.

Valentini, F., 2005, Physics of plasmas **12**, 072106.

Valentini, F., R. De Marco, V. Carbone, and P. Veltri, 2008, EPL (Europhysics Letters) **83**(5), 55001.

Vanneste, J., 1996, J. Fluid Mech. **323**, 317.

Volokitin, A., and C. Krafft, 2012, Plasma Physics and Controlled Fusion **54**(8), 085002.

Warn, T., and P. Gauthier, 1989, Tellus **41A**, 115.

Warn, T., and H. Warn, 1978, Stud. Appl. Math. **59**, 37.

Watson, J., 1960, J. Fluid Mech. **9**, 371.

Weitzner, H., 1963, Phys. Fluids **6**, 1123.

Wharton, C., J. Malmberg, and T. O'Neil, 1968, Physics of Fluids **11**, 1761.

White, R. L., 1986, in *The Use of Supercomputers in Stellar Dynamics* (Springer), pp. 167–174.

Willcocks, B., and J. Esler, 2012, Journal of Physical Oceanography **42**(2), 225.

Winant, C., and F. Browand, 1974, Journal of Fluid Mechanics **63**(2), 237.

Yamaguchi, Y. Y., J. Barré, F. Bouchet, T. Dauxois, and S. Ruffo, 2004, Physica A **337**, 36.

Yoshikawa, K., N. Yoshida, and M. Umemura, 2013, The Astrophysical Journal **762**(2), 116.

Zaslavsky, A., C. Krafft, L. Gorbunov, and A. Volokitin, 2008, Physical Review E **77**(5), 056407.